Development and Performance Evaluation of a Medium Scale Clustered LPG Stove with Porous Radiant Burner

A thesis submitted in partial fulfillment of the requirements for the degree of

Doctor of Philosophy

by

Sunita Deb

(Roll No: 166151107)

School of Energy Science and Engineering

Indian Institute of Technology Guwahati

Guwahati – 781039, India

March, 2022

School of Energy Science and Engineering

Indian Institute of Technology Guwahati

Guwahati – 781039, India

STATEMENT

This is to certify that the research work presented in this thesis entitled "**Development and Performance Evaluation of a Medium Scale Clustered LPG Stove with Porous Radiant Burner**" has been carried out by me at the School of Energy Science and Engineering, Indian Institute of Technology Guwahati, under the esteemed supervision of Prof. P. Muthukumar.

I hereby assure that there is no conflict of interest related to the research work and the and the results presented in this thesis were obtained by me and have not been submitted to any other Institute or University for the award of any other degree or diploma.

As per the general practice and ethics of reporting scientific information, due acknowledgements and citations have been made wherever the work described is based on the findings of other investigations.

Sunita Deb

Roll Number 166151107

Research Scholar

School of Energy Science and Engineering

Indian Institute of Technology Guwahati

Guwahati – 781039, Assam, India.

School of Energy Science and Engineering

Indian Institute of Technology Guwahati

Guwahati – 781039, India

THESIS CERTIFICATE

It is certified that the work embodied in the thesis entitled **Development and Performance Evaluation of a Medium Scale Clustered LPG Stove with Porous Radiant Burner** by **Sunita Deb**, a student in the School of Energy Science and Engineering, Indian Institute of Technology Guwahati, India, for the award of the degree of the **Doctor of Philosophy** has been carried out under my supervision and that the work has not been submitted elsewhere for the grant of any other degree.

Dr. P. Muthukumar

Professor

Department of Mechanical Engineering

Indian Institute of Technology Guwahati

Guwahati – 781039, Assam, India.

Dedicated to

All the previous researchers in the field of Porous Media Combustion

Acknowledgement

May almighty God accept my foremost gratitude as all words fall short before His benevolence in getting me admitted in the Ph. D program and finally getting me the degree while carving me out for the same. I am utterly thankful to Him for everything.

I take this opportunity to express my profound gratitude to my supervisor Prof. P. Muthukumar, Professor, Dept. of Mechanical Engineering, Indian Institute of Technology Guwahati, for his unflagging guidance, motivation and timely interventions. His diligence has inspired me to keep working and never lose hope. He has been extremely forgiving and kind and has always given me a comfortable platform to grow while making things easy for me. I extend my sincere thanks to my Doctoral Committee members, Prof. G. Pugazhendi, Prof. K. Mohanty and Dr. D. N. Basu for their advice and guidance towards improving my research work. I thank them for examining me and taking out time for the entire process.

I would like to offer my sincere thanks to the Ministry of Education, Government of India for providing me scholarship I would also like to acknowledge the heads and the staff, School of Energy Science and Engineering, Department of Mechanical Engineering and Department of Design for providing necessary help during my pursuit of Ph. D.

I would also like to acknowledge Dr. M. A. Mujeebu and Dr. K. E. Reby Roy for their advice and mentoring. Additionally, my gratitude is extended to Prof. Gautam Biswas, Dr. Pankaj Kalita, Dr. Vinayak Kulkarni, Dr. Pranab K. Mandal and Dr. Balkrishna Mehta for imparting me knowledge during my course work. In this regard, I would like to thank all my teachers who contributed to my education.

I thank Mr. G. Das, Mr. D. Chetri, Mr. J. Basumatary, Mr. M. Sharma and other Technical Assistants of the Central Workshop, IIT Guwahati, for their effort and contribution in the fabrication of the experimental set-up. The credit also extends to project technicians Pratap Chandra Das, Gabindo Boro and Pervez Ahmed for assisting me during experimental work. My gratitude is extended to all the vendors and suppliers of the materials used in the set-up development. In this regard I would like to thank Mr. Amit Jain for providing valuable suggestions regarding material selection.

I am highly obliged to Dr. L. K. Kaushik, M. Arun Kumar, S.H.V. Satish, K. Hemanth and Pratibha Maurya, for helping me perform experiments and simulations. All my friends and colleagues deserve a special mention for lending me an ear at the time of stress. In this regard, I would like to specially thank G. Sureandhar, Dr. Gayatri Nayak, Divya Kulkarni, Deepika Bishnoi, Umme Hani and Jhuma Debnath for bringing me peace. They have been a significant part of my life and helped me grow. Furthermore, all my lab mates, both who graduated and are currently pursuing Ph. D., deserve a special mention.

This research work required an emotionally stable and optimistic mind which was enhanced much more with the daily online motivation received from pastors Joel Osteen, Priscilla Shirer and Joyce Meyer, spiritual speakers, Sister B. K. Shivani, Quazi Johir and Swami Mukundanand, and thus I express my gratitude to all of them. In line with them, my relatives Suman Das, Purabi Das, Dr. Rahul Kar, Dr. Sudeshna Sarkar and Dr. Sudeep Sarkar have provided valuable advice and guidance at various times in making career decisions and thus I am grateful to them.

I am immensely thankful to my friend Maj. Bharat Mohan. Friendly company received from my friends Anil Kr. Rout, Muniraja Tippa, Samar Das, Ojing Siram, Mrinal Bhowmik, Shailendra Kumar and Ankita Pandey is acknowledged as they not only helped me during course work but also added fun and frolic into my stay at IIT Guwahati. I thank all the support staff at my hostel and IIT Guwahati fraternity who made my life comfortable and made me feel at home.

I am indebted to my mother for having my back and always providing unwavering support and motivation for my education and career building. I will be ever grateful to my late father Sachi Dulal Deb who has been divinely watching over me, guiding my steps and providing for me. My sister Bijoya Deb, my brother-in-law Dr. Pankaj Paul and my aunt Shipra Das equally deserve praise for sharing or rather taking up my responsibilities at home while I peacefully pursue higher education. Their expectations of me inspire me to work harder and impress them more. I am blessed to have them as my family members. Finally, I would like to thank my husband Dr. Prasenjit Sarkar and my new family especially my mother-in-law, for supporting me and encouraging me to pursue my dreams.

I thank all those whose names I have not been able to mention but have been inspired or rectified by them.

Abstract

Fossil fuels continue to be the most dominating source of energy required for transportation, production of electricity, agriculture, industrialization, cooking and many other small businesses. Due to the consistency of fuel characteristics, fossil fuels are reliable sources of energy. However, due to diminishing reserves and pollutants generated from combustion, the use of fossil fuels has become expensive and detrimental to the environment. Despite various advantages offered by renewable energy resources like environment friendliness, unlimited availability and low cost, their use remains limited mainly due to their inconsistent characteristics. Fast developing society and rapid advancement of industrialization and commercial sector demand cheap, environment friendly and reliable energy. Therefore, the use of energy efficient and environment friendly devices is a must.

Cooking is the one of the most energy intensive sector, as it is an activity concerning everyone irrespective of the geographical location, race, and profession. Apart from being a daily household activity, cooking has also led to the proliferation of various restaurant businesses which are a source of livelihood to many. Thus the expansion of commercial cooking has consequently increased the demand of non-domestic Liquefied Petroleum Gas (LPG) in India as indicated by a growth of 4.9% in the year 2021 (Petroleum Planning & Analysis Cell, 2021). The increasing fuel prices contribute to high operational costs and inhibit the growth of these enterprises, and thus necessitates maximum fuel usage. Therefore, the use of energy-efficient cooking appliances is a conspicuous solution.

LPG being clean, reliable and safe is the most commonly used cooking fuel in commercial kitchens. The LPG cookstoves used in such kitchens are based on free-flame combustion, in which the flame or the reaction zone is completely exposed to the atmosphere and thus gives rise to incomplete combustion, and excessive heat loss. Low thermal efficiency is the major disadvantage of such cookstoves. Over the years, various researches have been conducted research on improving the performance of cookstoves in terms of thermal efficiency, emissions and safety. Most of these improvements ensued from the design improvements that minimized the heat losses from the burner to the load. Various technological advancements in terms of improving heat transfer and combustion characteristics were explored. A major leap in the research works occurred with the advent of Porous Media Combustion (PMC) that gained immense research interests due to its unique heat transfer characteristics that enable wider power modulation, cleaner emissions

and operability with fuels with low calorific values. In this regard, the use of Porous Radiant Burners (PRBs) in cookstoves have been reported to be an advantageous option as the various advantages offered by PMC technology facilitate the maximum conversion of energy in fuels to heat and clean combustion.

Towards improving the performance of the cookstoves, investigations were carried out that included exploring the influence of the physical properties of the porous materials and the geometrical parameters impacting the flow properties, which in turn affected the combustion and heat transfer in the burners. Some of the observations from the literature reported that the thermal efficiency obtained from PRBs, when operated at lower power inputs (0.6 – 3 kW), was observed to be higher (~78%) (Mishra and Muthukumar, 2018; Pantangi et al., 2011) than that obtained from PRBs operating at higher power inputs (5 – 15 kW) (55%) (Mishra, 2015). This led to the necessity of research in order to improve the thermal performance of cookstoves operating at higher power inputs, which are generally used in commercial kitchens. Another critical observation from some of these investigations (Mishra et al., 2015; Mishra and Muthukumar, 2018; Muthukumar and Shyamkumar, 2013; Pantangi et al., 2011; Wu et al., 2014; Yoksenakul and Jugjai, 2011) revealed that smaller-sized PRBs yielded higher thermal efficiency than relatively larger porous burners of higher diameters. The above observations led to the hypothesis that the thermal efficiency of a PRB can be improved by keeping the burner size small. There was no research to investigate the influence of PRB size on the thermal efficiency and mitigation of large gaps in the thermal efficiencies obtained from burner operation at lower and higher power inputs.

In this regard, the main objectives of the present research work are the following –

1. To demonstrate the impact of clustering smaller-sized PRBs on the thermal performance of the burner in comparison with a single-PRB
    a. To perform experimental investigations with forced draft CPRB and evaluate the thermal performance at a power input of 12.5 kW.
    b. To determine the power modulation of the CPRB and thermal performance
2. To develop a self-aspirated CPRB applicable for medium scale cooking
    a. To study the thermal performance of the self-aspirated CPRB
    b. To determine the superiority of the CPRB over a Conventional Burner (CB) in terms of eco-friendliness

3. To perform numerical investigations on the air entrainment and combustion parameters of a self-aspirated Porous Radiant Burner

The present study was carried out in pursuit of an improved PRB that yielded high thermal efficiency while operating at power input corresponding to medium-scale cookstoves (5 – 15 kW). In this regard, a Clustered Porous Radiant Burner (CPRB) was developed, which was a combination of three individual PRBs (individual burner diameter 70 mm) having a total top surface area equivalent to that of a single-porous burner (individual burner diameter 120 mm) developed by Mishra (2015). The performance investigations were performed for a fixed power input of 12.5 kW corresponding to a fuel flow rating of 1 kg/h. The CPRB was found to yield higher thermal efficiency and lower emissions of CO as compared to that generated from the single-PRB. Subsequently, the CPRB was tested for its power modulation in order to ascertain its applicability to different applications. The range of stable power input was found to be 8 to 20 kW, with the burner being stable at different ranges of equivalence ratio obtained at each power input. A common range of equivalence ratio (0.7 - 0.8) was observed for power inputs 8, 10 and 14 kW and therefore, the comparative performance investigation in terms of thermal efficiency and emissions was carried out at these power inputs. At an equivalence ratio of 0.7, the maximum thermal efficiency reported for power inputs of 8, 11, and 14 kW were 59.7%, 57.3%, and 52.9%, respectively. The emissions of CO, NO_x and C_xH_y were found limited to 137, 21.5 and 318 ppm for the entire operational range. Compared to a CB, the CPRB was found to provide a maximum improvement of 26% in thermal efficiency and maximum reductions of 78.7%, 74.1% and 48.9% in CO, NO_x and C_xH_y emissions, respectively.

Towards improving the thermal performance of the CPRB further, the experimental investigations were carried out by increasing the burner diameter in steps of 10 mm up until an optimized diameter was obtained. The CPRB with individual burner diameter 80 mm (CPRB8) was found to yield thermal efficiency of 59.2% and lower CO and NO_x emissions as compared to the CPRB with individual burner diameter 70 mm i.e. CPRB7. With further increase in the burner diameter, i.e., in case of individual burner diameter 90 mm (CPRB9), the thermal efficiency was observed to decrease to 50%; however, the emissions of CO and NO_x were reported to be lower compared to the emissions from CPRB8. When compared to the CBs, a maximum thermal efficiency improvement of 27% was obtained with CPRB8, while a maximum reduction of 85.3% CO and 83.3% NO_x emissions were obtained with CPRB9. As the CO/CO_2 ratio in case of all the cases considered were much below the

prescribed Bureau of Indian Standards (BIS) limit of 0.02, CPRB8 was considered to be the optimized burner for maximum thermal performance.

The forced draft CPRBs developed operated with combustion air supplied by a compressor. For the applicability of the CPRB as a cookstove, the operation of the CPRB with self-induced air was mandatory. Therefore, the design and development of a self-aspirated CPRB was carried out in the second phase of the development of the CPRB. The advancements were made by carrying out geometrical optimization. Initially, when the self-aspirated CPRB was operated on submerged combustion mode, instabilities in the form of flashback were observed to occur. When the CPRB was operated in partially submerged combustion mode, stable combustion was observed to take place for some configurations of orifice diameter, orifice position and mixing tube diameter. The optimized self-aspirated CPRB was found to be stable for the power input range 8 – 14 kW. The parametric study revealed that the optimized burner geometry yielding the maximum thermal efficiency was obtained with orifice of diameter 0.35 mm, placed at a position of 20 mm from bottom of the mixing tube. Maximum thermal efficiency was obtained as 58.2% at a power input of 8 kW. Minimum CO emissions of 5 ppm were obtained at 8 kW, while the emissions of NO_x were untraceable. Maximum CO and NO_x emissions were limited to 122 and 15.2 ppm, respectively, which was equivalent to emission reduction up to 72% compared to a CB. The self-aspirated CPRB was subsequently assessed for its environment-friendliness with the help of Life Cycle Assessment (LCA). The assessments were carried out considering yearly consumption of fuel in a hostel mess. The LCA conducted on a single CPRB against a CB, for a period of one year highlighted that the use of a CPRB stove reduced the environmental damage significantly and minimized the damage to human health and resources.

Another aspect of the present research work was to study the air entrainment and flame stability of a single-PRB developed by Muthukumar et al. (2020) and obtain an optimized design for the PRB. The simulations were carried out for a power input of 5 kW and the orifice diameter, orifice offset from the bottom and the mixing tube diameter were optimized. The PRB was observed to operate under stable partially submerged combustion for orifice diameter 0.3 mm when positioned at 30 mm from the bottom of the mixing tube of diameter 29 mm. The insights obtained from the numerical study provided knowledge for geometrical optimization of a CPRB through numerical investigations.

Nomenclature

A_{ts}	Top surface area
c	Specific heat capacity
D_m	Mass diffusivity
D_t	Thermal diffusivity
h	Molar enthalpy
h_a	Convective heat transfer coefficient
h_i	Enthalpy of species 'i'
h_v	Volumetric heat transfer coefficient
$\dot{m}_f$	Mass flow rate of fuel
$\dot{m}_a$	Mass flow rate of fuel
P	Pressure
P_e	Peclet Number
Q_w	Wall heat transfer
R	CO/CO_2 ratio
S_L	Flame speed
T	Temperature
T_0	Ambient temperature
W	Molecular mass
$\dot{w}$	Molar rate of production
Y	Mass fractions

Symbols

ϕ	Porosity
Φ	Equivalence Ratio
ρ	Density
μ	Viscosity
η_t	Thermal efficiency
η_t	Radiation efficiency
σ	Stefan-Boltzmann constant
ε	Emissivity
k-ε	*k* : turbulent kinetic energy; ε : dissipation rate of turbulent kinetic energy

Subscripts

i	species number
s	solid
g	gas
Surr	Surrounding
Surf	Surface
p	Pan
w	Water

Abbreviations

CCT	Controlled Cooking Test
CZ	Combustion Zone
EZ	Extended Flame Zone
FFC	Free Flame Combustion
KPT	Kitchen Performance Test
LCA	Life Cycle Assessment
LCV	Lower calorific value
LPG	Liquefied Petroleum Gas
PM	Porous Matrix
PMC	Porous Media Combustion
PNG	Piped Natural Gas
PRB	Porous Radiant Burner
PRRB	Porous Radiant Recirculating Burner
PZ	Preheating Zone
ppcm	Pores per centimetre
ppi	Pores per inch
ppm	Parts per million
WBT	Water Boiling Test

Contents

List of Tables

List of Figures

Chapter 1

Introduction

Preface

The advancement in the living standard of the society depends on the increase in comfort and productivity of the people and is dependent on their safety, health, wealth and longevity. Most of these factors related to the improvement in the living standards require energy usages in activities like transportation, electrification, construction, cooking etc. In this regard fossil fuels have been a boon to mankind as they were initially abundant, consistent and have high energy density. However, of late, fossil fuels have become expensive and unaffordable due to growing demands and limited availability. The pollution caused after combustion have added to the health woes and climate change. Despite various advancements in renewable energy technologies to counter these shortcomings, the development of energy efficient and non-polluting fossil fuel based burners are mandatory.

The present chapter puts forward the various energy options and explains the need to develop gaseous burners that are energy saving and non-polluting. Additionally, a glimpse of the thesis work has been presented

1.1 Background and Motivation

The progress of human civilization in terms of transportation, industrialization, agriculture, electrification, and general wellbeing of the society has been favoured by the use of fossil fuels for energy generation. Fossil fuels like petroleum, coal and natural gas are known to have high energy densities and are considered to be reliable sources of energy. These advantages make them the most common sources of energy. A glimpse of the global energy consumption scenario for 2020 in Fig. 1.1. The global energy intake is mostly sourced from fossil fuels like coal, oil and gas in most countries. Fossil fuels continue to be the dominant source of energy globally due to their consistent nature of sources and operation.

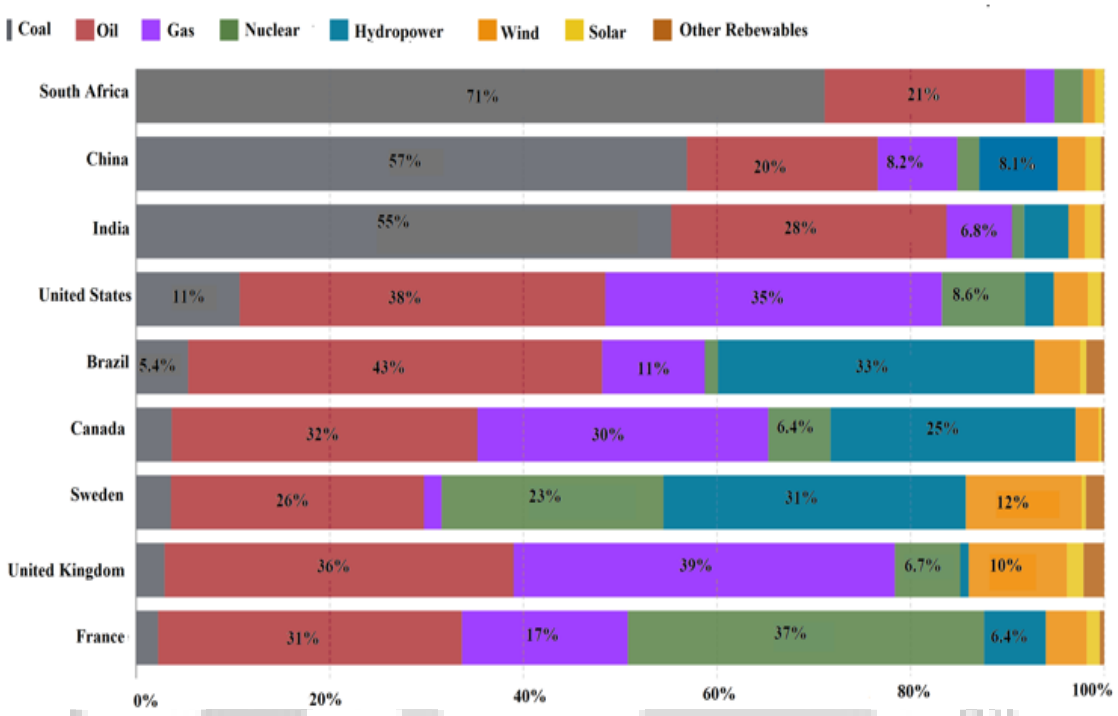

Fig. 1.1: Global energy consumption scenario, 2020 ("Primary energy consumption by source, 2020," n.d.)

Due to the requirement of combustion for the production of usable energy, the use of fossil fuels possesses the greatest disadvantage of emitting harmful pollutants. Additionally, their non-renewable nature makes them limitedly available and increasing demand has led to their fast depletion. Addressing the issue of health, energy and pollutant emissions, the United Nations (UN) laid down 17 Sustainable Development Goals (SDGs), one of which is the access to clean and efficient energy for all. The provision of clean and efficient electricity and cooking energy are the two major targets undertaken under SDG 7. Achieving these goals requires steps like substituting fossil fuels with renewable energy resources (solar, wind, hydro etc.), switching from higher carbon emitting fuels to lower carbon emitting fuels or to reduce the energy consumption itself. The use of renewable energy resources is mostly restricted due to their inconsistent nature and varying intensity as per geographic locations. Fig. 1.2 shows the global low-carbon energy usage for the year 2019.

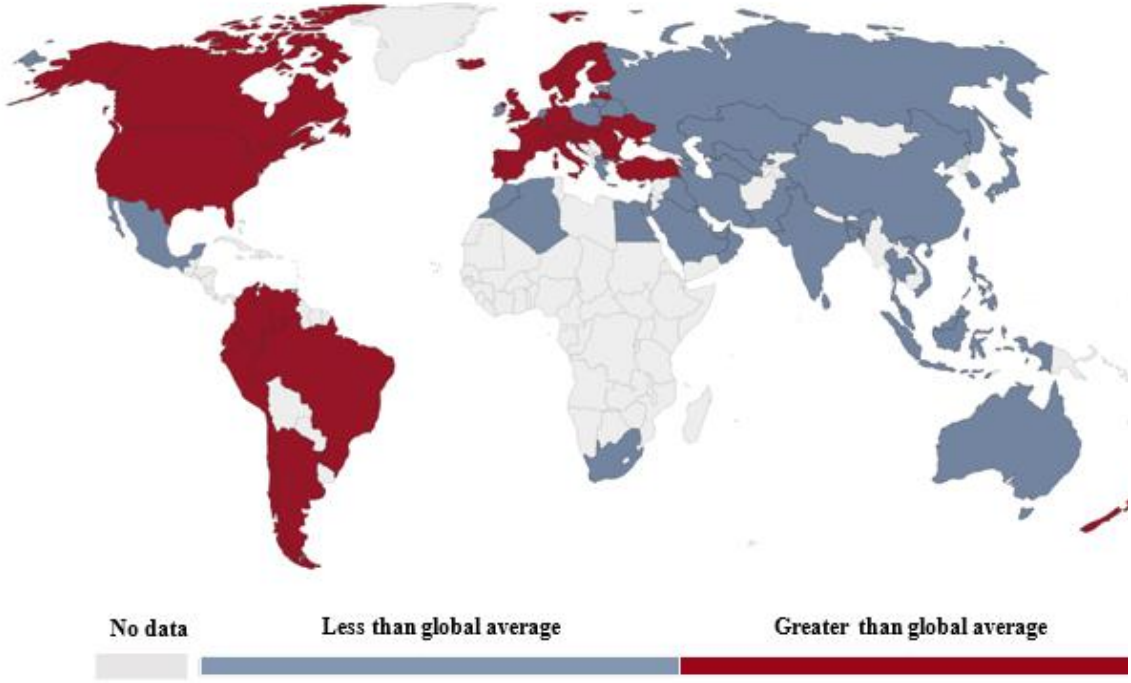

Fig. 1.2: Global consumption of renewable energy (Data, 2021)

Despite the environmental benefits offered by low-carbon fuels, the usage by the eastern part of the world was found to be less than the average of 15.8%. Minimizing the energy consumption is a preferable option as the complete switching over to low carbon emitting fuels is restricted as per availability and accessibility to remote areas. Increasing population and quality of life raises the energy demand and thus the goal of reducing the energy intake can be realized only with the use of energy efficient devices.

One of the major and basic energy demands for the existence of mankind is the requirement of food. Out of the vast majority of staple foods, 95% require the food to be cooked prior to serving ("Facts on Cooking Energy - energypedia," n.d.). Being an essential activity, cooking concerns almost everyone. Thus the provision of clean and efficient cooking energy is a significant step undertaken that can influence every individual for the better. As per reports, in the year 2020, 2.8 billion people still used biomass fuel for cooking. The harmful emissions from biomass fuels make the users prone to an unhealthy life and an unproductive lifestyle (*Global Energy Review 2021*, 2021) apart from deteriorating the environment. Gaseous cooking fuels are generally cleaner than their solid or liquid alternatives. Gaseous fuels like Liquefied Petroleum Gas (LPG) or Piped Natural Gas (PNG) have been found to be safe both for human health and the environment (Kapsalyamova et al., 2021). LPG being derived from fossil fuels is non replenishable and

is expensive and unaffordable to many. In order to make such a beneficial cooking fuel accessible to all, the development of energy efficient cook-stoves that enables the judicious consumption of cooking fuel is necessary. The demand of designing clean and energy efficient cookstoves calls for intensive research work and thus the study of the gas burner design is necessary. The following section presents a brief description of the various gas burner designs.

1.2 Design of Gas Burners

The design of gas burner is an intriguing activity as the fascinating concepts of combustion and heat transfer are finally applied to produce cooking appliances useful to both commercial and domestic settings. Careful design of a burner ensures burner stability establishing its safety, maximum energy output to the load ensuring minimum heat loss and optimum fuel use and minimum emissions of harmful pollutants establishing its environment friendliness. The achievement of these objectives require supply of proper air fuel mixture, reliable and controlled ignition, optimum operating and geometric parameters enabling the maximum heat transfer to the load and lastly, the burner to be inherently safe and stable in operation.

1.2.1 Classification of gas burners

Gas burners can be classified in generally two ways –

i) On the basis of interaction of fuel and air

a) Non aerated burners

Non aerated burners (Fig: 1.3 (a)) are those where the fuel and air interact only at the reaction zone and are unmixed prior to combustion and therefore the burners are based on diffusion flame. Primitive non-aerated burners were prone to produce soot due to the limited availability of air for combustion and therefore further researches were carried out to produce soot free burners. The shift to the use of natural gas from town gas as fuel favoured more research on the design improvements, however, the new designs required high manufacturing tolerances and their stability was restricted.

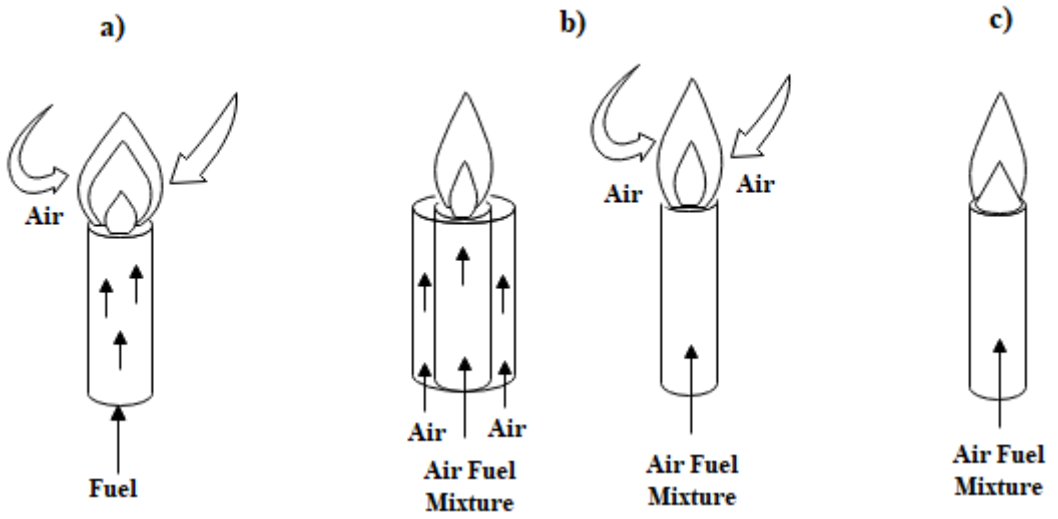

Fig. 1.3: Classification of gas burners on the basis of fuel and air interaction a) Non-aerated burner, b) Partially aerated burner and c) Fully aerated burner

b) Partially aerated burners

Partially aerated burners (Fig. 1.3 (b)) were developed as an advancement over non-aerated burners in order to overcome the problems of soot formation due to incomplete and unstable combustion. The combustion air is supplied in two parts; primary and secondary air. A part of the total air required for combustion is initially supplied along with the fuel and is known as the primary air. However, towards improving combustion, some extra air is supplied as secondary air. The supply of secondary air is either through air openings in the burner or through the entrainment of surrounding air by the flame jet formed as a result of combustion of the air-fuel mixture. Most of the burners used in domestic gas appliances are of the partially aerated type.

c) Fully aerated burners

The supply of air in two parts in a partially aerated burner require careful design considerations for placing the burner ports or maintain enough space in the combustor for the secondary air opening. These shortcomings are overcome by the fully aerated burners (Fig. 1.3 (c)) where all the air required for combustion is supplied along with the fuel and combustion is enabled in a relatively compact space. However, these burners may require some preheating of the air-fuel mixture when excess air provided for complete combustion results in decrease of the temperature (H.R.N. Jones, 2005). Thus these burners also require

careful design in order to handle the high flow rates of the air-fuel mixture and provide sufficient air for complete combustion without instabilities.

ii) On the basis of the provision of heat recirculation

Apart from the method of air supply, burners can also be classified based on the provision of heat recirculation in order to preheat the incoming air-fuel mixture. The burners that do not provide any means of heat re-circulation to preheat the incoming air-fuel mixtures are mainly based on Free Flame Combustion (FFC) where the entire flame is exposed to the surroundings. The energy balance of such burners, as depicted in Fig. 1.4, comprises heat generation from combustion, heat transferred to the load and the heat lost to the surroundings from the flue gases.

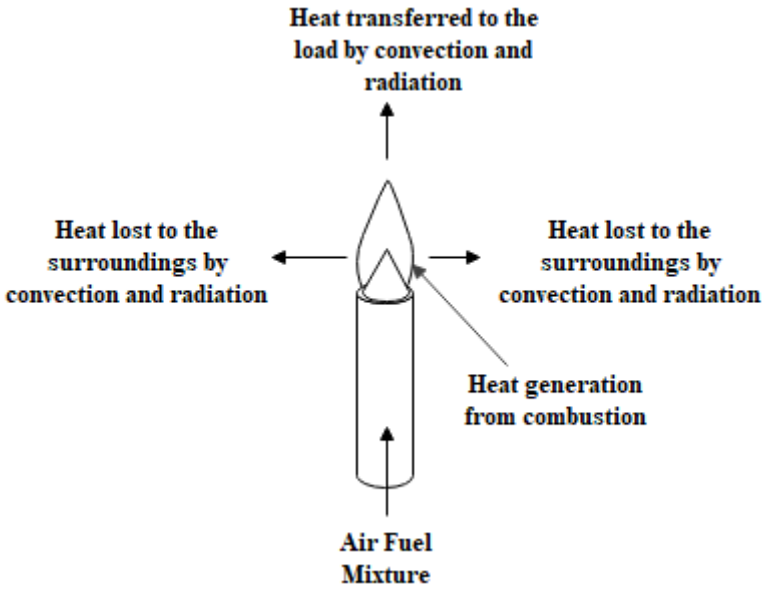

Fig. 1.4: Heat transfer mechanism in a free flame burner

As mentioned previously, as per the design requirements there may arise the need to preheat the incoming air-fuel mixture. Apart from assisting stable burner function, preheating the air-fuel mixture helps in widening stable operating range, decreasing pollutant emissions and increasing thermal efficiency. The preheating can be obtained by recirculating a part of the heat from the reaction zone or from the outgoing flue gases towards the incoming air-fuel mixture, thus enabling the utilization of a part of heat content of the flue gases which otherwise remains unutilized. Heat re-circulating burners provide a means to recirculate heat without dilution of the fresh air-fuel mixture. The heat re-circulating burners can be further sub-divided into external and internal types based on the separation

of the incoming air-fuel mixture from the outgoing product gases. The external type of heat recirculating burners were first introduced by Weinberg (1971), the illustration of which is shown in Fig. 1.5 (a).

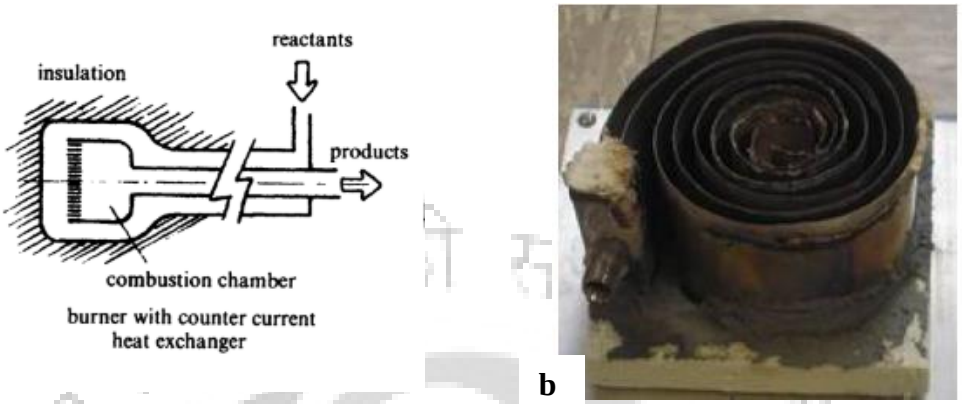

Fig. 1.5: Heat re-circulation burners of the external type a) Heat recirculating burner (Weinberg, 1971), b) An open top swill roll burner (Chen et al., 2009),

Subsequently, more research works were conducted and another such development was Swiss roll burner (Fig. 1.5 (b)) developed by Chen et al. (2009), which is a salient example of an external heat recirculating burner. With the help of a double spiral heat exchanger, a fraction of heat from the product gases is used to preheat the reactants.

In contrast to the external heat recirculating burners, internal heat re-circulating burners provide a means of recirculating the heat via an internal mechanism of heat exchange. In this kind, the combustion zone itself may act as a heat exchanger that can transfer the heat to the reactants from the combustion zone. These burners generally contain a Porous Matrix (PM) that have special thermal and physical properties supporting the process of combustion and heat transfer effectively and are called Porous Radiant Burners (PRBs). These burners generally are of the radiant heater type and can be further classified into two types: one is of the radiant plaque type where the flame remains close to the discrete holes forming the burner ports and the other one is the ceramic foam burner in which layers of ceramic foam or fibers sustain combustion taking place inside the voids (Fig. 1.6). This type of combustion is commonly known as Porous Media Combustion (PMC) and was first proposed by Takeno & Sato, 1979, based on the excess enthalpy flame theory proposed by Hardesty & Weinberg, 1973 and Weinberg, 1971.

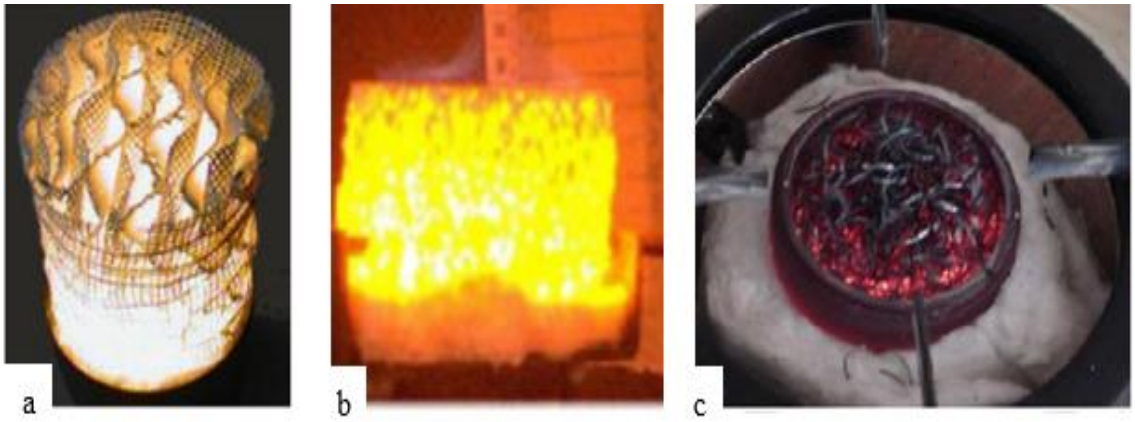

Fig. 1.6: Photographic views of Porous Media Combustion in a) Alumina lamellae (Wood and Harris, 2008), b) Silicon Carbide matrix (Laphirattanakul et al., 2016) and c) Metal fiber (Pantangi et al., 2011)

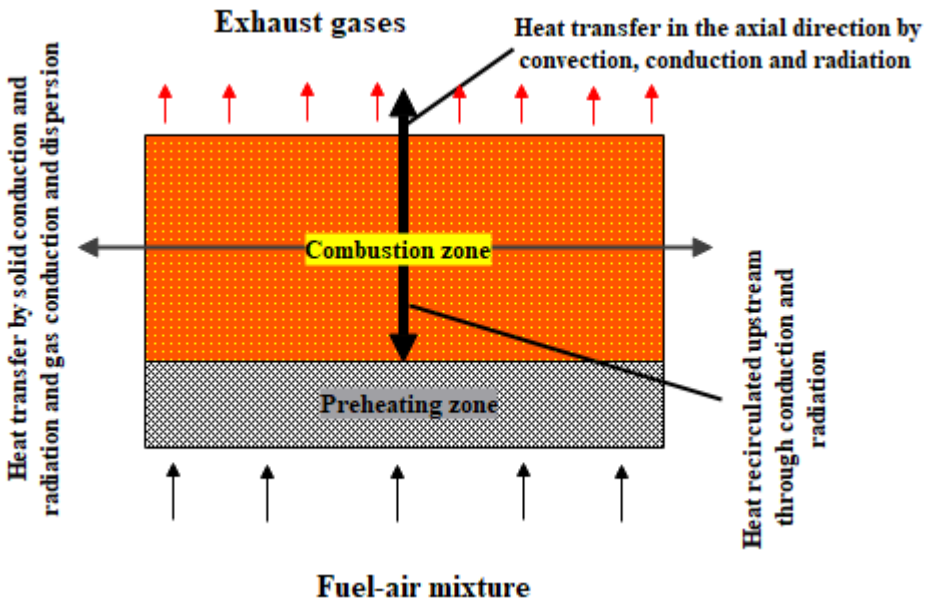

Fig. 1.7: Heat transfer mechanism in a double-layered layered Porous Radiant Burner (Wood and Harris, 2008)

The heat transfer process in a double-layered PRB, consisting of porous preheating and combustion zone, can be comprehended from the illustration shown in Fig. 1.7. Some of the heat generated in the combustion zone is transferred internally upstream by solid conduction and volumetric radiation. Improved heat transfer characteristics offered by PMC through conduction, convection and radiation modes enable the combustion of fuels having low calorific value and the attainment of high flame velocities, radiant output and flammability limits can be obtained. Higher thermal efficiency and lower emissions of CO and NO_x obtained from PRBs compared to the Conventional Burners (CB) operating on

FFC make them a desirable option for use in several applications, one of them being in cookstoves.

1.3 Cookstove Performance Parameters

A newly developed cookstove is required to be tested for its performance to establish the validity of the parameters that define its characteristics. Also a new cookstove requires to compete against the available ones and thus has to undergo several examinations ensuring its competence. A proper cook-stove should satisfy the following requirements of the end user.

(i) Fuel Saving: - it is the most desirable feature of a cook-stove because it provides economic benefit to the households. Also in many cases where home delivery is not provided by the gas agencies, fuel savings also mean that the consumer will have to refill after a longer time period thus reducing the inconvenience caused due to handling and transportation of the gas cylinders.

(ii) Less Polluting: - it is very much desirable and also an imperative feature ever since the UN set up the Global Alliance for Clean Cook-stoves in 2010. As mentioned previously, exposure to pollutants emitted by cook-stoves cause various respiratory diseases and other health problems.

(iii) Cooks local food: - it is expected that the cook-stove can be used to prepare local meals in a manner equal to or more efficiently than the conventional cook-stove. It should be able to cook large or small meals as per the number of members in the family and their food habits.

(iv) Cook in less time: - it is desired by the users that the cook-stove should be able to cook in less time and also the heat output can be controlled so that some items can be cooked at lower temperatures also.

(v) Accommodates local cooking equipment: - the cook-stove should be able to accommodate local cooking equipment so that a large variety of dishes can be prepared and conforms to the local cooking practices.

(vi) Easy maintenance: - the end user or the consumer should be able to easily maintain the cook-stove so that there is reduced or no inconvenience caused due to failure of any

part of the cook-stove. The user should also be able to clean the cook-stove regularly in order to maintain hygiene in the kitchen.

(vii) Safety: - it is the most important parameter for any device. The cook-stoves should have provisions so that physical contact of the people with the hot burner can be avoided and also most importantly the occurrences of flash-back and blow off should be eliminated. Additionally, reliable and safe stove operation enables the users to leave the cookstoves unattended during meal preparation, which allows the users to save time and increase their productivity as mentioned previously in section 1.1.

(viii) Affordable: - the cook-stove should not only save fuel but should also be inexpensive because high cost discourages the general public for opting for a new stove and abandoning their already functional conventional cook-stove. High cost of the cook-stove obstructs the users from availing various other advantages offered by the cook-stove.

1.3.1 Performance evaluation of a cookstove

The performance analysis of a cookstove is essential in order to quantify the energy-saving and emission characterisctics. Thermal efficiency and emissions are the most common performance paramters. Some of the various methods of performance analysis of a cookstove based on laboratory scale and field testing are described in the following:-

(i) Water Boiling Test (WBT): - it is the preliminary test performed to measure the thermal efficiency of cookstoves. It is used to measure how efficiently a fuel can be used to heat the water under controlled conditions. It is basically done to test a newly developed stove and ensure that it meets the intended performance. Performance evaluation of the stove is as per standards prescribed by a regulatory organisation.

(ii) Controlled Cooking Test (CCT): - it is a laboratory or a field test that evaluates the performance of the cooking stoves using a standardised local cooking task. This method evaluates behaviour of the stove under the ideal cooking conditions in a laboratory. The menu for cooking is prepared by consulting the local people. The test is performed in accordance with the set out procedures. It may also be performed to get an estimation of the stoves that can be sent for field testing. The results of the cookstove can be replicated, provided the menu and the cooking conditions are the same. Specialized cooks are required to prepare the meals. The outcomes of CCT for one project area cannot be translated to a different project area. It cannot, however, be used to measure the effectiveness and

sustainibilty of a cookstove. Therefore more detailed survery is necessary to evaluate the actual performance of a cookstove.

(iii) Kitchen Performance Test (KPT): - the results of WBT or CCT are not sufficient to determine whether a cookstove can be launched in the market because both of them are performed in laboratory environment. KPT measures the real performance of stoves in the households under the real operating conditions. This method assess the impact of stoves on fuel use and stove utilisation trends over long term. It is able to predict the outcomes of uncontrolled usage of the cook stoves in actual practice.

Some of the common gaseous fuel based cookstoves available in the market are presented in Table 1.1 Most of these cookstoves operate on FFC mode and thus the mechanism of heat recirculation is lacking.

Table 1.1: Some of the available gaseous fuel based cookstoves

Name	**Type of use**	**Efficiency**	**Image**
Domestic LPG stove	Domestic	68%	
KB-5 burner (Aroonjarattham, 2016) (LPG)	Commercial application	48 – 51%	
Biogas stove-KVIC model	Domestic	67%	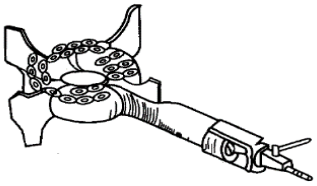
T-35 burner (LPG)	Commercial application	46.6%	

M-35 burner (LPG)	Commercial application	47%	
M-22 Burner (LPG)	Commercial application	47%	
C-35 burner (LPG)	Commercial application	30 - 36%	

1.4 Motivation of the Proposed Research Work

Growth in urban lifestyle, backed by a rise in income, supported the expansion of the restaurant services market, including the increase in the number of small eateries, hawkers and Dhabas categorized under the unorganized sector. The market share of Indian food services is predicted to be Rs. 6753 billion by financial year (FY) 2024 ("Indian Food Services Industry - Market Analysis - StockTalk," n.d.). With an expected cumulative growth rate of 6% and 44% for the FY 19 – 24, in the unorganized and organized (restaurants, hotels and standalone outlets) sectors, respectively, an increased consumption of cooking fuel can be foreseen. This can be seconded by the predicted growth of 4.9% in non-domestic LPG customers in 2021 (Petroleum Planning & Analysis Cell, 2021). High operational cost is a challenge to the sustenance of these businesses and therefore calls for measures to curb losses.

The use of energy-efficient cook-stoves can be an instrumental step towards reducing the operational costs of the commercial cooking sector. Recent developments in the field of

LPG cook-stoves reveal that the use of PMC technology can lead to significant fuel savings and reduction in pollutant emissions as compared to conventional burners operating on FFC. Unique features of PMC, such as high surface area to volume ratio and enhanced heat transfer by radiation and conduction, lead to high flammability limits and flame stability compared to that with FFC. Some of the previous research works exploited the advantages of PMC to build PRBs for cooking applications (Muthukumar et al., 2020; Muthukumar and Kaushik, 2020). Such burners have been effective in addressing the higher pollutant emissions and fuel consumption from their conventional counterparts. These burners enable natural air entrainment, thereby supporting the operation without the use of external devices for air supply. However, the suitability of these cook-stoves is limited to domestic (1 – 3 kW) and commercial (5 – 7 kW) usages only. Also, when operated at higher power inputs the energy-saving capability diminishes. Based on PMC, the present research work corresponds to cater to the requirement of higher fuel savings at higher power inputs and is advantageous in terms of providing wider power modulation. The present research is based on clustering three individual PRBs in order to provide higher peripheral surface area compared to single PRB. This innovative method results in more uniform heat distribution across the individual PRBs resulting in lowering of top surface temperature ensuing higher thermal efficiency and lowering emissions.

Moreover, the development of PRBs requires extensive experimentation with lot of resources. Numerical simulations were conducted to find an optimized burner dimension of the self-aspirated PRB developed by Muthukumar et al. (2020) and study the effects of the air entrainment and its influence on the combustion stability. The numerical technique can be used for studying the stability conditions for PRBs in cluster and the study contributes to the knowledge in the domain of PMC.

1.5 Thesis organization

Following the present chapter on the introduction to the thesis, the second chapter provides an overview of the previous research works conducted on the development of gaseous fuel operated porous burners. The literature survey has been divided into two sections; experimental and numerical investigations, with a focus on the performance evaluation of the burners and their investigation procedure. The identification of the literature gaps led to the outlining of the objectives for the present thesis work.

The third chapter is regarding the establishment of a Clustered Porous Radiant Burner (CPRB) as an improvement over a single PRB. The concept of clustering porous burners to improve the performance was proven with the help of experimental investigations at a fixed power input. Thereafter, the newly developed CPRB was investigated for its turn-down ratio to investigate its operable range. Performance comparison with the available CBs were also conducted.

The fourth chapter presents the development of a self-aspirated CPRB. After developing a CPRB operating stably on self-aspirated mode, the performance was investigated in terms of technical assessments (turn-down ratio, thermal efficiency and emissions) and Life Cycle Assessment (LCA). The capability of the self-aspirated CPRB to replace the existing CBs for medium scale applications was ascertained.

Another aspect of the thesis is to present a numerical study on the geometrical optimization of a PRB operating on partially submerged mode of combustion. The numerical investigation was detailed in the fifth chapter and the effects of variation of geometrical parameters like the orifice diameter, orifice position and the mixing tube diameter on the primary air entrainment, temperature and flame speed were presented.

The sixth chapter is on conclusion and future scope and provides insights to the key findings followed by the vision of future research works.

1.6 Summary

The present chapter on introduction emphasizes the need to develop fossil fuel based burners for energy efficiency and cleaner environment, with the focus on cookstove burners. Burners are then classified in to two types. The first one is based on the supply of fuel and air into the burner and the second one is based on the provision of heat re-circulation. The various advantages of Porous Media Combustion technology are put forward. The various performance evaluation methods are described and some commonly available gaseous cookstoves are presented. Finally, the motivation of the present research work and its objectives are elaborated.

Chapter 2

Literature Review

Preface

Porous Media Combustion (PMC) is a new paradigm in the field of combustion which offers to solve some of the important issues of our society related to energy efficiency and emissions. PMC finds application in various domains such as gas turbines engines, fuel cell, room heaters, cookstoves, etc. As the present thesis is intended towards providing an energy-efficient and clean combustion option, the literature is focused mainly based on the research works that present the combustion of gaseous fuels in Porous Radiant Burners (PRB). In this chapter, an extensive literature survey on the shift to research on PMC, methods of establishing stability, improving efficiency and lowering emissions are discussed. Also investigations on finding a suitable numerical model, optimizing the burner geometry, estimating thermodynamic entities like temperature, velocity, heat transfer etc. have been explored. From the various corollaries obtained from the literature survey, the literature gap was identified and the objectives of the present research work were presented.

2.1 Advent of Porous Media Combustion technology: A brief review

Investigations on burning lean mixtures began when Weinberg (1971) proposed the concept of excess enthalpy flames. Further investigations were conducted by Hardesty and Weinberg (1973) on producing excess enthalpy flames by recirculating the heat from the flame to the incoming premixed air and fuel mixture. By this method, lean mixtures of fuels with Lower Calorific Value (LCV) that are otherwise non-flammable can also be burnt, producing equivalent enthalpy as desired. This assists in producing reduced emissions and assists in adhering to emission norms. Their concept can be visualized by a comparison shown in two schematic diagrams in Fig. 2.1.

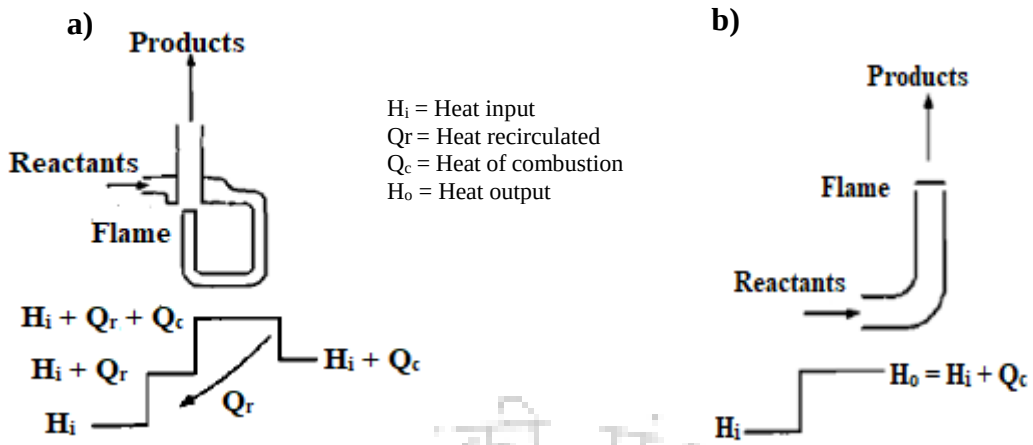

Fig. 2.1: Concept of excess enthalpy flames, a) Enthalpy with re-circulated heat from exhaust gas and b) Enthalpy without heat recirculation

Research work on PMC started in the last decade of 20th century. The main goal was to extend the flammability limit of lean fuel-air mixtures with the help of the concept of excess enthalpy flames given by Weinberg. Following the above research, Takeno and Sato (1979) proposed an embodiment of the concept of excess enthalpy flame by introducing the concept of combustion in a Porous Matrix (PM) of high thermal conductivity. With the help of one dimensional modeling, the flame propagation at different mass flow rates was studied. Combustion in the PM was found to be stable for increased mass flow rates and the abilities to combust low caloric fuels and emit low emissions were foreseen. The concept of PMC for creating excess enthalpy flames and its benefits in extending the flame stability was established experimentally by Kotani and Takeno, (1982). Subsequently, some of the early investigations to find the flame stability for various kinds of PM were carried out by Babkin et al. (1991) and Min and Shin (1991).

In another breakthrough, Durst et al. (1996) introduced a double-layered PRB, where the two layers of PM were used; (i) the upper layer with higher porosity such that the value of the Peclet Number (Pe) is more than 65 and supports combustion and (ii) the lower layer having low porosity where combustion is restricted and the Pe is lower than 65. The reaction zone originates at the interface of the two layers of PM with different porosity. In most of the investigations on double-layered PRBs, the upper layer acting as the combustor is termed as Combustion Zone (CZ), while the bottom layer functioning as the preheater is termed as Preheating Zone (PZ). More insights into the above concept have been described in the following section.

2.2 Investigation on Stability and Flame Characteristics of Porous Radiant Burner

Flame stability is an essential factor in developing a burner as the stable flame ensures safety to the people around the burner. Also, the performance of the burner can be evaluated only when flame stabilization has been achieved. In Conventional Burners (CBs), where the flame is exposed to the surroundings, flame stability is achieved when the flame is attached to the burner ports. Flame becomes unstable when the flame velocity exceeds the velocity of the incoming fuel and air mixture and travels upstream and reaches the mixing tube. This phenomenon is called flashback. When the velocity of the fuel and air mixture is much higher than the flame velocity, then the flame lifts off the burner ports, and this phenomenon is known as blow-off. Similarly, for PRBs, the flame is generally considered to be stable when the reaction zone is restricted within a desired limit. In the case of surface stabilized PRBs the flame is anchored to the surface of the CZ. However, in the case of submerged flame type of PRBs, the flame is restricted inside the CZ for single-layered PRBs or at the vicinity of the PZ and CZ interface for double-layered PRBs. Various factors impacting the stability of PRBs have been reported in various research works, and some of the notable research works are presented below.

2.2.1 Effect of equivalence ratio, flame speed and heat recirculation on PMC stability

Numerical investigations on PMC involving a reciprocating flow were carried out by Hanamura et al. (1993). Reciprocating flow regenerates the excess enthalpy of the combustion gases to an enthalpy increase of the combustible gas through PM. Results obtained from numerical simulation show that the temperature achieved is 13 times the ordinary temperature in free flame. The maximum temperature became higher with decreasing length of the half-cycle. The flame position was reported to be dependent on optical thickness, thermal conductivity, Reynolds number, and heat capacity ratio.

Leonardi et al. (2003) developed a one-dimensional model to predict flame stabilization. At low power inputs and Equivalence Ratio (Φ), surface flame was predicted. Drop in radiation efficiency (η_r) was predicted when the flame moved outside the burner.

The influence of various mixtures, basically highly diffusive gases, on flame stabilization was carried out by Trimis and Wawrzinek (2004). Modified Peclet Number (Pe) is a parameter to determine the flame stability within a PM and the critical Peclet (Pe_c) number was found to be 65 for mixtures having Lewis Number equal to one. For mixtures with Lewis Number less than 1, the Pe_c was found to be below 65 while, for gases having Lewis Number of about 0.4, the Pe_c was found to be as low as 17.

$$Pe = \frac{S_L d C_p \rho}{k}$$

Where, S_L is the flame speed, d is the pore diameter, C_p is the specific heat, ρ is the density and k is the thermal conductivity. A schematic diagram for the various modes of heat transfer in a double-layered PRB is shown in Fig. 2.2.

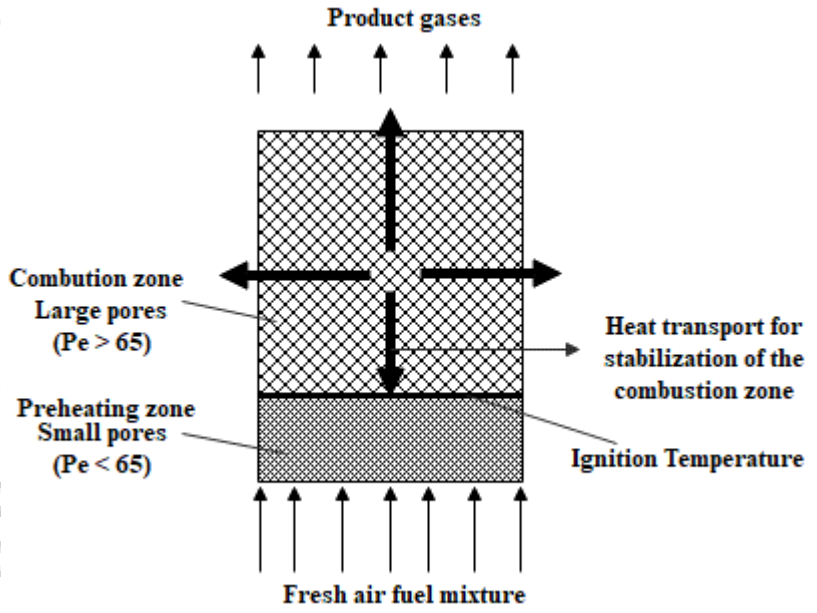

Fig. 2.2: Schematic diagram of various modes of heat transfer in a bi-layered PRB (Trimis and Wawrzinek, 2004)

Zhang et al. (2006) investigated low velocity gas combustion in a packed bed of inert alumina balls. The following conclusions were drawn:

- With an increase in combustion wave velocity, both the peak temperature and flame speed increase
- Higher flow rate and lower Φ combustion results in a greater steady combustion wave velocity

- Super-adiabatic temperatures are more easily achieved in the leaner flames (Φ< 0.3) with stream-wise propagating combustion waves

Zhao et al. (2007) used a one-dimensional laminar pre-mixed model using the software CHEMKIN to simulate the combustion of methane-air mixture. They studied the radiative heat transfer in solids and the convective heat transfer between the gas and the solid. The gas and solid temperatures were obtained by varying the extinction and volumetric heat transfer coefficients. It was concluded that the combustion in PRBs offers superior characteristics compared to CBs, such as super-adiabatic flame temperatures, better stabilization characteristics, higher flame speed, and wider flammability limits.

Bubnovich et al. (2010) studied the flame stabilization for methane combustion in a PM for two beds of different sizes of alumina balls, for different Φ. Stabilized flames were reported in the range of fuel flow rate from 7.01 l/min to 19.00 l/min at Φ of 0.6 and 0.7.

Bakry et al. (2011) carried out an experimental investigation to study the characteristics of combustion of methane-air premixed mixture in a nonhomogeneous PM. Experiments were conducted under high pressure and temperature to study the flame stabilization phenomenon. They found that the flame speed attained the highest value under high inlet pressure and temperature. Also, higher preheat temperature enhanced the stability of combustion.

Veríssimo et al. (2013) derived a relationship between the excess air ratio and air velocity and their impact on the establishment of flameless combustion using methane of 99.5 % purity. They found that the velocity of air increased with a constant excess air ratio of 1.3. The high velocity of the air jet, which comes centrally, increases the entrainment of the fuel and burnt gases. For excess air ratios of 1.7 and higher, submerged combustion couldn't be attained.

Dai et al. (2015) studied the effects of Φ, flow rate, and heat loss through the walls on the super-adiabatic combustion of methane. They reported that the peak temperature increased with the increase in inlet gas velocity while the upstream propagation velocity decreased. With the increase in the Φ, both upstream propagation velocity of combustion waves and the peak temperature increased.

Panigrahy and Mishra (2016) numerically analysed the combustion of LPG in SiC PM by taking into account the volumetric radiation. The energy equation was solved using the finite volume method. A comparison was drawn between methane and LPG combustion on Free Flame Combustion (FFC) and PMC mode. It was reported that LPG had lower flammability limits than methane both in FFC and PMC mode.

Laphirattanakul et al. (2016) conducted experiments to find out the combustion stability of an Alumina PM which was placed inside a hollow cylinder, for a rich premixed LPG mixture. Comparisons were made with a CB. It was reported that flame speed and convection are the major two factors which control the stability. Combustion stability was achieved for Φ less than 4.1 when flame speed dominated convection. For Φ more than 4.1, soot formation took place, however, at higher power inputs, the PM acted as a flame holder.

Hashemi and Hashemi (2017) analyzed the combustion of methane and air in a double-layered PRB, using finite volume method. Their results showed that flame stability limit and flame temperature increased with the increase in Φ. A parametric study of the burner geometry was also done which predicted an optimum outlet to inlet diameter ratio of 2 and optimum ratio of PZ to CZ length to be 0.33 for maximum flame stability.

2.2.2 Effect of porous media specifications on stability

The shape, size and porosity of the PZ and CZ have a significant impact on the combustion phenomenon in a PMC. Several researchers have conducted experiments and numerical simulation to find out the optimum dimensions of the set up.

Hsu et al. (1993) conducted experiments, with varying porosity of the submerged CZ while using the same preheater. Also, insulation was provided around the burner which decreased the lean flammability limit to 0.55 for porosity of 10 ppi. The flame speed was reported to increase with the decrease in pore size and increase in Φ. A comparison with the free flame burner showed better stability and higher range of flame speeds over a constant Φ.

A parametric study on the improvement in radiative output of a PRB was conducted by Kulkarni and Peck (1996) by using double-layered PM. They found that the upstream layer should be highly scattering, and the downstream layer non-scattering. The upstream layer should have lower porosity, shorter length, and higher optical thickness than the downstream layer.

Zhou and Pereira (1997) developed a numerical model to study the combustion phenomena of methane-air and emission of pollutants in a nonhomogeneous PM integrated with a heat exchanger. The peak temperature was found to decrease with the decrease in thermal conductivity of the PM and therefore they suggested the use of a PM with a lower value of thermal conductivity to reduce the emission of NO.

Muthukumar and Shyamkumar (2013) found out the influence of the porosity of SiC foam filter on the emissions and efficiency of PRB. They reported that with the decrease in porosity of the CZ from 90 % to 80 %, the efficiency decreases from 75 % to 71 %. Also CO emissions increase with the decrease in porosity of the foam filter.

Another dimension to the field of PRB was added by Baiquan et al. (2014) through their research on the combustion of low concentration coal mine methane in divergent PRB (inlet diameter 20 mm and outlet 180 mm). Results were compared with a cylindrical PRB of diameter 20 mm. They concluded that the operating conditions of divergent burner are wider than the cylindrical one. For large volume of low concentration methane, divergent structure is superior to cylindrical one.

Janvekar et al., (2017) carried out experiments to find out the effect of PZ thickness on the flame stabilization inside a PM with butane as the fuel. They used alumina foam as the CZ and porcelain foam as the PZ. They considered 5, 10, and 15 mm thick porcelain foams out of which the 10 mm thick porcelain foam was found to be the most suitable for attaining submerged flame stabilization.

Singh et al. (2017) experimented with a divergent shaped SiC reticulated foam, (outlet diameter 90 mm and 70 mm and a constant height of 50 mm) acting as the CZ and metal balls as the PZ. They reported efficiency of 78% with the divergent burner of 90 mm outlet diameter, for an Φ of 0.16. The schematic diagram of the burner is as shown in Fig 2.3. Basically, it can be asserted that CZ with porosity of 90 % are appropriate for stable operation. The PZ acts as a medium to exchange heat between the solid and the incoming fuel and air mixture and should also prevent the flame from travelling downstream. Thus, the porosity of the PZ should be lesser than the porosity of the burner. The divergent burners also act in a similar way.

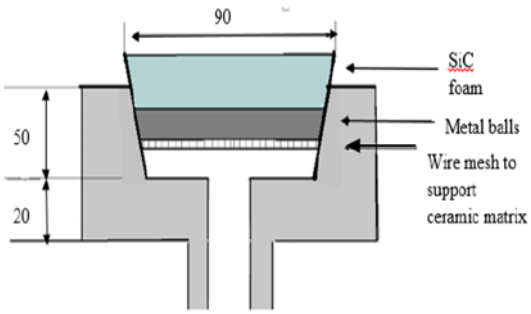

Fig. 2.3: Divergent shaped burner (Singh et al., 2017)

2.3 Studies on Air Entrainment and Design of Mixing Tube

The applications of PRBs are diverse ranging from use in gas turbine engines to fuel cells and cookstoves. Burners for various applications require naturally entrained combustion air in order to eliminate the usage of extra components like blower, accessories and other resources. The self-aspirated design discards the need of pressurized air, eliminating the requirement of extra equipment and electrical energy. Studies on the air entrainment is an important consideration as the fuel flow and air entrainment affect the combustion parameters significantly, as mentioned previously.

The concept of self-aspiration can be commonly found for burners operating with FFC technology. Very initial developments on the study of self-aspirated burners were made by Prichard et al. (1977), who proposed an expression for the Entrainment-Ratio (ER) which was found out from the mass and momentum balance inside the burner. ER was found to affect stability and was influenced by the type of gaseous fuel, loss coefficient of the mixing tube and the orifice and the mixing tube area. Subsequently several researches have been conducted to study the impact of the orifice and the mixing tube dimensions on the entrainment and the mixing characteristics of burners.

Investigations carried out by Kolluri et al. (1996) to study the effects of non-circular Venturi inlet geometries on the primary air entrainment. The use of an elliptical Venturi instead of a circular Venturi led to 30% increase of primary air entrainment. In a study conducted by Singh et al. (1999), the density ratio, aspect ratio and the position of the jet were found to be the most significant factors influencing the air entrainment and mixing. The air entrainment was found to initially increase with increase in the distance of the jet location from the tube inlet and decrease when the jet was positioned further away.

In another study by Singh et al. (2003) reported that non-circular jets enable higher entrainment of surrounding fluid than circular jets except for mixing tube with smaller diameters (39 mm). In the case of tubes with larger mixing tube diameters (90 mm), isosceles triangular jets were reported to yield maximum entrainment that was 10% higher than circular jets. A modified expression for the entrainment ratio applicable to non-circular jets was proposed, which incorporated the impact of jet location. Mishra et al. (2014) ascertained that the ratio of mixing tube length to the nozzle diameter was the most influential parameter affecting air entrainment, followed by the ratio of the mixing tube diameter to the nozzle diameter. An increase in air entrainment with mixing tube diameter was reported in another research by Mishra and Paramanik (2019).

Similar principle of self-aspiration was further extended to the development of PRBs. Some of the notable research works on air entrainment in eductors of PRBs are presented below-

In one of the initial studies of air entrainment in a PRB, Namkhat and Jugjai (2010) determined the Primary Aeration (PA) and its variation with fuel mass flow rate for a single layered surface stabilized PRB. Additionally, a correlation between the air entrainment for hot flow and cold flow conditions was derived. Laphirattanakul et al. (2016) reported that the additional pressure drop created due to the presence of a PM increases the resistance to the fluid flow, which affects the primary air entrainment. The air entrainment was observed to increase with power input, up to a certain limit, beyond which the air entrainment was reported to decrease due to the increase in the fuel flow. Addamane et al. (2016) developed a PRB to study the effect of fuel flow rate on Φ. The Φ, which is directly related to the air entrainment, was observed to increase with porous bed temperature. An analytical model was developed to study the air entrainment and predict the Φ for a specified set of geometrical parameters. Chaelek et al. (2019) designed a self-aspirated Annular Porous Radiant Burner (APMB) and an APMB with Porous Radiant Recirculation Heater (APMB with PRRH) for power inputs from 21 to 44 kW. The air entrainment was found to increase with the increase in the power input. The increased heat recirculation obtained in APMB with PRRH caused a reduction in the air entrainment as compared to the APMB.

2.4 Development and Performance assessment of PRB

Based on the various concepts of flame stabilization, methods of heat recirculation, effect of equivalence ratio and geometrical parameters on combustion, various researchers have

developed PRBs for domestic, medium and industrial applications. Basically performance evaluation in terms of thermal efficiency and emission have been carried out to find out their feasibility and a comparison was drawn to find out the advantages PMC offers over the CBs

In one of the first developments, Jugjai and Sanitjai (1996) explored the usage of PM as a means to reflect and recirculate the heat from the exhaust gases from a cookstove to preheat the combustion air. The proposed design was termed as Porous Radiant Recirculated Burner (PRRB) and was reported to yield improved thermal efficiency and a wider operating range than a CB, while producing low CO emission.

Attempts to increase the efficiency of domestic burners were made by Jugjai and Rungsimuntuchart (2002) by utilizing the concept of heat recirculation in PRBs and integrating it with the CBs. The proposed PRRB integrated CB had a thermal efficiency of 12 % higher than the CBs. They also introduced the concept of swirl in the PRRB by inclining the port angle, shown in Fig. 2.4, and that led to an increase in efficiency to 60%.

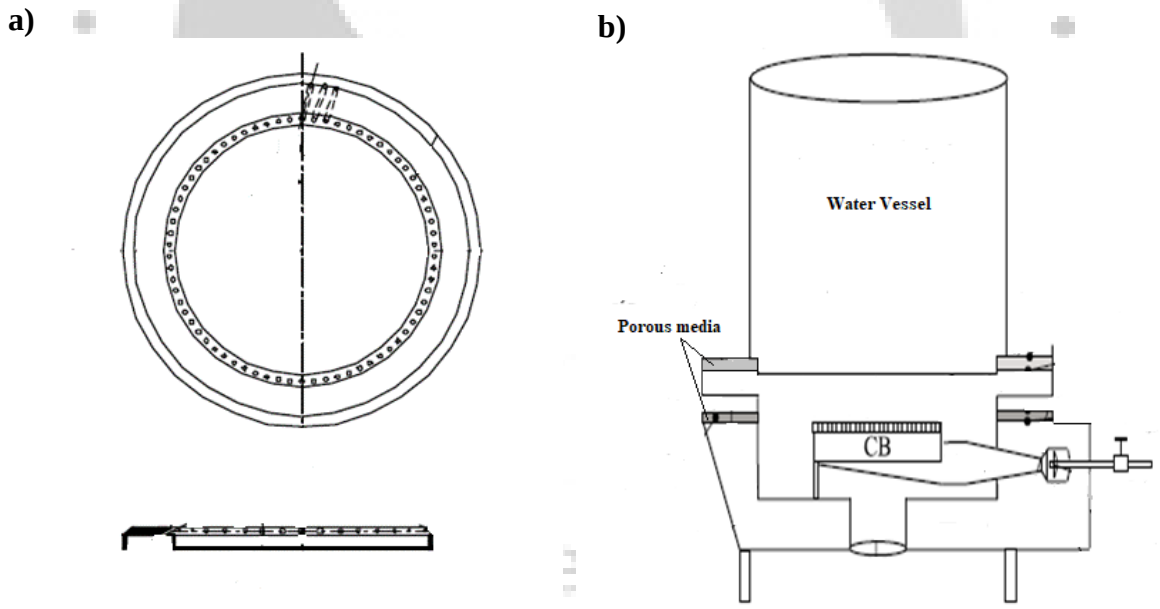

Fig. 2.4: Porous Radiant Recirculation Burner (PRRB) with a) Swirling central flow and b) in combination with a CB

Pantangi et al. (2007) explored the scope of PMC in the field of domestic LPG cook-stove. Three different combinations of PM (metal balls, chips and gravel) were used to conduct experiments as shown in Fig. 2.5 (a) and (b). Observations revealed that the thermal efficiency increased up to 73 % with pebbles in the PZ and mild steel chips in the CZ. This

led to energy savings and that in turn led to cost savings for the customers. Also there was an increase in the percentage volume of CO_2 (0.6875 to 0.9375) and decrease in the levels of CO (225 ppm to 118 ppm) in the exhaust gas which verified better combustion in case of PM as compared to CB.

a)  **b)** 

Fig. 2.5 Domestic cookstoves developed with different porous media a) alumina balls, b) metal chips (Pantangi et al., 2007)

Avdic et al. (2010) developed a combined heating system based on 8 kW PRB by coupling it with a heat exchanger. With this they could achieve CO and NO_x emissions of 48 mg/kWh and 45 mg/kWh, respectively which was less as compared to the conventional gas burners. Thus, the PRB was found to comply with the Blue Angel limit. They could also increase the dynamic power range of the burner up to 1:8. The system developed was efficient and the capacity of the water storage tank could also be reduced substantially.

As an extension of their previous research (Pantangi et al., 2007), Pantangi et al. (2011) used SiC reticulated foam as the CZ and Alumina balls as the PZ. Experiments were conducted by varying the burner casing diameter, CZ and PZ thicknesses, Φ at different power inputs. They found that at higher wattages and Φ, the thermal efficiency decreases as lean mixtures favour complete combustion and heat loss is more at higher heat inputs. The optimum burner diameter was found to be 90 mm. They reported a thermal efficiency of 68 % and much lower emissions (CO: 25-350 mg/m^3 and NO_x: 12-25 mg/m^3) which proved to be more advantageous than conventional domestic cookstove.

Mujeebu et al. (2011b) developed two LPG fired PRBs; one on submerged combustion mode and the other on surface combustion mode. The efficiency and emission characteristics of both the burners were compared to a CB for a thermal load of 0.62 kW. Both the PRBs developed showed higher efficiency and lower emissions as compared to the CB. They also developed a compact LPG PRB based on surface combustion (Mujeebu et al., 2011a). Alumina foam of 26 ppcm and 8 ppcm were used as PZ and CZ respectively.

For an air-fuel ratio of 4:0.5, 80 % fuel savings and significant reduction in NO_x emission could be achieved as compared to CB.

Yoksenakul and Jugjai (2011) developed a self-aspirated PRB (packed bed of Aluminium Balls), as shown in Fig. 2.6, which operated in the range 23-61 kW, which had a turn-down ratio of 2.64. The power input was the most important controlling factor in the performance of the burner as it controlled the PA, which in turn controlled the flame temperature. The power input had not effected the CO emissions while it increased the NO_x emissions. The self-aspirated burner offered a platform for complete combustion which reduced the level of CO emissions to 200 ppm and NO_x emissions to 98 ppm which were significantly low as compared to CB.

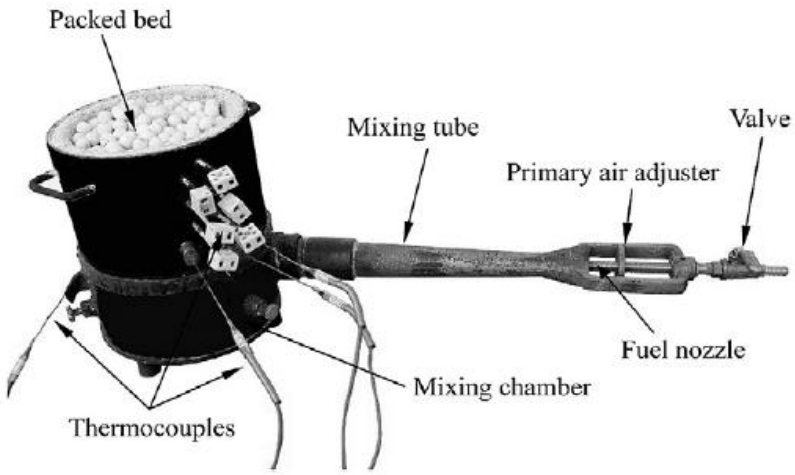

Fig. 2.6: SPMB of Alumina Balls developed by Yoksenakul and Jugjai (2011)

Wu et al. (2014) studied the uses of flat flame burner by using porous metal in comparison to the traditional Bunsen burner flame in domestic stove applications. They reported that the flat flame burner offers superior performance in terms of operating range, turn-down ratio and emission characteristics. Uniform temperature was attained over the flame and however their work leaves a scope to obtain a convincingly higher thermal efficiency over various ranges of Φ, so that a significant development can be introduced in the field of domestic cook-stoves.

PRB with Al_2O_3 particles obtained from grinding wastes and SiSiC foam was developed by Herrera et al., (2015) and its combustion stability and emission characteristics were evaluated with respect to CB used for food industry. The emission of CO was found to 25 ppm when operated at a heat input lower than 194 kW/m^2. The burner was reported to have

lower efficiency than the CB when the pan was kept 5 cm above the surface of the burner. However, the efficiency could be improved by 14 % by keeping the pan directly above the surface.

Mishra et al. (Mishra et al., 2015; Mishra and Muthukumar, 2018) have carried out extensive research on the development and performance analysis of LPG stoves on domestic and medium scale with a two layered PRB. Initially for medium scale applications having power input in the range of 5-10 kW (Mishra et al., 2015), compressed air was used. It was reported that at a heat input of 5 kW and Φ of 0.56, the CO and NO_x emissions were found less as compared to the medium scale burner with CB. The axial temperature was 200°C lower than that of a CB. The efficiency calculated was 58% whereas in case of CB, it was 45%. So with the use of compressed air as oxidiser for medium scale LPG stoves, it was found that the efficiency is much higher and the emissions were lesser than that of an LPG stove with a CB. Subsequently, a self-aspirated PRB for medium scale cooking applications (Mishra, 2015) was developed which yielded 44 – 55 % thermal efficiency in the power input range of 5 – 15 kW.

Later, a self-aspirated PRB for domestic cooking applications (Mishra and Muthukumar, 2018) for the power input range 1 – 3 kW was developed. The performance analysis for the self-aspirated domestic PRB was done by varying the burner port diameter and orifice diameter. Use of smaller orifice diameters or large port diameters resulted in better combustion and thus lowered emissions of CO and NO due to entrapment of sufficient air for the combustion. The thermal efficiency for porous LPG burner at heat input of 1 kW was reported to be 75.1 % which was way higher than that obtained from CB. The temperature across the cross-section of the PRB was also found to be uniform as compared a CB. Therefore, the domestic PRB developed promises to be both energy saving and feasible for domestic applications as it is self-aspirated. Schematic diagram of domestic LPG PRB stove is as shown in Fig. 2.7.

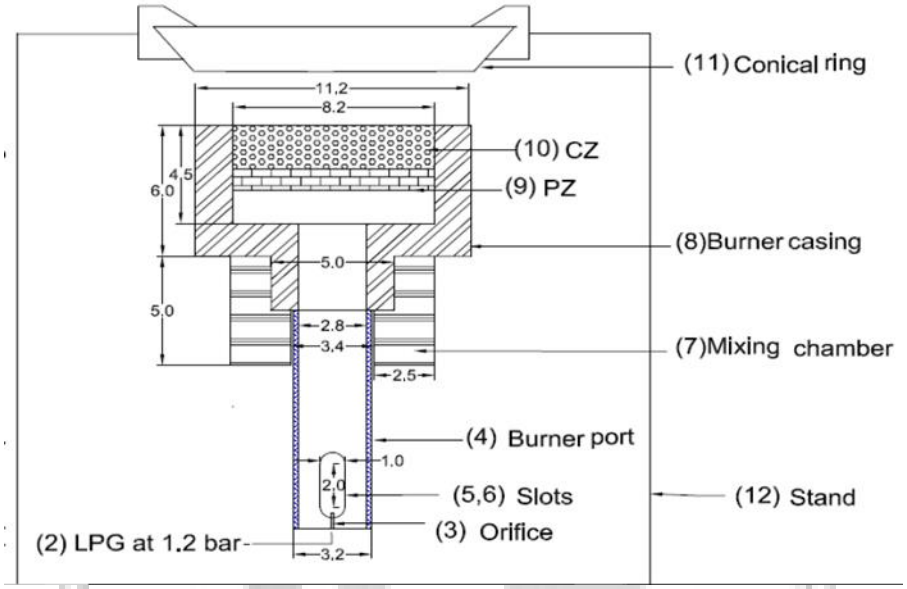

Fig. 2.7: Schematic diagram of self-aspirated domestic LPG PRB stove

Meanwhile, Panigrahy et al. (2016) analysed the combustion in a domestic LPG cook-stove with PRB. The effect of scattering albedo, Φ, PZ thickness and thermal conductivity were observed on the emissions from burners of different sizes. For Φ of 0.4, all burners emitted CO less than 5 ppm. CO emissions from the burner, having PZ thickness 12 mm and CZ thickness 30 mm, were found to be below WHO limits when the scattering albedo was decreased by 50 % and the thermal conductivity was increased by 10 %. The PZ thickness has little effect on the emission of CO.

Muthukumar et al. (2020) and Muthukumar and Kaushik (2020) developed self-aspirated PRBs for medium scale and domestic cooking applications as an improvement over self-aspirated PRB developed by Mishra and Muthukumar (2018). The domestic cookstove (Muthukumar and Kaushik, 2020) operates with available domestic LPG regulator and eliminates the need of pressurized fuel supply and provides high thermal efficiency. The self-aspirated medium scale cookstove (Muthukumar et al., 2020) offers a simple design for commercial cooking (5-7 kW) applications and operates with the help of an unreduced pressure regulator commonly available in the market.

2.5 Numerical Modelling

Numerical modelling assists in predicting the behavior of systems and reduces the usage of resources and effort incurred in experimentation. The numerical methodology influences

the prediction of the results and thus the selection of an accurate model is essential. Some significant research works on numerical modeling of PMC are presented below.

Bouma et al. (1995) carried out numerical simulations on flame stabilization of a lean methane-air premixed flame in a ceramic foam using one dimensional model. They took into account the heat transfers between the flame and the burner surface and the burner radiative properties. They concluded that, to accurately predict the presence of CO in the post-flame zone, modelling of gas radiation is required.

Zhou and Pereira (1998) compared four combustion models to predict methane and air combustion in a PM. The combustion models were full mechanism (FM, 49 species and 227 elemental reactions), skeletal mechanism (SM, 26 species and 77 elemental reactions), 4-step reduced mechanism (4RM, 9 species) and 1-step global mechanism (1GM). The 4-step reduced mechanism was prescribed as the most suitable model for such type of simulation processes, as it provided computational stability and was less costly. Shi et al. (2011) investigated the methane combustion considering 2-D structure in a single layer PRB. Implementing a one-temperature energy model, they investigated the effect of power input and Φ on emissions and energy extraction efficiency. Nimvari et al. (2013) compared two turbulence models for their suitability in predicting the combustion behaviour in a PM. The accuracy of the turbulence model prescribed by Pedras and de Lemos (2001) was reported to be higher than that suggested by Nakayama and Kuwahara (1999). Reis et al. (2014) conducted numerical modelling using standard, RNG, and Realizable k-ε models and Reynolds Stress Model (RSM) method to design an orifice for an industrial burner. Out of these models, the Realizable k-ε model has been found to be most appropriate as its saves time and memory. The numerical tools assisted in redesigning a gas burner orifice, in case of change in composition of the gas and determining the correct pressure for burner operation.

Wasinarom et al. (2019) developed a 1-D numerical model to investigate LPG combustion and validated the results with experiments. The reaction kinetics were calculated using the Arrhenius law, and the energy transfer was modelled using two-temperature model. The effects of extinction coefficient and convective heat transfer effective area on the temperature profiles were found to be stronger with increase in power input.

Hoda et al. (2019) performed numerical simulation on a 3-D rectangular single layer PM to study methane combustion and heat transfer. A five-step reaction was employed to depict the combustion mechanism. The temperature difference between the solid and gas was found to decrease with increase in the average velocity due to increase in the porosity of the packed bed. The optical thickness of the PM was found to significantly influence the thermal behavior of PRB.

Liu et al. (2019) numerically studied propane-air combustion in a 2-D PRB. Two-step mechanism, k-ϵ turbulence model and two-temperature model were employed to model the combustion, turbulence, and energy transfer, respectively. The predicted velocity of the filtration flame was found to be lower than that obtained from experiments. However, in case of flame structure and axial temperature, the results of simulations agreed well with the corresponding experimental results.

2.6 Corollaries Derived from Literature and Literature Closure

From the literature review on experimental studies, some important takeaways are:

i. Heat recirculation is responsible for the unique characteristics of flames in PM.
ii. The heat feedback from combustion by PM makes it possible to sustain combustion for a wide range of power inputs (turn-down ratio) and Φ.
iii. The performance of a PRB is greatly influenced by the geometry, properties, and operating parameters.
iv. Improved performance of PRBs compared to their conventional counterparts put it on a high pedestal to develop clean, efficient and fuel-saving burners.
v. The air entrainment in naturally aspirated burners depend on the geometrical dimensions of the educator components like jet location, shape of the jet, orifice diameter etc.

From the literature review on numerical studies, important corollaries are:

i. Results predicted by numerical tools are found to agree well with experimental results.
ii. The system of complex PRB geometry and combustion mechanisms were simplified using 1-D or 2-D planar geometries and reduced reaction mechanisms, respectively.

iii. The energy transfer in the PM was modelled either by considering one-temperature or two-temperature models.

iv. Similarly, the flow phenomenon inside the PM was represented either by considering laminar or turbulent flow, and in the case of turbulent flow, different turbulence models were employed.

Apart from the above generalized observations, a brief summary on the performance of the PRBs has been presented in Table 2.1.

Table 2.1: Brief description of some notable published works on PRB

Authors (year)	Details of research and burner description	Findings
Jugjai and Rungsimuntuchart (2002)	Conventional domestic burner combined with Porous Radiant Recirculated burner PRRB (CB) PPRB combined with swirl flow PRRB(SB)	12% and 30% higher thermal efficiency (η_t) obtained with PRRB(CB) and PRRB(SB) respectively compared to CB
Abdul Mujeebu et al. (2011)	Matrix stabilised burner (MSB)– porcelain foam and Alumina spheres Submerged burner (SSB)– Alumina (Al_2O_3) foams of porosity 26 ppcm and 8 ppcm, diameter – 85 mm Thermal load – 0.62 kW	Up to 12% and 24% higher η_t obtained with MSB and SSB respectively compared to Conventional Burner (CB)
Yoksenakul and Jugjai (2011)	Self-aspirated PRB formed by a conical shaped packed-bed of alumina spheres with an average diameter 150 mm for 23-61 kW	Up to ~94% reduction in CO emissions and 40% increase in NO_x emissions compared to CB at 54 kW
Pantangi et al. (2011)	Developed domestic stoves with two-layer PRB with SiC and Alumina balls as Combustion Zone (CZ) and Preheating Zone (PZ) and compared with CB	Up to 3% increase in η_t with respect to CB Maximum reduction of ~93% and ~92% in CO and NO_x emissions compared to CB
Muthukumar and Shyamkumar (2013)	Developed two layer PRB with porosities (80 %, 85% and 90%) of CZ. Diameter of CZ – 90 mm	~95% and 100% reduction in CO and NO_x emissions and 10% increase in η_t with respect to CB (domestic) for CZ porosity of 90%.
Wu et al. (2014)	Development of a flat flame burner of 1 kW using a porous matrix	Higher turn-down ratio, operating range and lower

	stabilizer of 50 mm diameter. Conducted analytical and numerical study of heat transfer.	emissions as compared to conventional Bunsen burner flames
Mishra et al. (2015)	Development of (5-10 kW) PRB of diameter 120 mm with SiC as CZ and Alumina Balls as PZ	Up to 29 % improvement in η_t and up to 92% reduction in CO and NO_x emissions compared to CB
Mishra and Muthukumar (2018)	Developed self-aspirated PRB for 1-3 kW with burner diameter 80 mm.	Up to 15% improvement in η_t and 86% and 96% reduction in CO and NO_x emissions compared to CB
Chaelek et al. (2019)	Annular Porous Radiant Burner with Porous Radiant Recirculated Heater for 21-44 kW. Diameter: 174 mm	Up to 40% improvement in η_t. Increased emissions of CO by 1900 ppm and reduction in NO_x emissions compared to CB
Muthukumar et al. (2020)	Medium scale PRB for 5 – 7 kW with burner diameter 120 mm	Maximum η_t.: 65% at 5 kW
Muthukumar and Kaushik (2020)	Domestic PRB cookstove of burner diameter 80 mm	Maximum η_t. 80% at 1 kW

Keen observations from the literature revealed that PRBs with smaller diameters (60 to 80 mm) operating in the power range of 1-3 kW generated higher thermal efficiency (72-80%) whereas PRBs of larger diameter (120 – 160 mm) and power range of 5-10 kW yields only 45 - 65%. However, no research work had been carried out to mitigate the large difference in the efficiencies of domestic and medium scale LPG PRB cook-stove. Moreover, no work has been carried out on the numerical simulation to optimize domestic and medium scale LPG PRB stove.

2.7 Objectives of the Thesis Work

From the generalized and critical conclusions on the literature, a hypothesis was developed that the thermal efficiency of a PRB can be improved by keeping the burner size small. To address the above mentioned research gaps and test the validity of the hypothesis, the objectives for the present research work are as follows: -

1. To demonstrate the impact of clustering smaller-sized PRBs on the thermal performance of the burner in comparison with a single-PRB

a. To perform experimental investigations with forced draft Clustered Porous Radiant Burner (CPRB) and evaluate the thermal performance at a power input of 12.5 kW.
b. To determine the power modulation of the CPRB and thermal performance

2. To develop a self-aspirated CPRB applicable for medium scale cooking
   a. To study the thermal performance of the self-aspirated CPRB
   b. To determine the superiority of the CPRB over a Conventional Burner (CB) in terms of eco-friendliness with the help of Life Cycle Assessment
3. To perform numerical investigations on the air entrainment and combustion parameters of a self-aspirated Porous Radiant Burner

2.8 Summary

An elaborate review on literature concerning developments of Porous Radiant Burners (PRB) has been presented. The parameters influencing the stability and performance of a PRB such as equivalence ratio, power input, porosity, heat recirculation and burner geometry were studied. Additionally, studies on the air entrainment in self-aspirated systems were carried out in order to imbibe knowledge for designing a self-aspirated PRB. Numerical modelling techniques and their part in accurately predicting various performance parameters like flame speed, emissions, temperature etc. were explored. Deriving corollaries from the literature review, the literature gap was identified and the objectives for the present thesis work were outlined.

Chapter 3

First Phase Investigations – Development of a Forced Draft Clustered Porous Radiant Burner

Preface

In order to validate the hypothesis developed, as described in the previous chapter, a Clustered Porous Radiant Burner (CPRB) was developed, and its performance was compared with a single Porous Radiant Burner (PRB) operating at the same power input. The operation was on forced draft mode, where the pressurized air was used for combustion. The characterization was conducted in terms of radial temperature distribution, thermal efficiency, and emissions. The novel method of clustering PRB was proven to generate higher thermal efficiency and reduced CO emissions as compared to a single-PRB.

The CPRB was further evaluated for its capability of being suitable for various applications requiring at different power inputs. The turn-down ratio was determined and the performance over the stable range of power inputs was determined. Additionally, design improvement of a forced draft CPRB has been presented.

3.1 Forced Draft Clustered Porous Radiant Burner as an improvement over a single Porous Radiant Burner

The main objective of the present study is to ascertain the correctness of the hypothesis deduced from the literature review that improved performance can be obtained by maintaining a smaller size of the Porous Radiant Burner (PRB). The medium-scale Liquefied Petroleum Gas (LPG) operated PRB cookstove developed by Mishra (2015) was chosen for comparison. The medium-scale PRB is a double-layered PRB with a burner diameter of 120 mm. Upon decreasing the diameter of the burner to 110 mm, incidences of

flame movement outside the top surface of the burner were reported, and therefore, the operation was considered unstable. Therefore, the stable operation of the PRB while maintaining the small size was attained with the help of clustering smaller PRBs such that the total top surface area of the PRB remained unchanged. The selection of the design mode of clustering burners was based on the shape of the burner and the pan. The burners are circular in shape and so is the base of the pan. Since the shape of the burner is circular, clustering two burners would have led to a longitudinal construction. Therefore, a cluster of three burners was chosen so that the symmetry of the system i.e. burner and pan is maintained. The preceding chapter on the literature on burner development for cookstoves implied that the burner performance depends upon combustion and heat transfer features, which are in turn influenced by the burner dimensions, materials and fluid properties, and operating parameters. A major contribution is obtained from the combustion air supply, which is obtained through natural entrainment or through external pressurization. The provision of correct amount of air for stable and efficient combustion through natural entrainment is significantly dependent on the mixing tube geometry. Therefore, for the purpose of focusing only on the advantage of clustering smaller PRBs over a large single-PRB and a subsequent study essentially on Clustered Porous Radiant Burner (CPRB) behavior, initial developments were carried out for forced draft operation.

3.1.1 Construction and operation of a Forced Draft Clustered Porous Radiant Burner

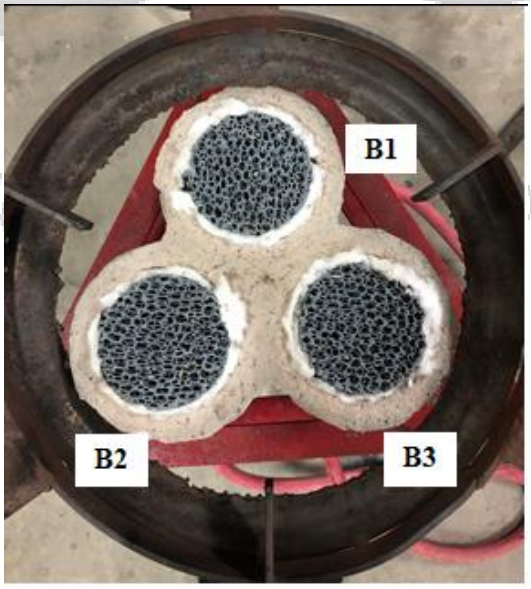

Fig. 3.1: Photographic view of CPRB

The CPRB is a cluster of three individual double-layer PRBs, as shown in Fig. 3.1. The schematic of one individual burner of the CPRB is shown in Fig. 3.2. The air and fuel are introduced in the burner through a Mixing Tube (MT) through separate streams, where it travels towards the Porous Matrices (PMs). The air and fuel then expand in the Mixing Chamber (MC) and form an air-fuel mixture before being preheated in the Preheating Zone (PZ) and combusted in the Combustion Zone (CZ).

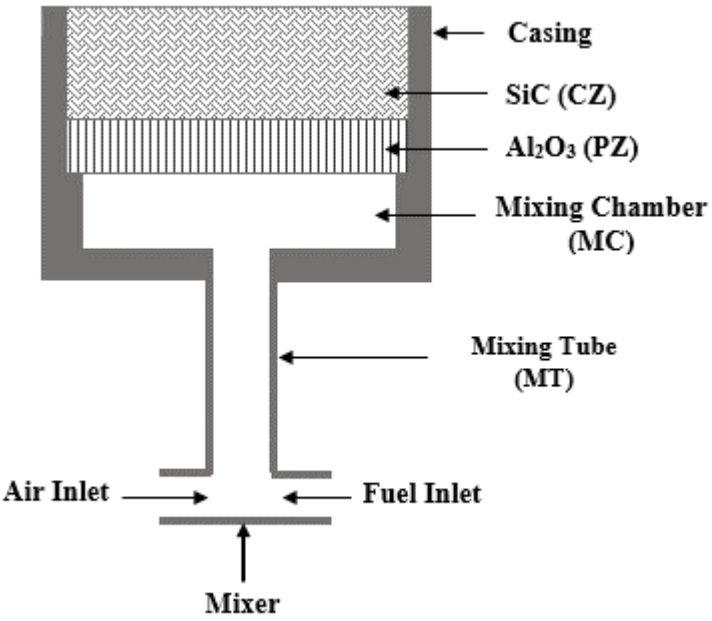

Fig. 3.2: Schematic of the internal structure of an individual burner of CPRB

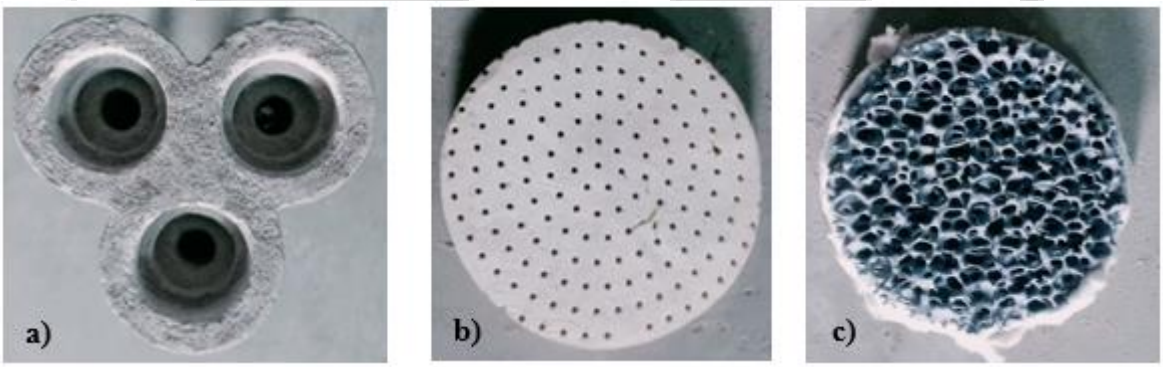

Fig. 3.3: Components for CPRB: a) Refractory cement casing, b) Alumina filter and c) SiC reticulated foam

The upstream or the bottom layer of PM acting as PZ is constituted by an Alumina (Al_2O_3) filter (Fig. 3.3 (b)) while downstream or the top PM layer, serving as the CZ is formed by Silicon Carbide (SiC) reticulated foam (Fig. 3.3 (c)). The PMs are enclosed in a casing (Fig. 3.3 (a)) made up of refractory cement that can withstand high temperatures and prevent

heat loss to the surroundings. The individual burners of the CPRB are named B1, B2, and B3, as shown in Fig. 3.1. The dimensions of the CZ, PZ, and MC are listed in Table 3.1, and the thermo-physical properties of the materials constituting the PM are summarized in Table 3.2. The burner diameter of 70 mm is chosen because the sum total of the top surface areas of the three individual burners of the CPRB (115 cm^2) is equivalent to the top surface of the single PRB (113 cm^2) developed by Mishra (2015).

Table 3.1: Specifications of CPRB

	Burner diameter (D) (mm)	**Thickness (mm)**	**Porosity**
Combustion Zone	70	20	90%
Preheating Zone	70	10	7%
Mixing Chamber	65	20	-

Table 3.2: Properties of materials (Mishra, 2015; "NIST Property Data Summary - NIST Ceramics Data Portal," n.d.)

Properties	**Alumina Ceramic (Al_2O_3)**	**Silicon Carbide Ceramic (SiC)**
Thermal conductivity (W/mK)	33	114
Emissivity	0.28	0.9
Density (kg/m^3)	3984	3160
Specific heat (J/kgK)	755	715

Description of the set-up

The forced draft operation of the CPRB required the provision of regulated quantities of fuel and air supply to each individual burner to maintain the desired Equivalence Ratio (Φ). An experimental set-up was therefore prepared in order to support the CPRB operation. The process flow diagram of the experimental set-up of the CPRB is illustrated in Fig. 3.4. The experimental set-up enables the supply and distribution of equal quantities of fuel and air to the individual burners of the CPRB. LPG (Composition: 60% Butane and 40% Propane; Lower Calorific Value (LCV): 45605.6 kJ/kg) was obtained from a 19 kg commercial cylinder (Indane) and pressurised air was supplied with the help of an air compressor. The power input was varied by controlling the fuel mass flow rate ($\dot{m}_f$) and was calculated using Eq. (3.1). At a certain power input, the Φ was varied by fixing the

$\dot{m}_f$ while varying the air mass flow rate ($\dot{m}_a$). Eq. (3.2) is used for calculating Φ corresponding to the given $\dot{m}_f$ and $\dot{m}_a$.

$$\dot{m}_f = \text{Power input/LCV} \tag{3.1}$$

$$\Phi = \frac{(\dot{m}_a/\dot{m}_f)_{stiochiometric}}{(\dot{m}_a/\dot{m}_f)_{actual}} = 15.45 \times \left(\frac{\dot{m}_f}{\dot{m}_a}\right)_{actual} \tag{3.2}$$

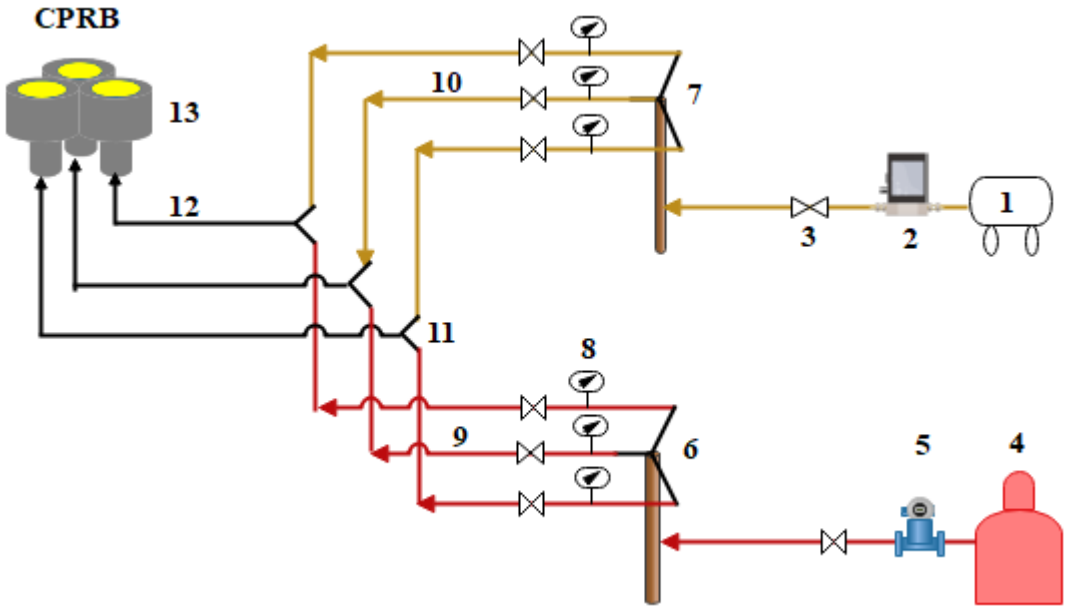

1. Compressor, 2. Mass flow meter for air, 3. Flow control valve, 4. LPG cylinder, 5. Mass flow meter for fuel, 6. Fuel header, 7. Air header, 8. Pressure gauge, 9. Fuel-line, 10. Air-line, 11. Air-fuel mixer, 12. Air-fuel mixture line and 13. CPRB

Fig. 3.4: Process flow diagram of CPRB set-up

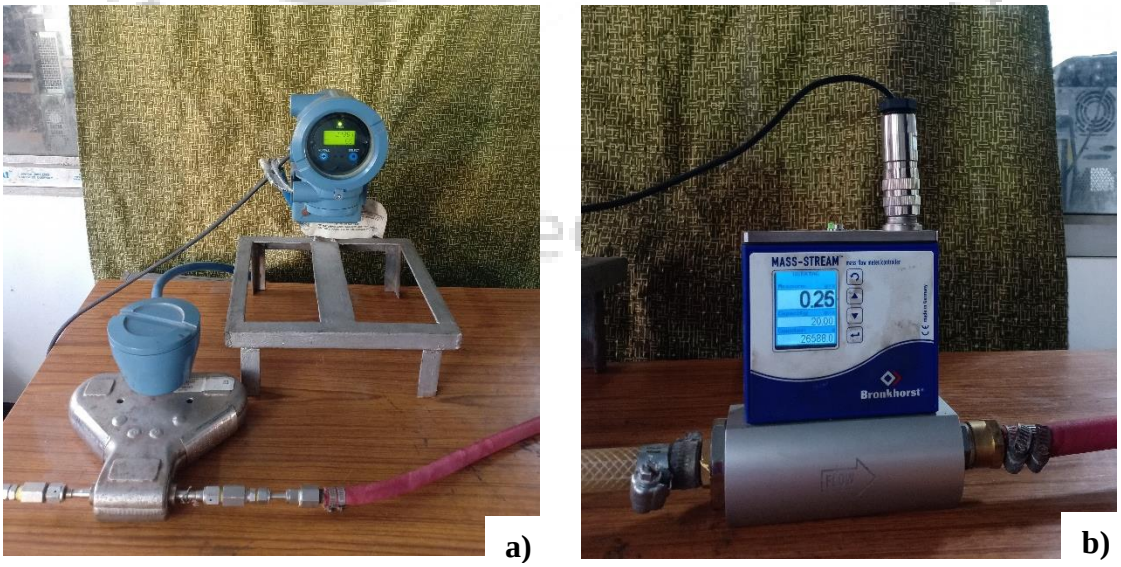

Fig. 3.5: Mass flow meter a) for fuel and b) for air

The valves, placed in each line, help to control the rate of the gas flow. The mass flow rates of both fuel and air are measured by mass flow meters (Fig. 3.5 (a) and (b)) installed in the respective fuel and air lines. The fuel and air are collected in their respective fuel and air headers. The headers, as shown in Fig. 3.6, are equal in shape and size and are so constructed that they equally distribute the gas amongst the lines placed at equal distances and height along the outer periphery. Pressure gauges are connected in each air and fuel line of the headers to indicate and ensure the equal distribution of the gases. The air and fuel flowing through their respective lines are mixed in the air-fuel mixers and the resultant mixture is supplied to the individual burners of the CPRB.

Fig. 3.6: Header for fuel or air

3.1.2 Performance parameters

The CPRB's temperature profiles, thermal efficiency (η_t) and emissions were assessed to find out the burner's characteristics. The experiments were conducted for a fixed gas (fuel) flow rate of 1 kg/h that corresponded to a power input of 12.5 kW. The performance parameters and their measurement techniques are explained in the following sub-sections.

Turn-down ratio

The ratio of the maximum to the minimum power input is called the turn-down ratio of a burner. It determines the capability of the burner to work stably over a range of power inputs.

Stability limits

Stable operation ensures reliability and smooth functioning of a burner. Flashback, flame-quenching and blow-off are the three main phenomena that determine the stability limits. The CPRB was considered to be stable when the individual burners performed stably and similarly. The CPRB was operated on submerged flame mode, in which the presence of a sustained flame beyond the CZ towards the downstream was regarded as blow-off. The extinguishing of the flame in any one of the burners was considered as flame-quenching. While the occurrences of blow-off and flame-quenching were monitored through visual inspection, the incidences of flashback (movement of the flame upstream of the PZ) were monitored through temperature measurement below the PZ, as shown in Fig. 3.7. The temperatures at the positions 5'', 5', and 5, as shown in Fig. 3.7, represent the PZ inlet temperature, the CZ and PZ interface temperature, and the temperature at the outlet, respectively. As the establishment of burner stability is essential before the measurement of η_t and emissions, the temperature measurements were carried out without any load.

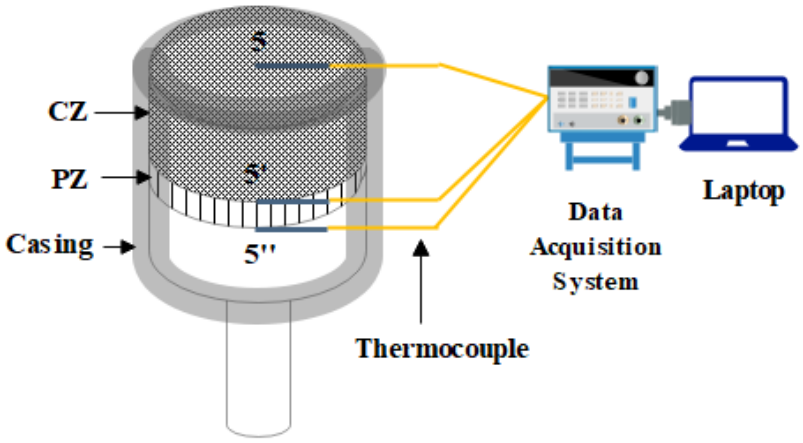

Fig. 3.7: Thermocouple positions for axial temperature measurement

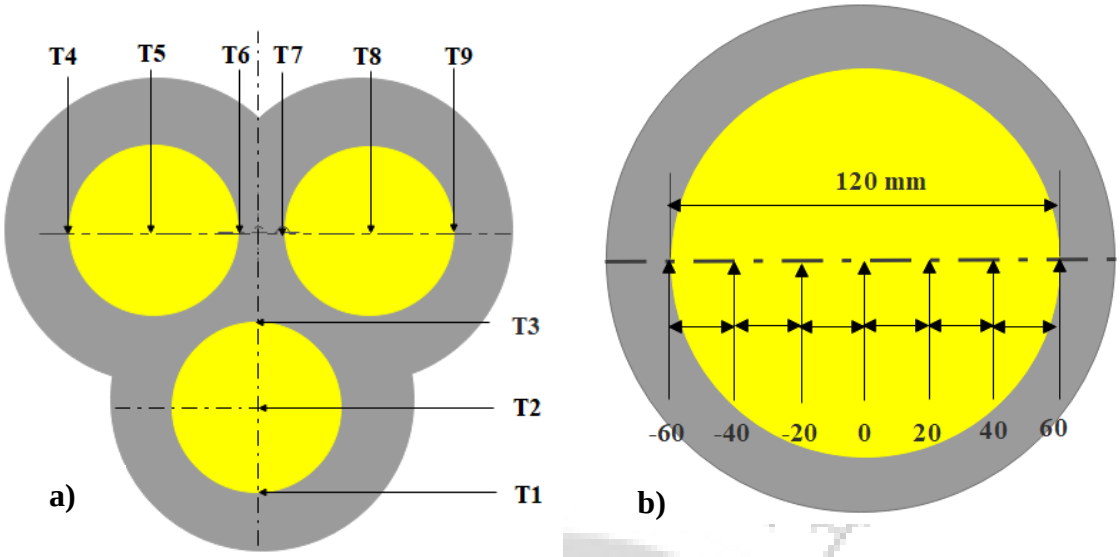

Fig. 3.8: Position of thermocouples for surface temperature measurement in a) CPRB and b) single-PRB (Mishra, 2015)

The stable combustion of a CPRB was also governed by the condition that the individual burners yielded similar heat output, which was checked with the help of radial temperature mapping at the top surface, as shown in Fig. 3.8 (a). When the variation of the temperature at the corresponding thermocouple positions remained within ±10°C for a minimum duration of 30 min (Gao et al., 2011), the burners were considered to be yielding similar heat output. All temperature measurements were carried out with the help of K-type thermocouples connected to a data acquisition system (Agilent make). After obtaining the stability limits, the CPRB was assessed for the other performance parameters viz. η_t, radiation efficiency (η_r) and emissions. The procedures for measuring these parameters are described in the following sub-sections.

Thermal efficiency

The thermal efficiency (η_t), defined as the capability of the CPRB to deliver the heat of combustion effectively to the load, was evaluated by performing Water Boiling Test (WBT) as per the protocols laid down in IS 14612:1999 (Bureau of Indian Standards, 1999) by the Bureau of Indian Standards (BIS). Fig. 3.9 illustrates the schematic of the arrangement for estimating the η_t.

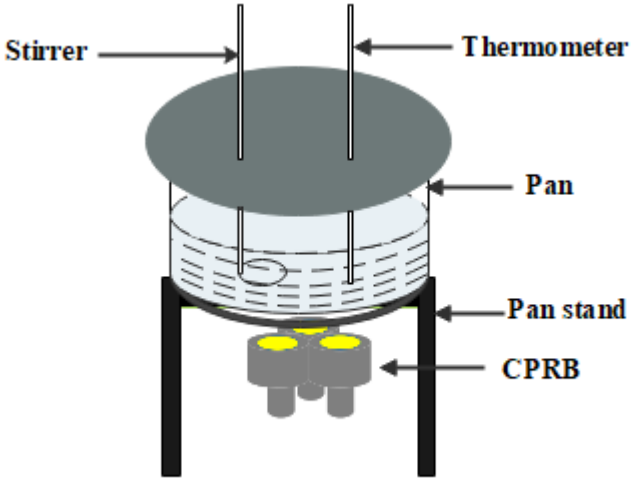

Fig. 3.9: Schematic of thermal efficiency test

A 2.99 kg Aluminium pan was used to heat 16.5 kg of water from the initial temperature of 30°C to the final temperature of 90°C. Eq. (3.3) was used to calculate the η_t(%).

$$\eta_t(\%) = \frac{(m_w c_w + m_p c_p) \times \Delta T}{m_f \times LCV} \times 100 \quad (3.3)$$

The notations 'm', 'c' and 'T' denote the mass, specific heat capacity and temperature, respectively, while the subscripts 'w', 'p' and 'f' denote water, pan and fuel respectively. The comparison of the η_t has been expressed in terms of percentage improvement (η_{imp}), which is defined as the ratio of the difference in the thermal efficiencies of the CPRB and respective burner being compared (i.e. PRB or CB) to the thermal efficiency of the burner being compared. The expression for the η_{imp} is specified in Eq. (3.4).

$$\eta_{imp}(\%) = \frac{(\eta_{t,CPRB} - \eta_{t,PRB/CB})}{\eta_{t,PRB/CB}} \times 100 \quad (3.4)$$

Radiation efficiency

The radiation efficiency (η_r) is a vital performance parameter that determines the capability of a burner to transfer the radiant heat output to the load effectively. In the case of CPRB, the η_r (%) is determined using Eq. (3.5).

$$\eta_r(\%) = \frac{3\varepsilon\sigma(T_{Surf}^4 - T_{Surr}^4)A_{ts}}{\dot{m}_f \times LCV} \times 100 \quad (3.5)$$

The notations 'ε', 'σ' and 'A_{ts}' denote the emissivity, Stefan-Boltzmann constant (5.67×10^{-8} W/m^{2}K^4) and the top surface area of the individual burners, respectively. The notations

T_{Surf} and T_{Surr} denote the top surface temperature and the surrounding temperature, respectively. The values for the T_{Surf} were obtained after averaging the temperature at the radial locations of the top surface, while T_{Surr} was taken as 27°C.

Emissions

Pollutants like CO and NO_x are components of greenhouse gases and are harmful to the environment (Gal et al., 2017). The CPRB was examined for its clean burning characteristics with the help of emission measurements of harmful pollutants like CO, NO_x and hydrocarbons (C_xH_y). The emission measurements were carried out according to the standards as prescribed in IS 14612. To measure the emissions, the flue gases were confined and collected by a hood. The probe of the Flue Gas Analyser (FGA) (Fig. 3.10) was inserted in the sampling tube of the hood. The emissions were corrected to 3% reference amount of oxygen and were measured on a dry basis. The measured values were recorded on a laptop that was connected to the FGA. The schematic of the arrangement to measure the pollutant emissions is shown in Fig. 3.11. The clean burning capability of the CPRB is expressed in terms of reduction in the emission (CO or NO_x), which is defined as the ratio of the difference in emission of the CPRB and the respective burner being compared (i.e., PRB or CB) to the emission of the burner being compared. The equation used to calculate the percentage reduction in emissions is given below.

$$\text{Emission}_{\text{reduction}}(\%) = \frac{\left(\text{Emission}_{CPRB} - \text{Emission}_{PRB/CB}\right)}{\text{Emission}_{PRB/CB}} \times 100 \qquad (3.6)$$

Fig. 3.10: Flue Gas Analyser

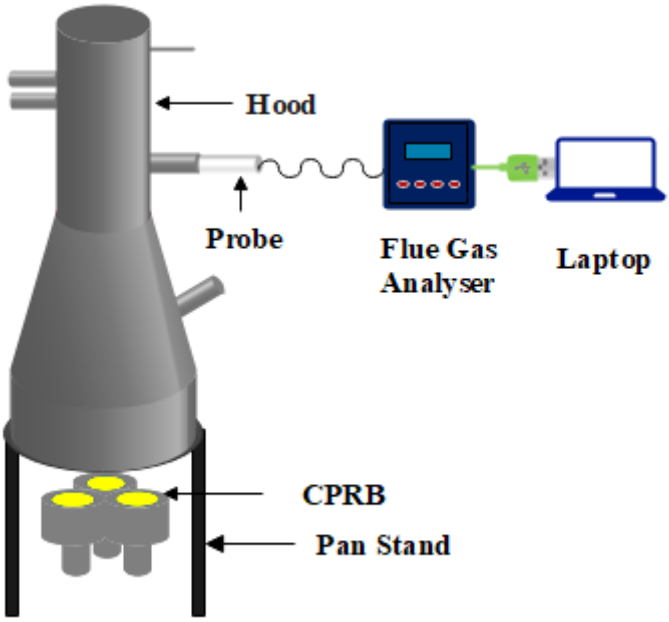

Fig. 3.11: Arrangement to measure pollutant emissions

To check the repeatability, the experiments were performed three times for each performance parameter and the average values are presented.

3.1.3 Uncertainty calculation

Instrumental errors contribute to the deviation of the measured values from the true values. Therefore, the uncertainties of the measured data are ascertained to estimate the experimental errors. The calculated values are Φ, η_t, η_r and the CO/CO_2 ratio (R), which are dependent on the accuracy of the instruments used to measure parameters like temperature, mass flow rates and emissions. The accuracies of the instruments used to measure the parameters are listed in Table 3.3.

Table 3.3: Accuracy of the measuring instruments

Instrument		Accuracy
Mass flow meter for fuel		±0.35% of full scale
Mass flow meter for air		±0.5% of full scale
Thermocouple		±1°C
Thermometer		±0.5°C
Flue Gas Analyser	CO and NO	±5% of reading
	C_xH_y	±10% of reading
	CO_2	±1% of reading

The uncertainties in the measurement of Φ, η_t, η_r and R are obtained from Eqs. (3.7) – (3.10).

$$\delta\Phi = \left(\left(\frac{\partial\Phi}{\partial\dot{m}_a}\right)^2 \times (\delta\dot{m}_a)^2 + \left(\frac{\partial\Phi}{\partial\dot{m}_f}\right)^2 \times (\delta\dot{m}_f)^2\right)^{\frac{1}{2}} \tag{3.7}$$

$$\delta(\eta_r) = \left(\left(\frac{\partial\eta_r}{\partial T_{Surf}}\right)^2 \times (\delta T_{Surf})^2 + \left(\frac{\partial\eta_r}{\partial T_{Surr}}\right)^2 \times (\delta T_{Surr})^2 + \left(\frac{\partial\eta_r}{\partial\dot{m}_f}\right)^2 \times (\delta\dot{m}_f)^2\right)^{\frac{1}{2}} \tag{3.8}$$

$$\delta(\eta_t) = \left(\left(\frac{\partial\eta_t}{\partial m_f}\right)^2 \times (\delta m_f)^2 + \left(\frac{\partial\eta_t}{\partial m_p}\right)^2 \times (\delta m_p)^2 + \left(\frac{\partial\eta_t}{\partial m_w}\right)^2 \times (\delta m_w)^2 + \left(\frac{\partial\eta_t}{\partial\Delta T}\right)^2 \times (\delta\Delta T)^2\right)^{\frac{1}{2}} \tag{3.9}$$

$$\delta(R) = \left(\left(\frac{\partial(R)}{\partial CO} \times \delta(CO)\right)^2 + \left(\frac{\partial(R)}{\partial CO_2} \times \delta(CO_2)\right)^2\right)^{\frac{1}{2}} \tag{3.10}$$

3.2 Performance Comparison of a CPRB with PRB (at 1 kg/h)

3.2.1 Stability and temperature mapping

As described in section 2.3.2, the CPRB was visually monitored for the incidences of blow-off or flame-quenching. Figs. 3.12 (a) and (b) show the unstable burning conditions for the submerged combustion mode of the CPRB.

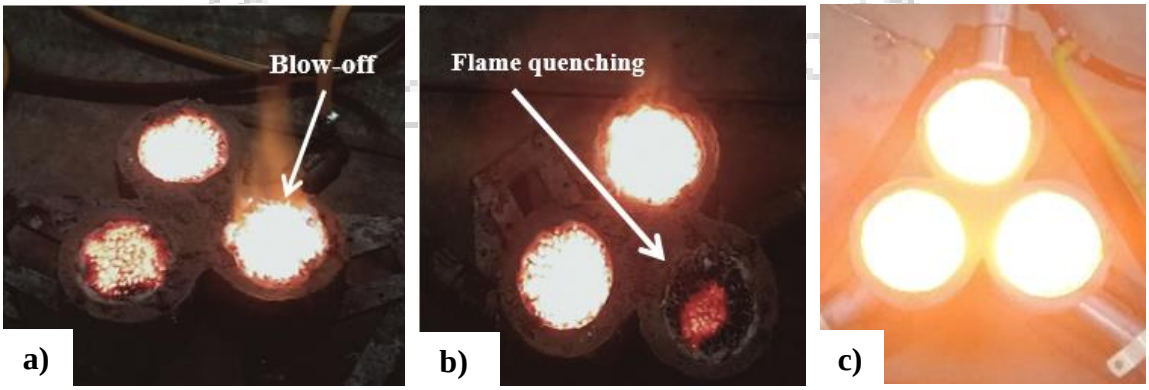

Fig. 3.12: Photographic views of a) Blow-off, b) Flame quenching and c) Stable combustion conditions of a CPRB

Blow-off occurred under two conditions; i) when the excess fuel was passed through any of the burners and ii) when the flame travelled towards the downstream. Flame-quenching resulted from the excess heat loss through the walls due to insufficient insulation. In case of the CPRB, the thermal stability was a result of the equilibrium established amongst the individual burners.

The excess heat gains from any of the burners resulted in unstable combustion in the other burners. The CPRB was thoroughly checked to rule out such discrepancies and the thermal performance was assessed after attaining stable combustion as shown in Fig. 3.12 (c). Experiments on the measurement of η_t and emissions were conducted after similar temperature profiles were obtained for each burner.

The results presented are the average obtained from three sets of experiments conducted for each performance parameter. The CPRB in a stable operation is shown in Fig. 3.13.

Fig. 3.13**:** Photographic view of the CPRB under stable operation

Temperature distribution

The temperature measurements at positions shown in Fig. 3.8 are considered to be an indicator of the overall burner stability. From the visual inspection and the surface temperature measurement, CPRB was found to be stable within the Φ range of 0.7 to 0.85. Beyond Φ of 0.85, stable submerged combustion couldn't be attained, and below Φ of 0.7,

flame quenching was observed. The unstable condition is due to the fact that the air-fuel mixture is unable to generate the required amount of heat for stable combustion.

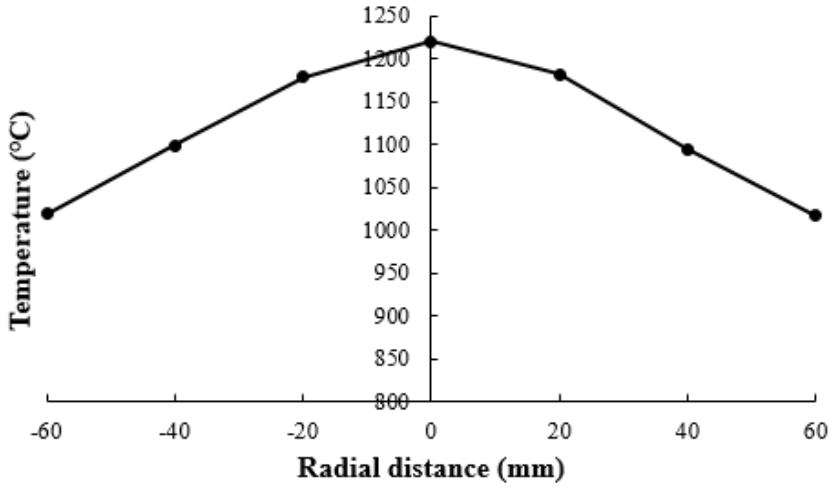

Fig. 3.14: Surface temperature distribution in a single-PRB (Mishra, 2015).

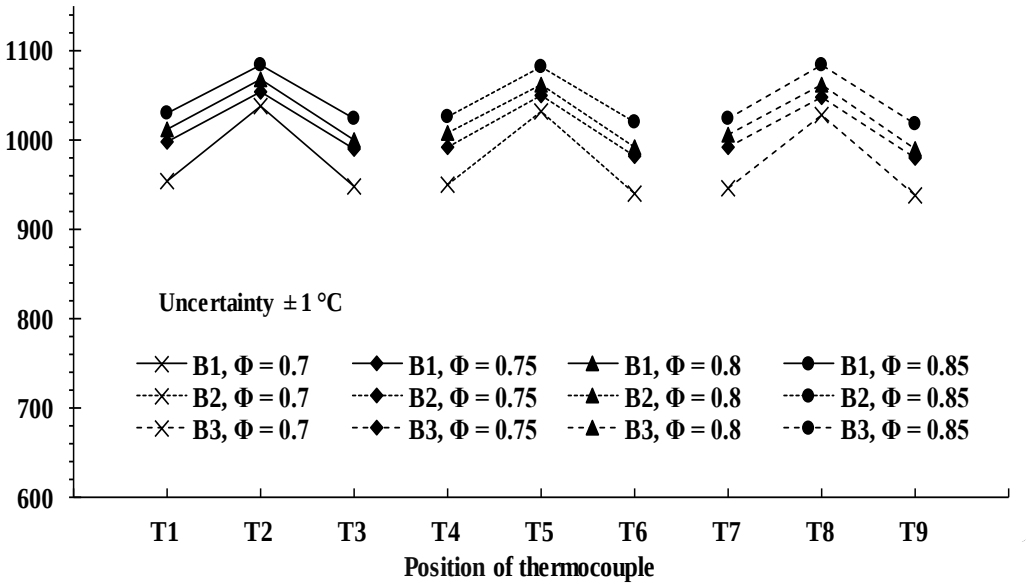

Fig. 3.15: Surface temperature distribution in a CPRB

The plots of the radial surface temperature measurement for single-PRB and CPRB are shown in Fig. 3.14 and Fig. 3.15, respectively. The surface temperature was highest at the centre of each burner and gradually lowered towards the periphery. Similar trends of surface temperature distribution were also obtained by Wu et al. (2014) for a porous metal burner. In the case of the single-PRB, the maximum temperature was found to be approximately 1200°C, as shown in Fig. 3.14, which was higher than the maximum temperature of 1085°C obtained from CPRB.

The peripheral surface area of the single-PRB (diameter 120 mm) is 132 cm^2, whereas the total peripheral surface area of the CPRB (70 mm individual diameter) is 198 cm^2. For a fuel flow rate of 1 kg/h, the mass-flux in the lateral direction of the single-PRB is 75.82 kg/m^2h, whereas, in CPRB, it is 50.55 kg/m^2h. The gases inside a PRB are homogeneously mixed and evenly distributed inside the volume of the combustion zone before the start of combustion. Some amounts of the gaseous mixture also travel towards the periphery to form an even distribution. Therefore, the gaseous mixture has more area to travel in a CPRB, as compared to a single-PRB, before the formation of a homogeneous mixture. Due to the movement of the air-fuel mixture towards the periphery, the mass-flux density in the CPRB is low to generate the same temperature as that of a single-PRB.

The maximum temperature obtained in the CPRB was observed to increase linearly with an increase in the stable Φ, and an analogous relationship of the peak temperature with the Φ was obtained by Baiquan et al. (2014). In the case of the CPRB, the peripheral positions (T3, T6 and T7) near the individual burners exhibited higher temperatures than the outer peripheral positions (T1, T4 and T9) near the surroundings. This temperature variation is due to the fact that the outer peripheral positions are exposed to the surroundings, which is at a lower temperature than the burner. Whereas the other peripheral positions are subjected to heat transfer from other burners. Despite this difference, the surface temperature distribution across the burner surface can be considered to be uniform because the temperature difference between the centre and the peripheral positions are found to be within 50°C (Mishra and Muthukumar, 2018).

3.2.2 Thermal efficiency

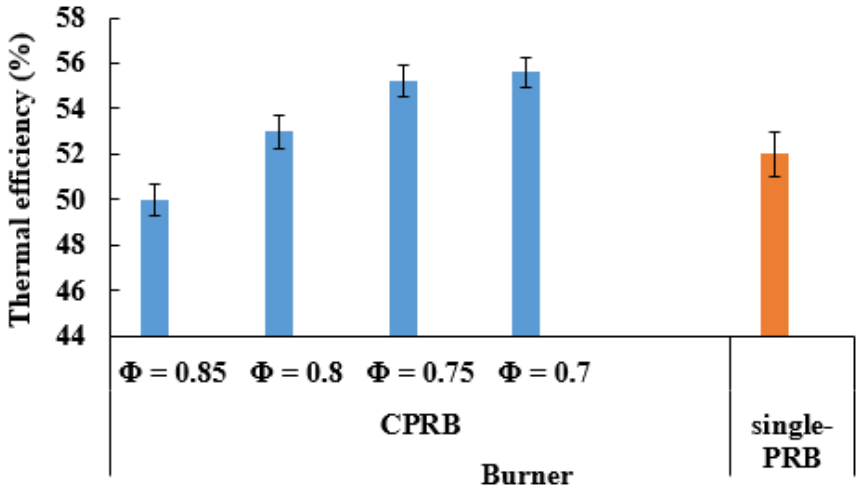

Fig. 3.16: Thermal efficiency of CPRB and comparison with a single-PRB

A comparison of the η_t of CPRB with a single-PRB is shown in Fig. 3.16. With decrease in Φ, the η_t was found to increase. The highest η_t of 55.6% was found at Φ of 0.7, while the lowest η_t of 50% was found at Φ of 0.85. The decrease in η_t with respect to increase in Φ is due to increase in heat losses to the surroundings because of increase in temperature with Φ. Similar results were obtained by Mishra et al. (2015).

The η_t of a single-PRB was reported as 52% (Mishra, 2015), which was 3.6% lower than the CPRB. The higher surface temperature obtained in a single-PRB as compared to the CPRB couldn't result in higher η_t because the high temperature also supported more heat loss to the surroundings through convection.

3.2.3 Emissions

The variation in emissions of CO and NO_x with Φ for the CPRB and their comparison with the emissions from a single-PRB are shown in Fig. 3.17. The emissions of both CO and NO_x were found to decrease with decrease in Φ. The increase in CO emission with Φ is due to the deficiency of excess oxygen for oxidising CO to CO_2. An increase in Φ favours the prompt NO_x formation by increasing the number of carbon atoms per unit volume. Similar trends of increase in CO and NO_x emissions with Φ were also reported by Mishra et al. (2015).

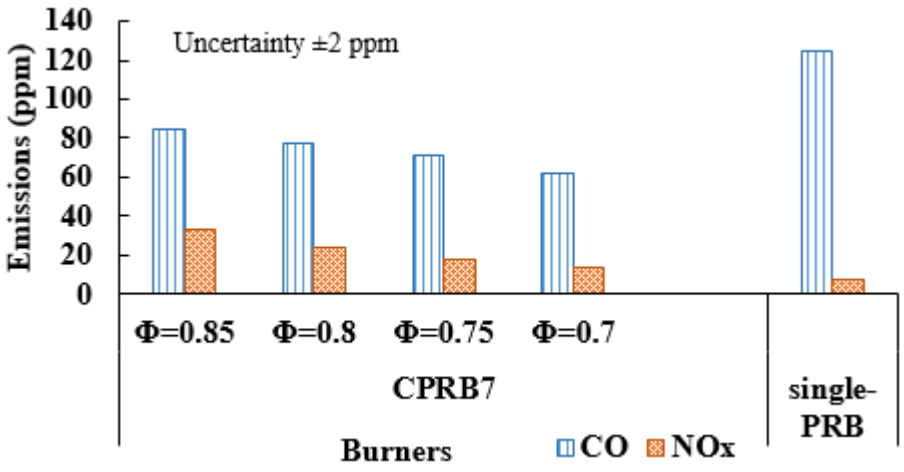

Fig. 3.17: Emissions of CO and NO_x for CPRB and comparison with single-PRB

The highest amount of CO (85 ppm) emitted from CPRB was lesser than the CO emission of 125 ppm produced from the single-PRB (Mishra, 2015). The higher peripheral surface area offered by the CPRB increases the residence time for the species and hence supports the oxidation of CO to CO_2. However, the single-PRB produced NO_x comparable to CPRB.

The formation of thermal NOx is favoured at temperatures more than 1300°C. As the maximum temperatures for both the CPRB and the single-PRB were below 1300°C, therefore it is considered that prompt NO_x is formed, which is favoured by the presence of carbon atoms. At equivalence ratio 0.7, the NO_x emission from a CPRB was found to be comparable with that of the single-PRB as the single PRB is also operated at lean equivalence ratio of 0.7. When the CPRB was operated at equivalence ratios 0.75, 0.8 and 0.85, the NO_x emissions increased because with increase in equivalence ratio, the amount of fuel increased for a given air supply and thus the number of carbon atoms were higher.

3.3 Determination of Turn-down Ratio and Performance in the Stable Power Inputs

3.3.1 Determination of stability range

Fig. 3.18 presents the range of turn-down ratio and Φ, for which the CPRB was found to be stable. The CPRB was observed to be stable at varied ranges of Φ for different power inputs. At lower power inputs, the burner was found to stabilize at lower Φ, which is in accordance with the results obtained by Pantangi et al. (2011).

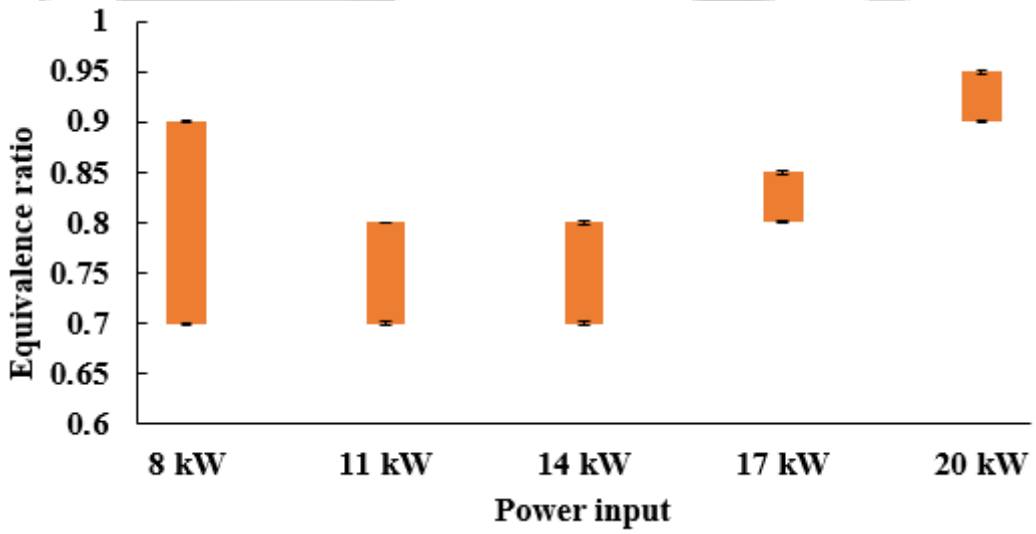

Fig. 3.18: Range of stable equivalence ratios at varied power inputs

The flame-movement, air-fuel mixture velocity and heat loss are important factors that determine the stability of a burner. At higher power inputs, the flame position moves towards the downstream (Pantangi et al., 2011). However, at higher Φ the flame stabilizes closer to the interface between the PC and CC while at lower Φ, the flame moves

downstream (Al-attab et al., 2015). Therefore, when the CPRB was operated at higher power inputs and higher Φ, the flame which previously moved towards the downstream was then shifted towards the upstream thus preventing blow-off. Similarly, when the CPRB is operated at lower power inputs, the stable flammability limits are obtained at leaner Φ because the flame was relocated towards the downstream thus preventing flashback. As the temperature beneath the PC remained below the ignition temperature of LPG (480–500°C) for the stable range of power inputs and Φ, the occurrence of flashback was ruled out. Operation of the CPRB below Φ of 0.7 at a power input of 8 kW resulted in flame quenching due to insufficient heat generation for sustained combustion. The CPRB was hence found to function under stable submerged condition for power inputs of 8 – 20 kW, thus yielding the turn-down ratio of 1:2.5.

From the stability assessment, the power inputs 8, 11 and 14 kW were observed to have a common stable Φ range of 0.7 to 0.8. Therefore, the thermal performance of the CPRB was determined for power inputs of 8, 11 and 14 kW for Φ of 0.7, 0.75 and 0.8. The capability of the CPRB as an improved technology over CBs was estimated through the performance assessment as described in the following sections.

The radial surface temperature distribution at the outlet of the burner provides an estimate of the heat output of the burner. The surface temperature distributions of the individual burners of the CPRB were observed to be similar. However, to maintain the succinctness of the thesis, the temperature distribution of only one of the individual burners have been presented.

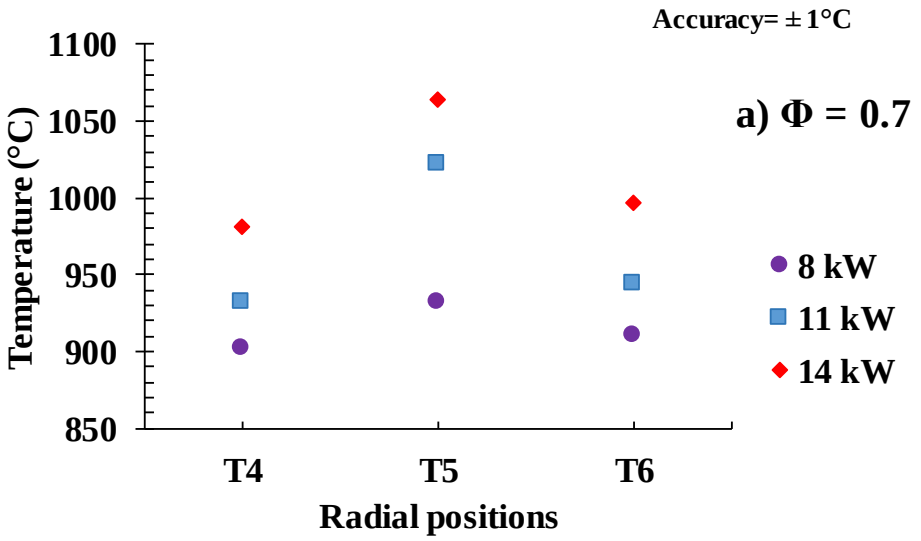

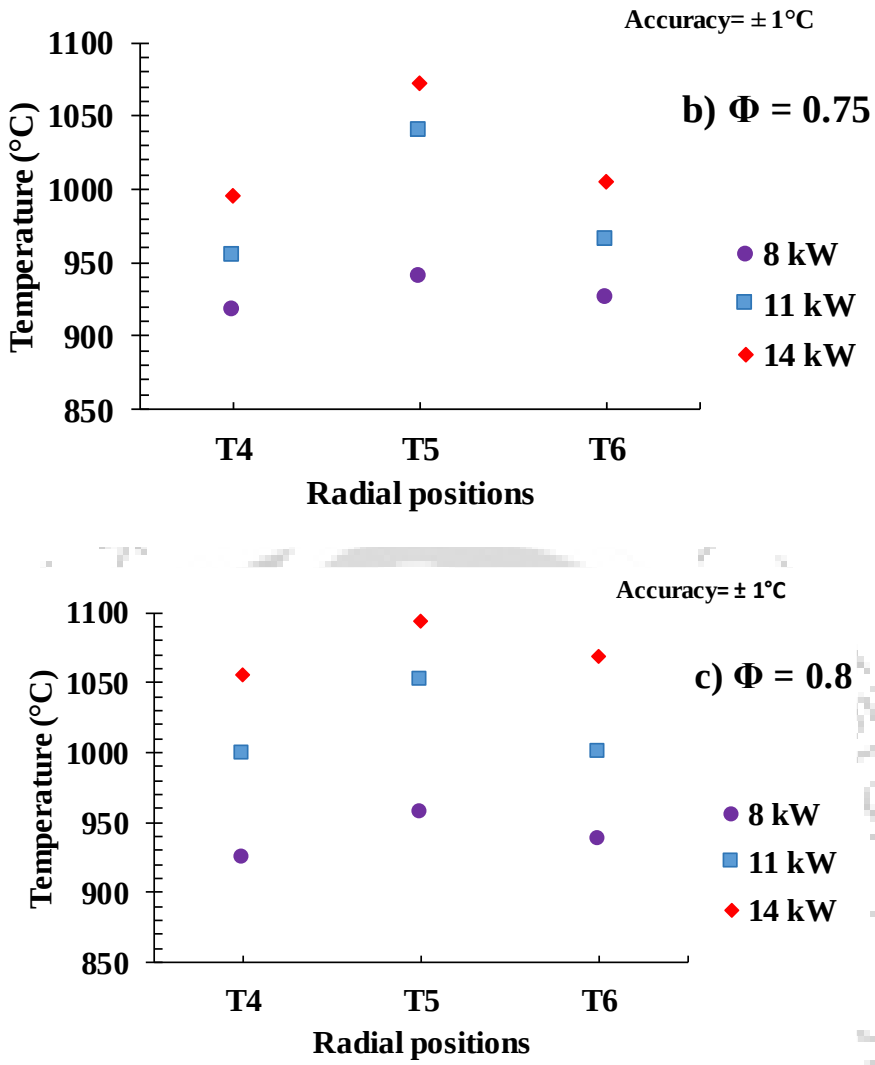

Fig. 3.19: Variation in radial temperature distribution with power input at equivalence ratios a) 0.7, b) 0.75 and c) 0.8

The variation of the radial surface temperature with power input and Φ is shown in Fig. 3.19. Similar to the temperature distribution across the surface of the CPRB as described previously in section 3.2.1, the maximum surface temperature was obtained at the centre of each burner as the heat loss through the wall resulted in a lower temperature than that at the centre. The temperature at T6 was found to be higher than that at T4, as the position T6 was exposed to the heat exchange with the other individual burners while the position T4 was exposed to the surroundings at lower temperatures (Fig. 3.8 (a)). Highest surface temperature of 1094°C was obtained at a power input of 14 kW at Φ of 0.8 while the lowest surface temperature of 932°C was obtained for a power input of 8 kW at Φ of 0.7. This variation can be explained by the movement of the flame location with power input. The

downstream movement enabled the heat to be transferred more towards the outlet, due to which the surface temperature was observed to increase for all the power input considered.

Fig. 3.20 represents the variation in axial temperature with power input for the stable range of Φ. The results reveal that the increase in the power input elevated the temperature at the corresponding positions attained in the CPRB with Φ.

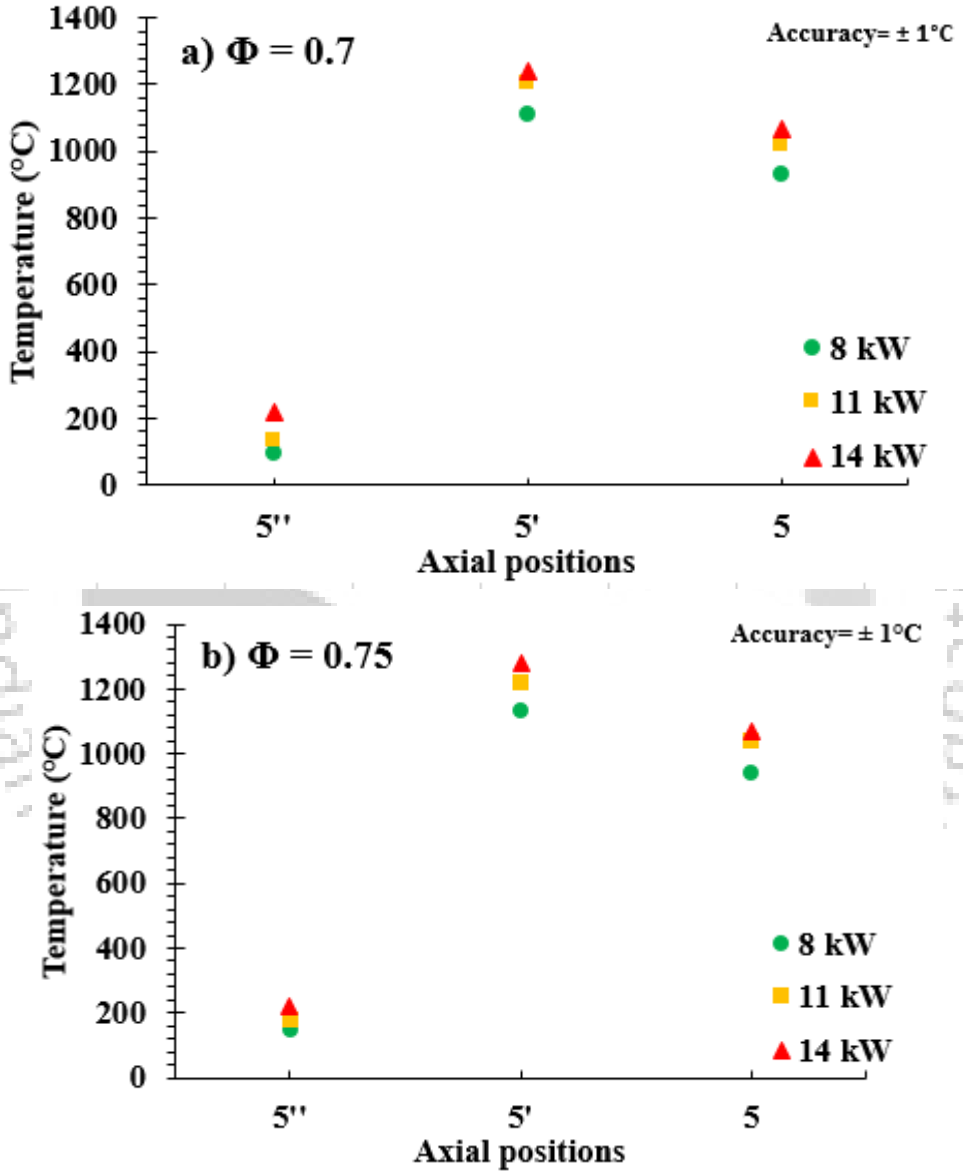

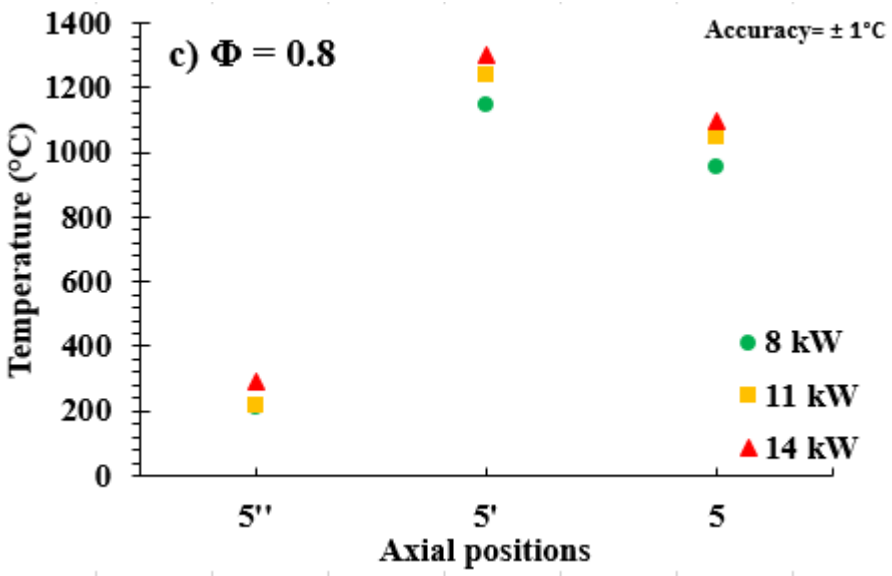

Fig. 3.20: Variation in axial temperature distribution with power input at equivalence ratios a) 0.7, b) 0.75 and c) 0.8

Within the power input range of 8 to 14 kW, the maximum interface temperature was found to vary from 1112 – 1238°C, 1135 – 1279°C and 1151 – 1304°C for Φ of 0.7, 0.75 and 0.8, respectively. The corresponding values of temperature at 5'' varied from 101 – 218°C, 150 –222.6°C and 210 – 290°C, respectively. The increase in the heat of combustion with power input leads to the increase in the heat recirculation towards the upstream and thereby leading to the current temperature trend.

3.3.2 Radiation and thermal efficiencies

Figs. 3.21 and 3.22 present the impacts of power input and Φ on η_r and η_t of a CPRB, respectively. With increase of Φ from 0.7 to 0.8, the η_r increased from 14.6 to 16.4% for a power input of 8 kW. Similarly, at power inputs from 11 to 14 kW, the η_r varied from 12.6 to 14.8% and 11.5 to 13.7%, respectively. Conversely, a rise in the power input decreased the η_r, for a given Φ. The rise of the η_r is favoured by an increase in the top surface temperature attained with increasing Φ. However, with increase in the power input, the rise in the surface temperature is less than the rise in the fuel flow rate, due to which a drop in η_r is noticed.

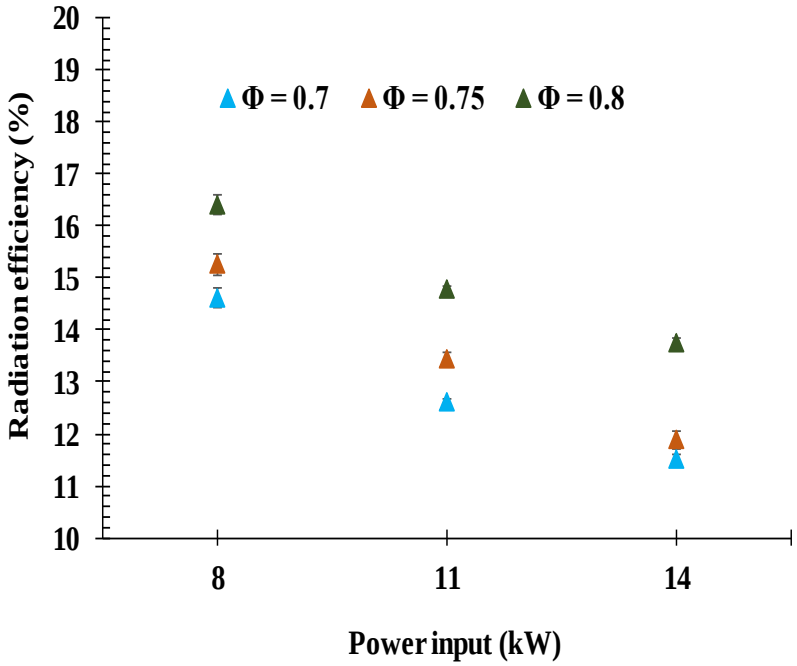

Fig. 3.21: Variation in radiation efficiency with power input and equivalence ratio

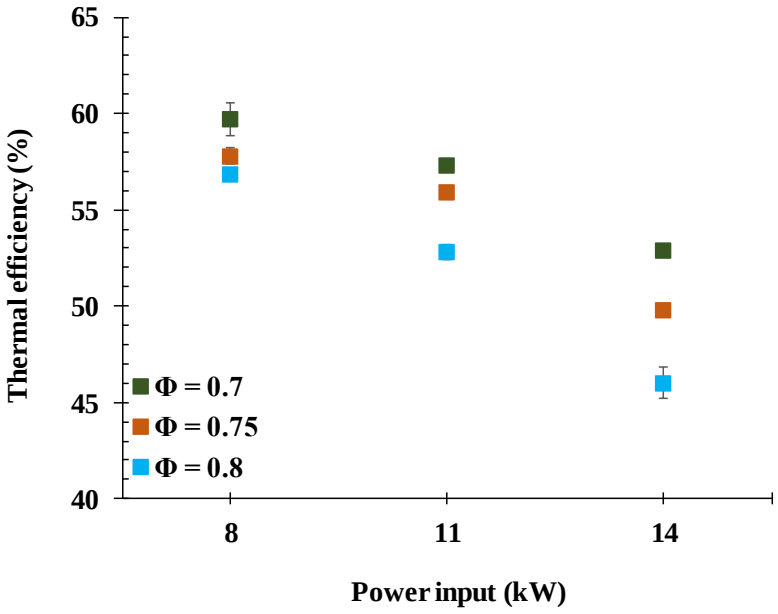

Fig. 3.22: Variation in thermal efficiency with power input and equivalence ratio

For each power input, the highest value of the η_t was obtained at Φ of 0.7. Maximum η_t were obtained as 59.7%, 57.3%, and 52.9% for 8, 11, and 14 kW, respectively. Unlike the variation of η_r, the η_t was found to decrease with an increase in Φ and power input. Higher top surface temperature attained with the increase in Φ and power input leads to the rise in heat losses from the burner, which resulted in lowering of the η_t. Similar trends of η_t were previously reported by Pantangi et al. (2011). When operated at Φ of 0.7, the CPRB yielded

η_t more than 50% and thus, it can be categorized as an energy-efficient Tier 5 cook-stove as per the protocols of the World Health Organisation (WHO) (Clean Cooking Alliance, Voluntary Performance Targets, 2020).

3.3.3 Emission measurement

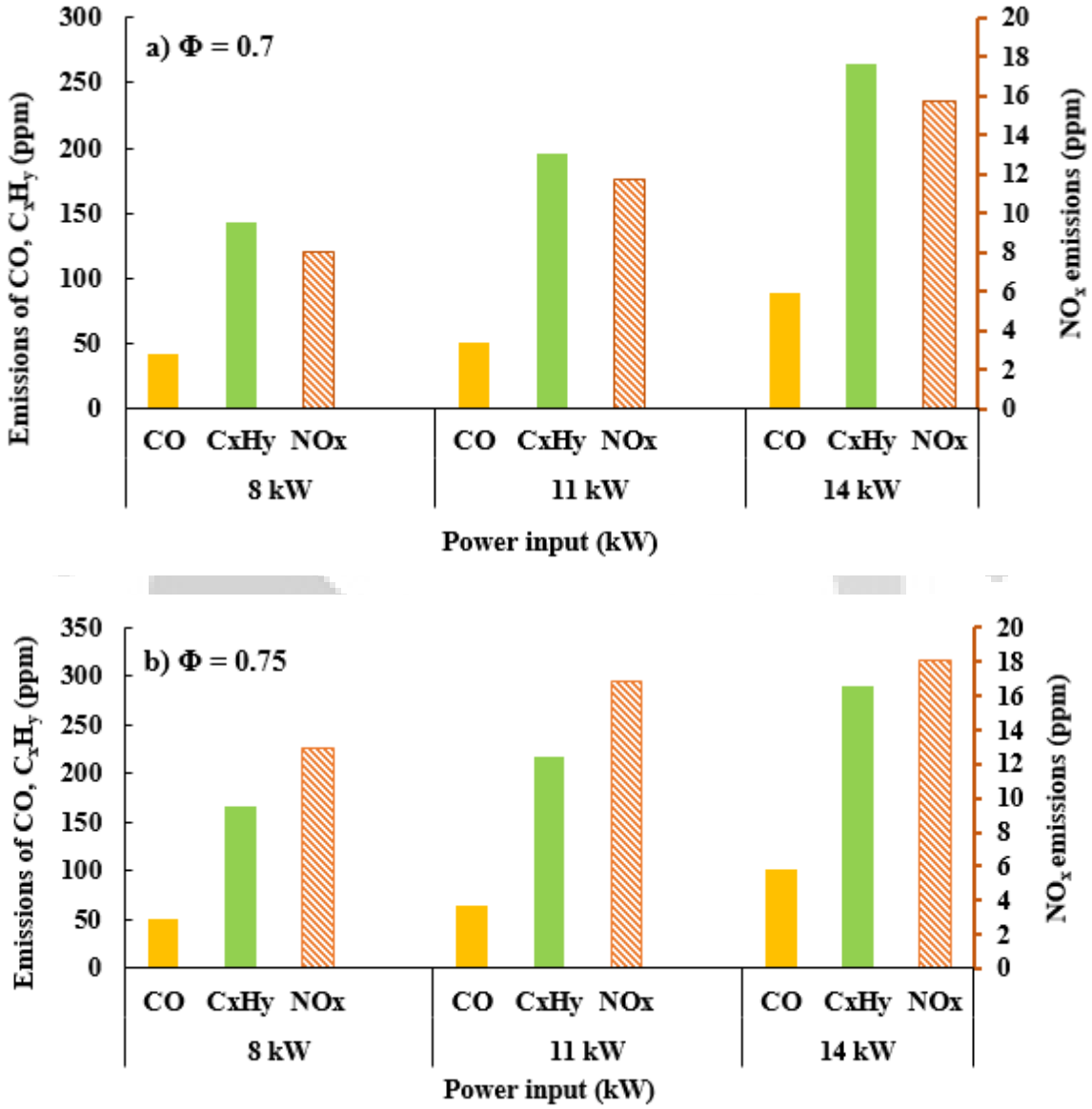

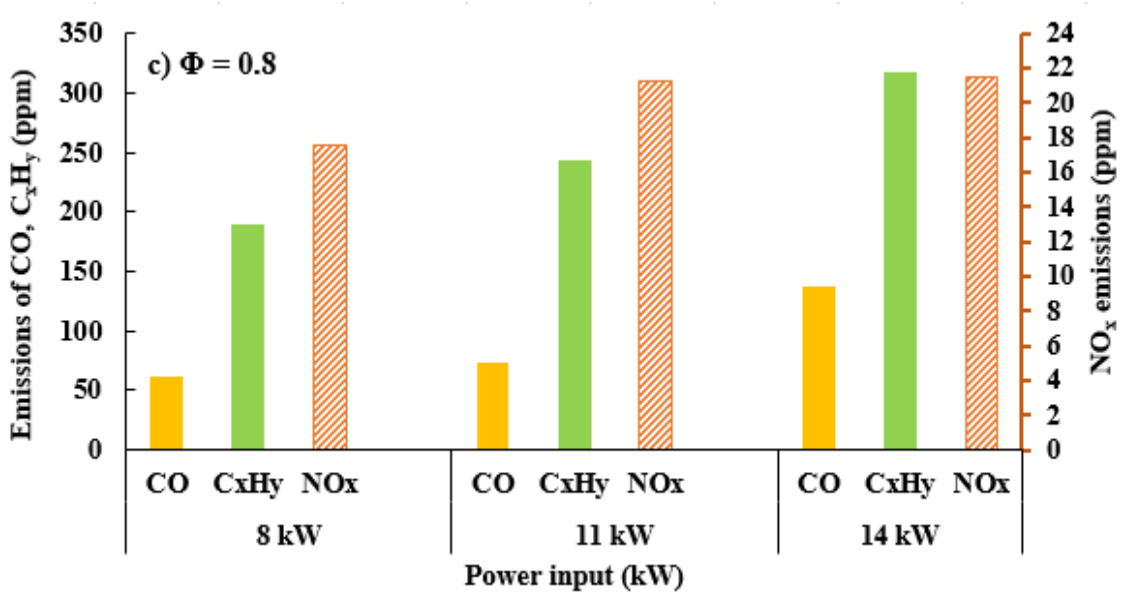

Fig. 3.23: Variation in emissions with power input at equivalence ratio a) 0.7, b) 0.75 and c) 0.8

The emission measurements of the CPRB are presented in Fig. 3.23 (a) – (c). The emissions of CO and NO_x were found to increase with both Φ and power input. For the maximum stable Φ of 0.8, the values of CO emissions were obtained as 62, 73 and 137 ppm for power input of 8, 11 and 14 kW, respectively. The values of NO_x at the corresponding points were found to be 17.5, 21.2 and 21.5 ppm, respectively. Similarly, the lowest CO and NO_x emissions were reported at an Φ of 0.7. The corresponding values were 42, 50 and 89 ppm, and 8, 11.7 and 15 ppm, respectively. Similar trends of CO and NO_x emissions were obtained by Mishra et al. (2015). With the increase in power inputs, the CO emission increases due to the lesser time available for complete combustion because of higher mixture velocity. For a given power input, the CO emission increases with Φ due to the decrement in the availability of excess air for complete combustion. With an increase in power input, the temperature rise leads to the formation of more quantities of NO_x. The C_xH_y emissions were found to increase with Φ and power input due to similar reasons as mentioned for the increase of CO emissions (Wood and Harris, 2008).

The CO/CO_2 ratio (R), an indicator of the burner combustion efficiency, for the stable operating ranges is shown in Fig. 3.24. The CO/CO_2 ratios were observed to increase with both power input and Φ. The increase in the reaction temperature with power input favours the rise in the CO/CO_2 ratio (Du et al., 1991). Apart from the increase in reaction temperature with Φ, the lack of excess air for complete combustion led to the rise in

CO/CO_2 (Du et al., 1991). For all the test cases, the values of CO/CO_2 were much below the BIS limit of 0.02.

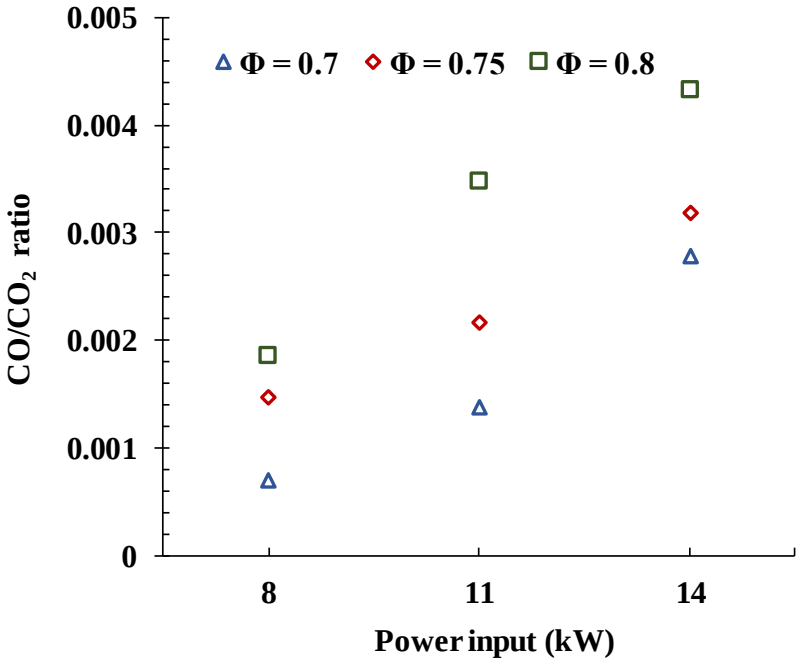

Fig. 3.24: Variation in CO/CO_2 ratio with power input and equivalence ratios

3.4 Determination of flame movement through numerical investigation

From the plots of the axial temperature distribution of the CPRB, the flame movement could not be ascertained due to the limitations in placing more thermocouples along the axis. To overcome this shortcoming, a numerical investigation was carried out to estimate the location of the flame.

3.4.1 Computational domain of the CPRB

Numerical simulations are carried out using CFD software Ansys Fluent 19 to predict the flame movement inside the individual burners of the CPRB. The computational domain shown in Fig. 3.25, represents one of the individual burner of the CPRB. The individual burners of the CPRB operate independently and exhibit similar thermal behaviour as determined from the stability assessment described in section 3.3.1. Due to the symmetry of the CPRB, the numerical simulations were carried out for one individual burner to reduce the complexity of the numerical model. The computational domain comprises three zones viz. Mixing Zone (MZ), PZ, and CZ, where the phenomena of fluid flow and heat transfer take place. The zone MZ includes MC, MT and the air-fuel mixer. Zones PZ and CZ are

porous zones, while zone MZ is a simple fluid zone. The dimensions of the zones are listed in Table 3. The axial and the radial temperature distributions are obtained along the locations shown in Fig. 3.25.

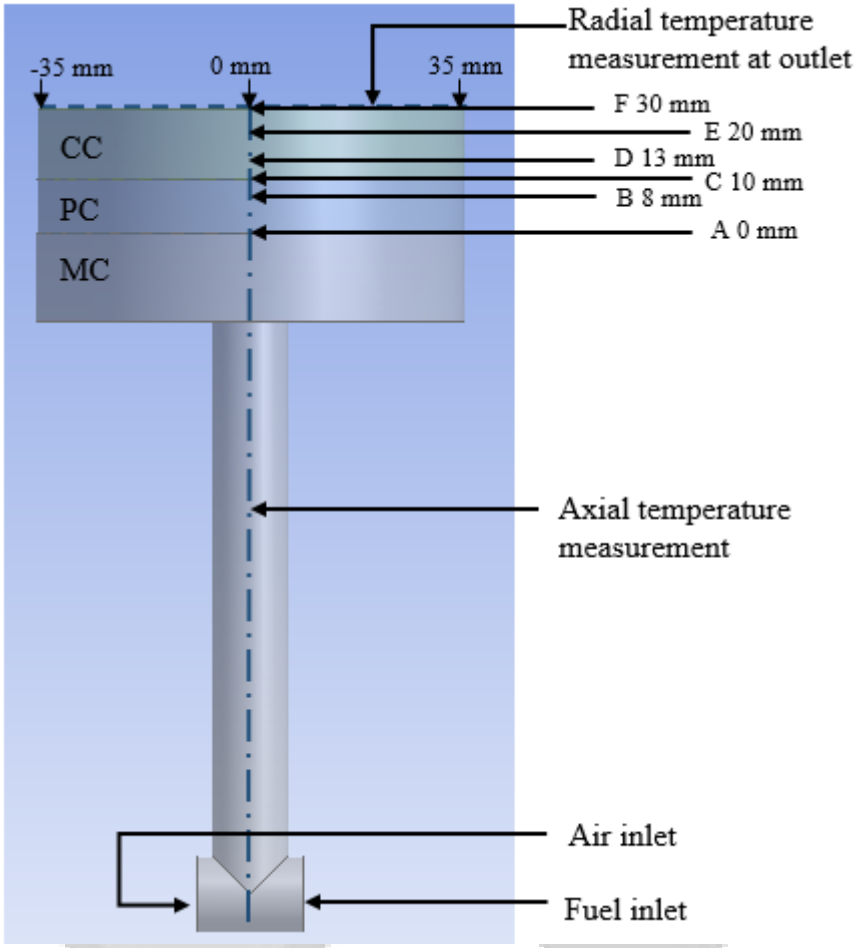

Fig. 3.25: Computational domain of the burner and positions of temperature measurement

3.4.2 Numerical Methodology

The literature on numerical investigations revealed that the heat transfer process in PMC can be modelled based on two idealizations of the temperature field: (i) Local Thermal Equilibrium model (LTE) (one temperature model), and (ii) Local Thermal Non-Equilibrium (LTNE) model (two temperature model). Numerical simulations are initially carried out for a power input of 11 kW and Φ of 0.8, considering both the LTNE and LTE models. Separate grid independence studies are conducted for both the temperature models and the mesh independent result from each model is compared with the experimental result. The model showing the least deviation from the experimental results is chosen for carrying out the subsequent simulations in the stable range of power inputs and Φ. The numerical

simulations are performed on Dell Precision 5820 with 64 GB RAM and 3.7 GHz processor.

The simulations are carried out for a steady flow process, and to simplify the model, the buoyancy effects and the thicknesses of the walls are neglected. The reactants and products are considered to be ideal gases and the thermal properties like specific heat capacity, density and thermal conductivity are assumed to be constant.

Table 3.4: Dimensions of the zones of computational domain

Zones		Height (mm)	Diameter (mm)
CZ		20	70
PZ		10	70
MZ	MC	20	70
	MT	150	21

Governing equations

Continuity Equation –

The conservation of mass is represented by the continuity equation as shown in the following:

$$\nabla.\left(\rho_g \vec{u} \phi\right) = 0 \tag{3.11}$$

where ϕ, $\vec{u}$ and ρ_g are porosity of the medium, velocity vector and density of the gas, respectively.

The conservation of momentum is represented by the momentum equation as expressed in Eq. 3.12.

Momentum Equation –

a) For the zone MZ:

$$\nabla.\left(\phi \rho_g \vec{u}\vec{u}\right) = -\phi \nabla P + \nabla.\left(\phi \mu \nabla \vec{u}\right) \tag{3.12}$$

where P and μ denote pressure and viscosity, respectively.

b) For the porous zones (CZ and PZ), additional source term S_i is added to the right-hand side of Eq. 3.12:

$$S_i = -\left(\frac{\mu}{K_1}\vec{u} + C_2\frac{1}{2}\rho_g|\vec{u}|\vec{u}\right) \tag{3.12a}$$

The permeability of the PM is represented by K_1 and the inertial resistance factor is represented by C_2 (Donoso-García and Henríquez-Vargas, 2015).

Species Conservation Equation –

$$\nabla.\left(\rho_g\vec{u}Y_i\right) = -\nabla.\left(\rho_g D_m\right)\nabla Y_i + \dot{w}_i W_i \tag{3.13}$$

Energy Equation –

The energy conservation equations have been formulated by referring Turns (2000) and Dai et al. (2015). The energy conservation equations for the LTE and LTNE are shown in Eqs. 3.14 – 3.15 (b).

Local Thermal Equilibrium Model (LTE):

$$\nabla\left(\phi c_g\rho_g T\vec{u}\right) = \nabla(k_{eff} + \phi c_g\rho_g D_t)\nabla T - \phi\sum_i \dot{w}_i h_i W_i \tag{3.14}$$

$$k_{eff} = \phi k_g + (1-\phi)k_s \tag{3.14 a}$$

Local Thermal Non-Equilibrium Model (LTNE):

a) For the gas phase:

$$\phi\nabla\left(c_g\rho_g T_g\vec{u}\right) = \phi\nabla\left(k_g + c_g\rho_g D_t\right)\nabla T_g - \phi\sum_i \dot{w}_i h_i W_i - h_v\left(T_g - T_s\right) \tag{3.15 a}$$

b) For the solid phase:

$$k_s\nabla(\nabla T_s) - h_v\left(T_s - T_g\right) = 0 \tag{3.15 b}$$

In Eqs. 3.14 – 3.15 (b), T, W, $\dot{w}$, Y, h_i and k represent temperature, molecular mass, molar rate of production, mass fraction, molar enthalpy of species 'i', and thermal conductivity, respectively. The subscripts 's', 'g' and 'i' stand for solid, gas and species number, respectively. The terms D_m and D_t represent the mass diffusivity and the thermal diffusivity

respectively and k_{eff} is the effective thermal conductivity of the PM. The volumetric heat transfer coefficient 'h_v' is incorporated in Eqs. 3.15 (a) and (b) to couple the gaseous and the solid phases.

The combustion of LPG is represented by the chemical reactions shown in Eqs. 3.16 (a) – (c). The rate of reaction is calculated by the eddy-dissipation model.

$$C_3H_8 + 3.5O_2 \rightarrow 3CO + 4H_2O \quad (3.16a)$$

$$C_4H_{10} + 4.5O_2 \rightarrow 4CO + 5H_2O \quad (3.16b)$$

$$CO + 0.5O_2 \rightarrow CO_2 \quad (3.16c)$$

Boundary conditions

The numerical model is subjected to the following boundary conditions: -

a) At the fuel inlet (mass flow inlet)

$$\dot{m}_f = \frac{\text{Power input}}{3\times LCV} \text{ g/s} \quad (3.17)$$

The mass fractions (Y (species)) of the various species constituting the fuel are Y (C_3H_8) = 0.335, Y (C_4H_{10}) = 0.665, Y (O_2) = 0, Y (N_2) = 0, Y (CO_2) = 0 and Y (CO) = 0.

b) At the air inlet (mass flow inlet)

$$\dot{m}_a = 15.45 \times \dot{m}_f/\Phi \quad \text{g/s} \quad (3.18)$$

The mass fractions of the various species constituting the air are: Y (C_3H_8) = 0, Y (C_4H_{10}) = 0, Y (O_2) = 0.233, Y (N_2) = 0.767, Y (CO_2) = 0 and Y (CO) = 0.

c) At the outlet (pressure outlet)

$$P_{gauge} = 0, T = 300 \text{ K} \quad (3.19)$$

P_{gauge} denotes the gauge pressure at the outlet. The mass fractions of the various species were initialized as: Y (C_3H_8) = 0, Y (C_4H_{10}) = 0, Y (O_2) = 0, Y (N_2) = 0, Y (CO_2) = 0 and Y (CO) = 0.

d) At the PC and CC wall

$$Q_w = -\varepsilon\sigma\left(T_g^4 - T_{Surr}^4\right) - h_a\left(T_g - T_{Surr}\right) \quad (3.20)$$

In Eq. 3.20, Q_w represents the wall heat transfer, 'T_{surr}', 'ε', 'σ' and h_a denote ambient temperature, emissivity, Stefan-Boltzmann constant and convective heat transfer coefficient, respectively.

Solution procedure

The SIMPLE algorithm was used to solve the pressure-velocity coupling. The first order upwind discretization was used to solve the convective and diffusive terms. The effects of turbulence in the PM were predicted by employing the RNG *k-ϵ* model with standard wall functions. The solution was considered to be converged when the residual error of the energy equation and the other equations were in the order of 10^{-6} and 10^{-4}, respectively (Dai et al., 2015).

3.4.3 Grid independence test and validation

The numerical simulations are useful in predicting the flame movement based on the shift in the location of maximum temperature points in the axial direction. The computational domain was meshed with the help of automatic method with a maximum orthogonality of 0.98. The results of the grid-independence studies for the LTE and LTNE models at a Φ of 0.8 and power input of 11 kW are presented in Table 3.5. For the grid comparison, the maximum temperature at the outlet was chosen. The grid independence study reveals that the optimum number of elements required to attain mesh independence for LTE and LTNE models are 315180 and 723941, respectively.

Table 3.5: Grid independence test for LTE and LTNE models

Thermal equilibrium model		**Thermal non-equilibrium model**	
Mesh elements	Temperature (°C)	Mesh elements	Temperature (°C)
255295	1289	592315	1200
283662	1189	658128	1189
315180	1108	723941	1077.2
350200	1112	796335	1077.5

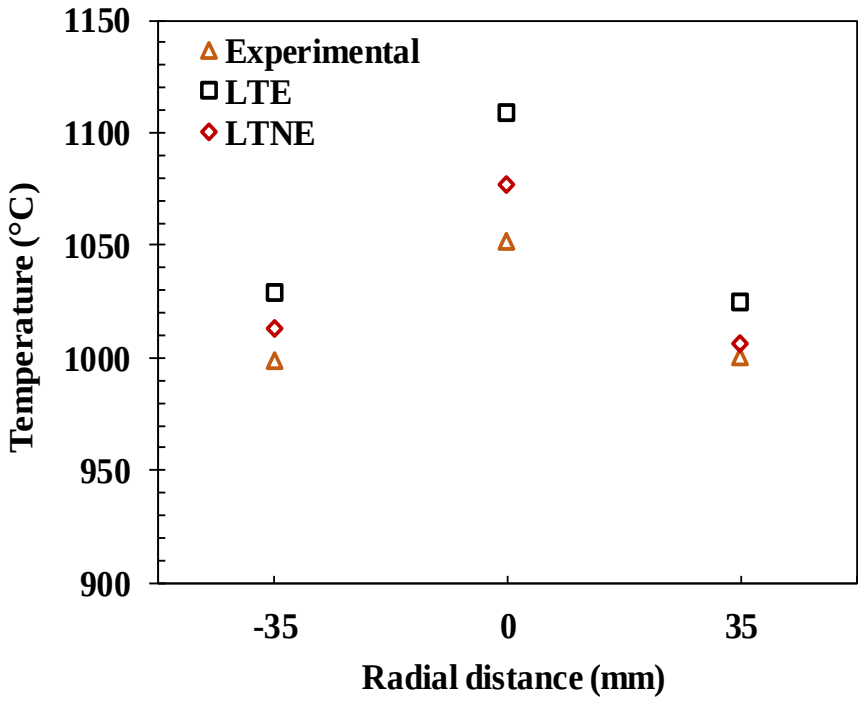

Fig. 3.26: Comparison of LTNE and LTE models with the experimental results

Fig. 3.26 shows the comparison between the LTE and the LTNE models with the experimental results. It is evident that the LTNE provides a more accurate solution than the LTE. The presence of large open pores, existence of source terms, and a large difference in the PM properties lead to a difference in the gas and the solid temperatures (Nimvari et al., 2013), which makes the LTNE model comparable to the actual combustion process in a PRB. Both the models yielded higher temperatures than that of the experimental results. This happens since the specific heat capacity was assumed to be constant which affects the prediction of the rise in the system temperature (Dai et al., 2015). Moreover, the computational domain and the numerical models were simplified based on assumptions, due to which the heat loss from the outlet and the walls was not exactly predicted. The maximum deviation of the temperature for the LTNE model from the experimental results is obtained as 22°C (< 3%) and is found to be lesser than the LTE model. Therefore, the LTNE model was chosen for the simulations to study the flame location at different power inputs.

3.4.4 Determination of the flame movement with power input

The flame position was estimated from the location of the maximum temperature points along the burner axis. The variation in the axial temperature with power input and Φ, obtained from numerical simulations is shown in Fig. 3.23.

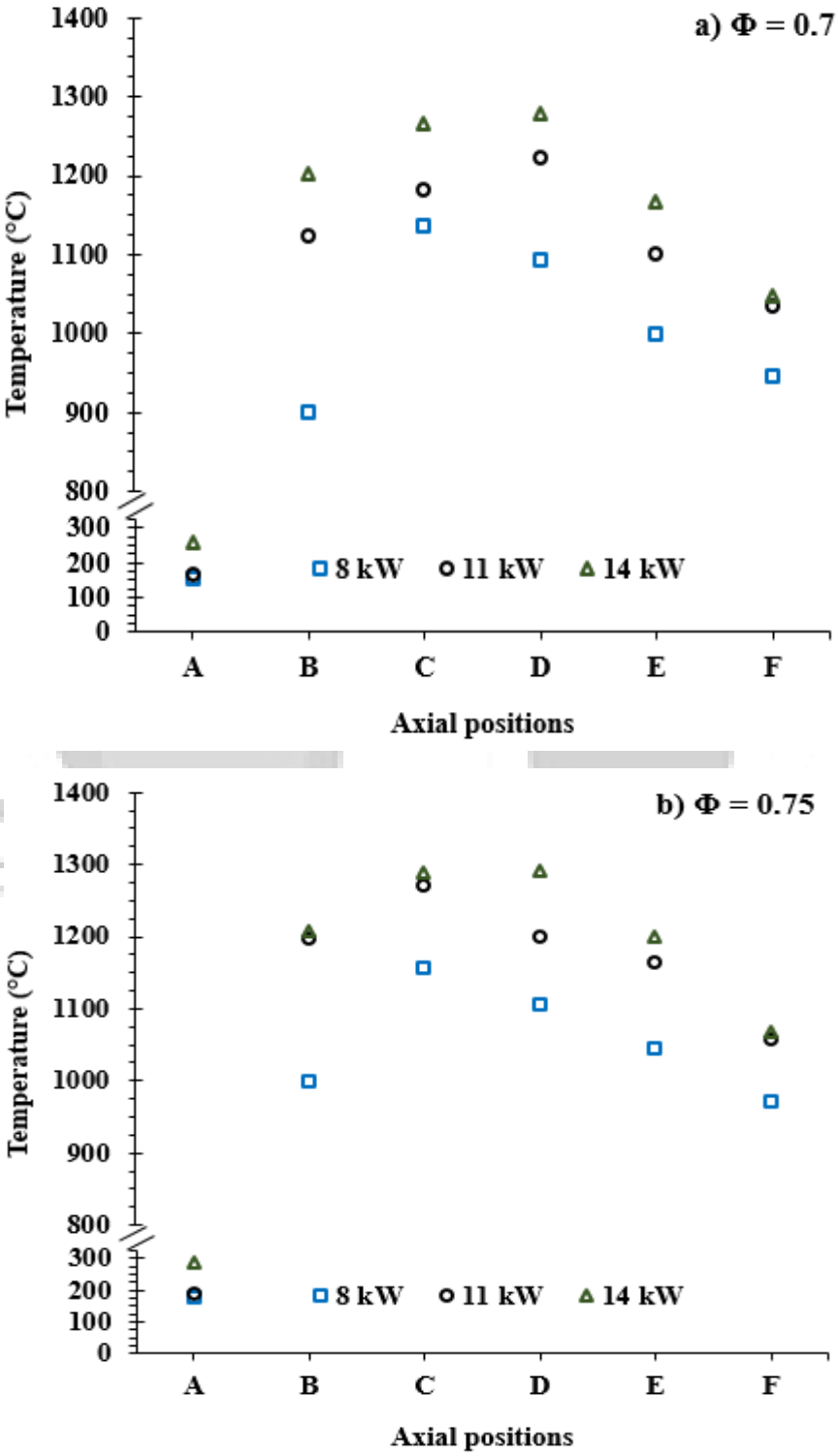

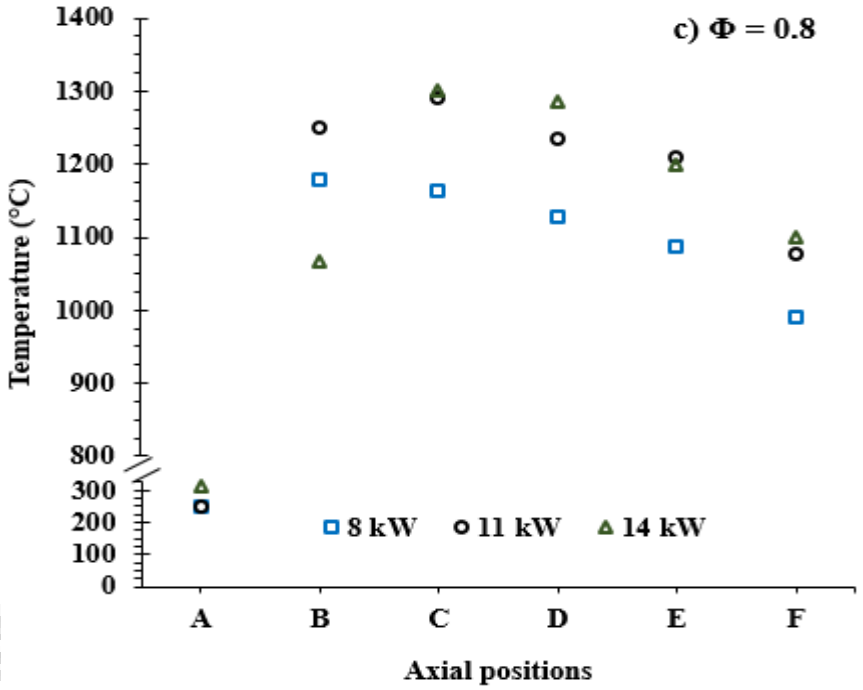

Fig. 3.27: Numerical results of axial temperature distribution with power input at equivalence ratios a) 0.7, b) 0.75 and c) 0.8

At Φ of 0.7, as shown in Fig. 3.27 (a), maximum temperature of 1137°C was obtained for power input of 8 kW at the position C, which is the interface of the CC and PC. Maximum temperatures reached for power inputs 11 and 14 kW were 1221°C and 1278°C, respectively, which were located at position D located at 3 mm downstream of the CC and PC interface.

In case of Φ of 0.75 (Fig. 3.27 (b)), the maximum temperatures obtained for power inputs 8, 11 and 14 kW were 1156°C, 1271°C and 1291°C, respectively. While the maximum temperature was obtained at position C for 8 and 11 kW, the flame shifted further downstream to location D for power input 14 kW. For Φ of 0.8 (Fig. 3.27 (c)), the maximum temperatures obtained for power inputs 8, 11 and 14 kW were 1178°C, 1289°C and 1301°C, respectively. While the maximum temperature for 8 kW was obtained at position B located at a distance of 2 mm beneath the interface of the CC and the PC and the maximum temperature was obtained at the interface for power inputs 11 and 14 kW.

The flame movement upstream or downstream leading to blow-off or flashback are related to matching of the flow velocity of the inlet mixture and the flame speed. For example, the flashback occurs when the flame travels at a higher speed than the incoming air-fuel

mixture, and the high temperature of the flame ignites the incoming fresh air-fuel mixture upstream of a reaction zone. Finally, the flow is stabilized at the position where the inlet mixture velocity matches the flame speed. The inlet mixture velocity and the temperature are dependent on the power input and the Φ and therefore, these factors collectively influence the flame movement. The same has been highlighted by the present numerical simulations. The variation in stability limits of CPRB results from the collective influence of power input and the Φ. The same has been highlighted by the present numerical simulations.

3.5 Experimental Study on Performance Improvement of CPRB

The results obtained from emission tests (section 3.2.3) left scope for further performance improvement of the CPRB. Research work carried out by Pantangi et al. (2011) indicated that an increase of burner diameter led to an increase of η_t till the point of a maximum burner diameter beyond which the increase in burner diameter led to the decrease in η_t. Therefore, CPRBs of higher diameter were tested for their thermal performance.

3.5.1 Effect on surface temperature

The radial surface temperature distributions at the top surface of CPRB8 and CPRB9 are illustrated in Fig. 3.28 and Fig. 3.29, respectively. Results show that the burner diameter significantly influences the top surface temperature distribution.

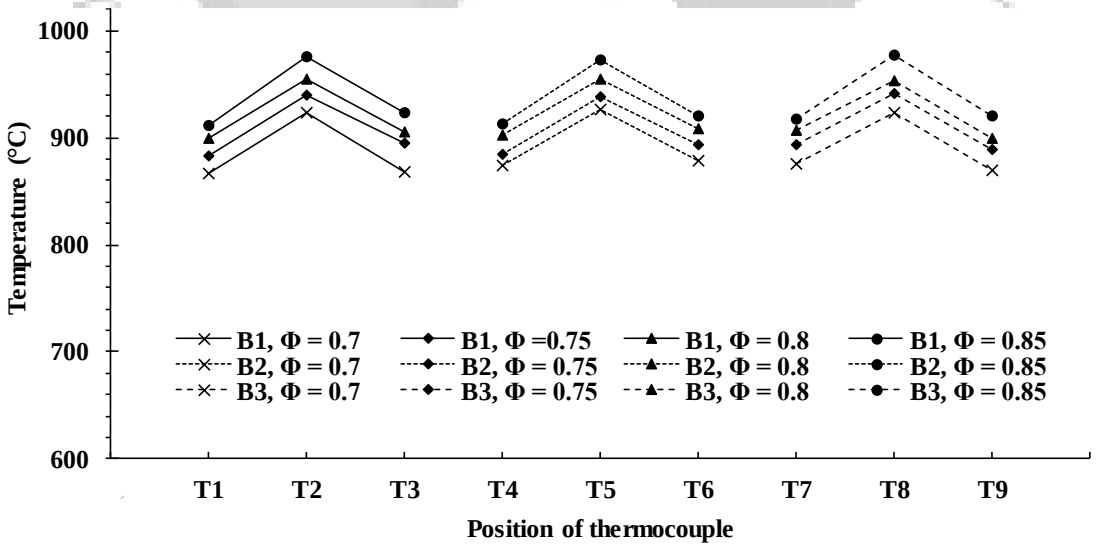

Fig. 3.28: Surface temperature distribution for CPRB8

A maximum surface temperature of 1085°C was obtained for CPRB7 (Fig. 3.15), whereas the same was 977°C (Fig. 3.28) and 949°C (Fig. 3.29) for CPRB8 and CPRB9, respectively. The radial temperature plots show that as the burner size increases, the top surface temperature becomes lower on account of an increase in surface area and more uniform distribution of heat.

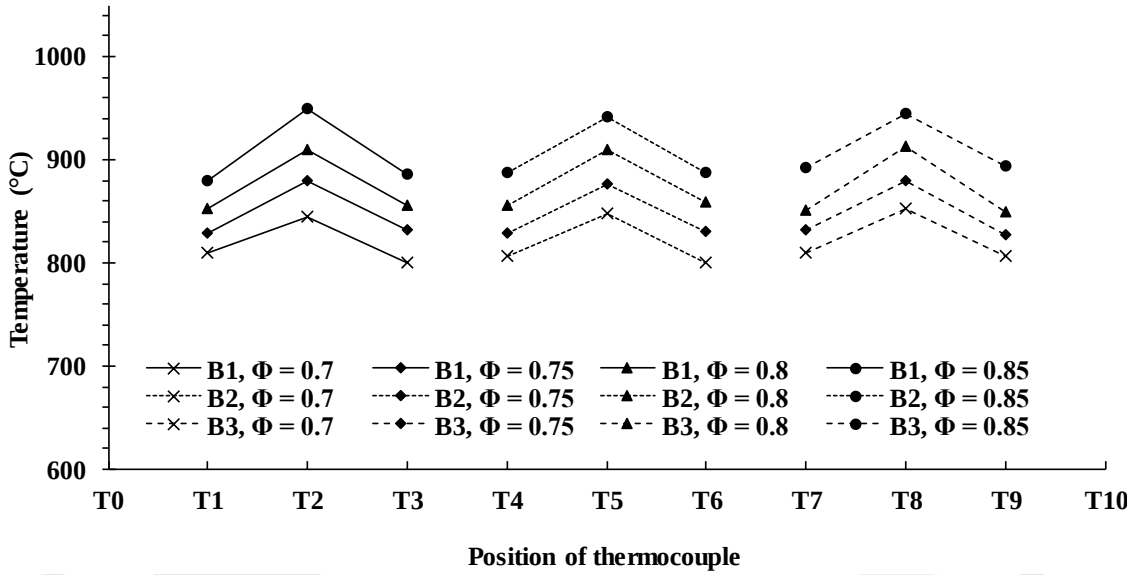

Fig. 3.29: Surface temperature distribution for CPRB9

3.5.2 Effect on thermal efficiency

The variation in η_t with Φ for CPRBs is shown in Fig. 3.30. The η_t within the studied range of Φ (0.7-0.85), varies in the range of 50 – 55.6%, 54 – 59.2% and 49 – 55% for CPRB7, CPRB8 and CPRB9, respectively. The maximum η_t was obtained at Φ of 0.7 for all the test cases. The η_t of CPRB8 was found to be higher than both CPRB7 and CPRB9. The increase in the diameter of the CPRB from 70 mm to 80 mm results in higher surface area for the radiative heat transfer, which is the predominant mode of heat transfer in a PRB. This enabled higher thermal efficiency to be obtained from CPRB8 (59.2%) as compared to CPRB7 (55.6%). When the size of the burner is further increased from 80 mm to 90 mm, the surface area available for the radiative heat transfer increases, but at the same time the heat loss from the burner periphery to the ambient also increases. The effect of the heat loss from the burner periphery is more dominant than that of the effect of increase in surface area for radiative heat transfer to the load. As a net result, the η_t of the CPRB is found to decrease from 59.2% (CPRB8) to 55% (CPRB9). Therefore, there is an optimum diameter of the CPRB (80 mm) beyond which the further increase in the diameter will lead to a reduction in η_t. This finding is consistent with the experimental results of Pantangi et al.

(2011) where the η_t was reported to increase with burner diameter from 60 to 80 mm and decreased beyond burner diameter of 90 mm.

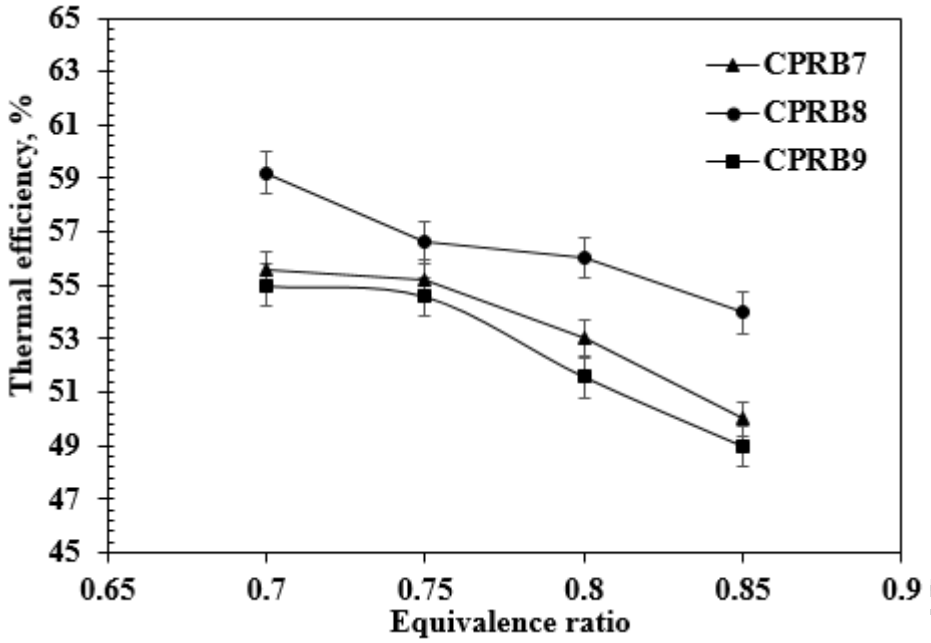

Fig. 3.30: Variation in thermal efficiency of CPRBs with equivalence ratio

3.5.3 Effect on emissions

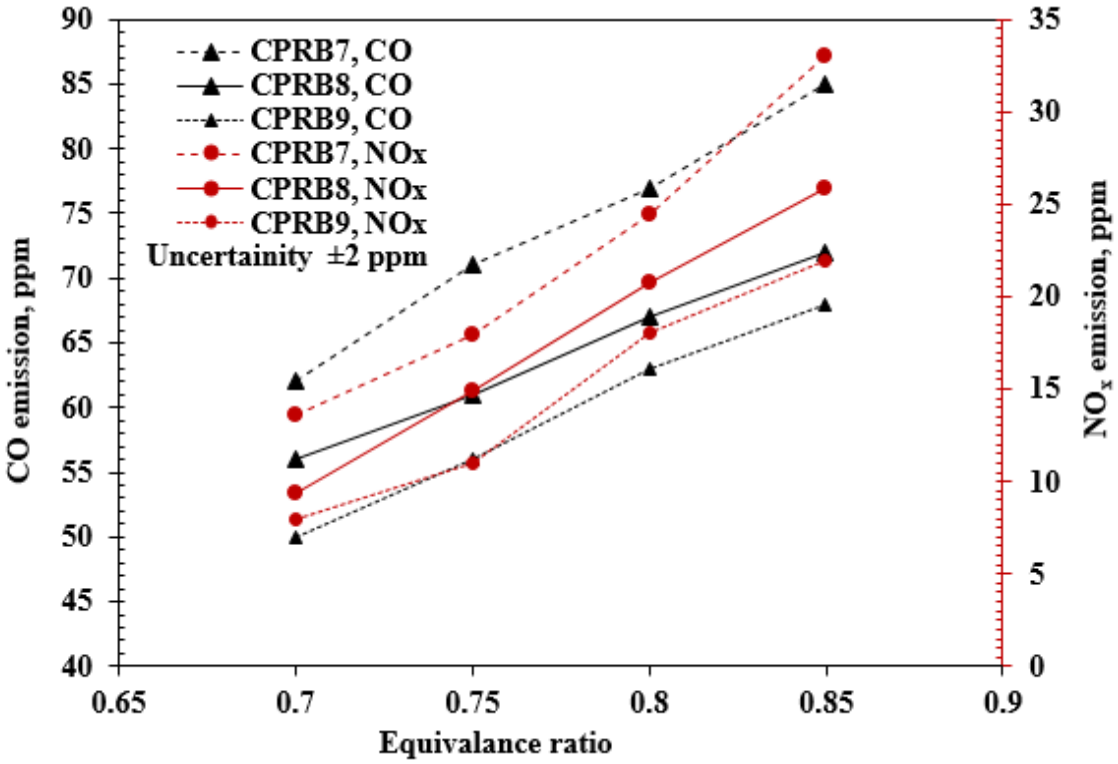

Fig. 3.31: Variation in CO and NO_x emissions with equivalence ratio of CPRBs

The variations in CO and NO_x emissions with Φ for CPRBs are shown in Fig. 3.31. The CO and NO_x emission were found to be highest for Φ of 0.85. The measured CO values were 85 ppm, 72 ppm and 68 ppm for CPRB7, CPRB8 and CPRB9, respectively. Similarly, the corresponding values for NO_x were 33 ppm, 25.8 ppm and 22 ppm, respectively. The lowest CO and NO_x emissions were obtained for Φ of 0.7. The values of minimum CO were 62 ppm, 56 ppm and 50 ppm for CPRB7, CPRB8 and CPRB9, respectively. Likewise, the corresponding values of NO_x emissions were 13.6 ppm, 9.4 ppm, and 8 ppm, respectively.

The increase in CPRB diameter facilitated the homogeneous mixing and complete combustion of the fuel that helped in reducing CO emissions. Likewise, the increase in CPRB diameter also resulted in a lowering of temperature that resulted in the reduction of NO_x formation.

Effect on CO/CO_2 ratio

The variation in CO/CO_2 ratio of the CPRBs with respect to Φ is shown in Fig. 3.32. Within Φ of 0.7-0.85, the CO/CO_2 ratio was found to increase from 0.00103 to 0.00425 for CPRB7. The same values for CPRB8 and CPRB9 were 0.0007 to 0.0024 and 0.000625 to 0.0011, respectively.

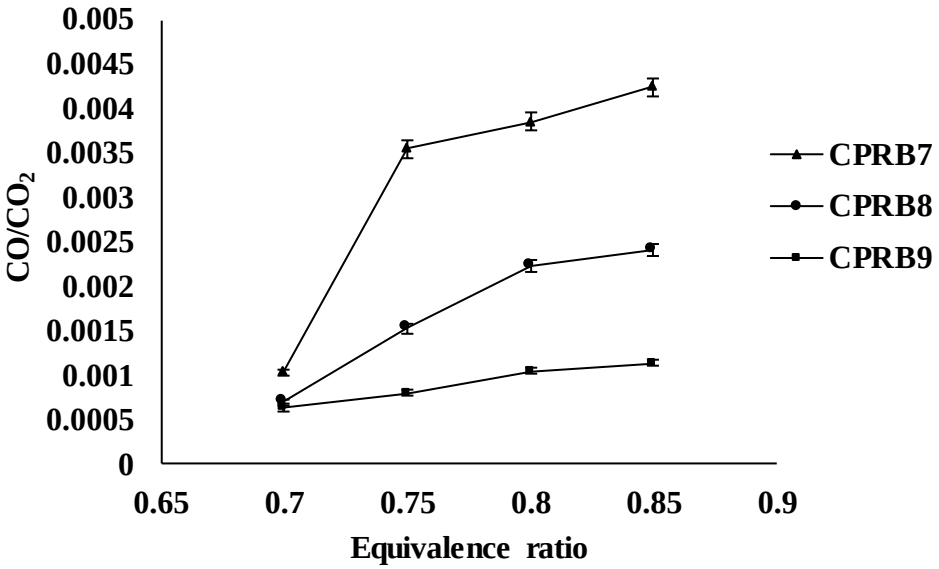

Fig. 3.32: Variation in CO/CO_2 with equivalence ratio for CPRBs

The combustion efficiency (η_c), defined by the ratio of CO_2 to the sum of CO and CO_2 (Decker et al., 2018), is suggestive of the extent of complete combustion of the fuel. From

the results of emission, it is observed that the amount of CO produced is negligible in comparison to the amount of CO_2, and therefore η_c more than 99% was obtained for all the CPRBs within the stable range of Φ.

3.6 Comparison with Conventional Burners

3.6.1 Description of the Conventional Burners (CBs)

The Conventional Burners (CBs), as described previously, work on the principle of a Bunsen burner in which the flame is attached to the burner port and is exposed to the surroundings. This phenomenon is generally termed as Free Flame Combustion (FFC). For medium-scale (5-15 kW) cooking, the commonly available CBs in the Indian market are namely T-22, T-35, M-22 and M-35 (Fig. 3.33 (a) – (d)). A T-type (Torch-type) burner is identified by a flame impinging out of a wire mesh located at the top of the burner head (as shown in Fig. 3.33 (a)), whereas in M-type (Marguerite) burners, a spreading flame is produced from the ports at the periphery of the burner head (Figs. 3.33 (c) – (d)). The T-22 burner has a head diameter of 63 mm and length of 185 mm. The T-35 burner is a torch type burner with a burner head diameter of 83 mm and a length of 200 mm ("Liquified Petroleum Gas Burners and Equipment," 2009) (Fig. 3.33(b)). The M-35 and M-22 burners with burner diameters of 83 and 63 mm respectively, and length of 200 mm, respectively ("Liquified Petroleum Gas Burners and Equipment," 2009). The rated fuel flow rate and pressure are 1 kg/h and 0.3 kg/m^2 respectively.

(a) **(b)** **(c)** **(d)**

Fig. 3.33: Pictorial views of a) T-22 burner, b) T-35, c) M-35 and d) M-22 burners

3.6.2 Performance comparison

The CPRBs were developed as an improved version of a single-PRB that can be used as a medium-scale cookstove. The performance of the CPRBs were compared with some of the

available LPG burners for medium-scale cooking. The methodologies to measure the η_t and emissions were the same as that for a CPRB. Fig. 3.34 shows a comparison of η_t of a single-PRB and CBs (M-22, M-35, T-35 and T-22) with CPRBs operated at Φ of 0.7 and power input of 12.5 kW. The CPRBs were found to have significantly higher η_t than the CBs under consideration. The lower η_t of CBs is because it operates on the phenomenon of FFC. In FFC, the flame is completely exposed to the surroundings and is therefore subjected to higher convective heat losses as compared to a PMC based burner where the flame resides below the top surface of the burner. The CBs have a maximum η_t of 47%, whereas the minimum η_t of CPRBs is 49%. A maximum of 13.8% and 31.5% improvement in η_t over single-PRB and CB, respectively, could be attained with CPRB8.

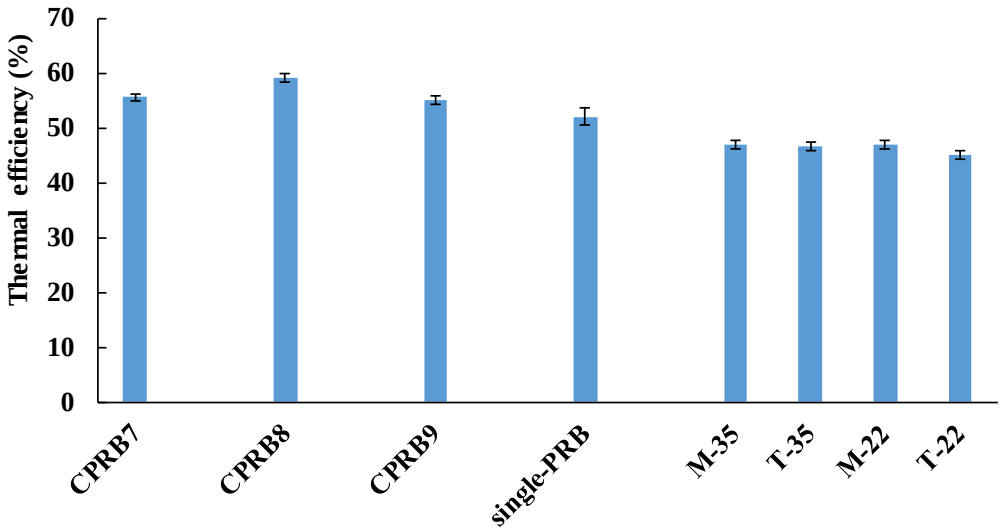

Fig. 3.34: Comparison of thermal efficiencies from CPRBs, PRBs and CBs

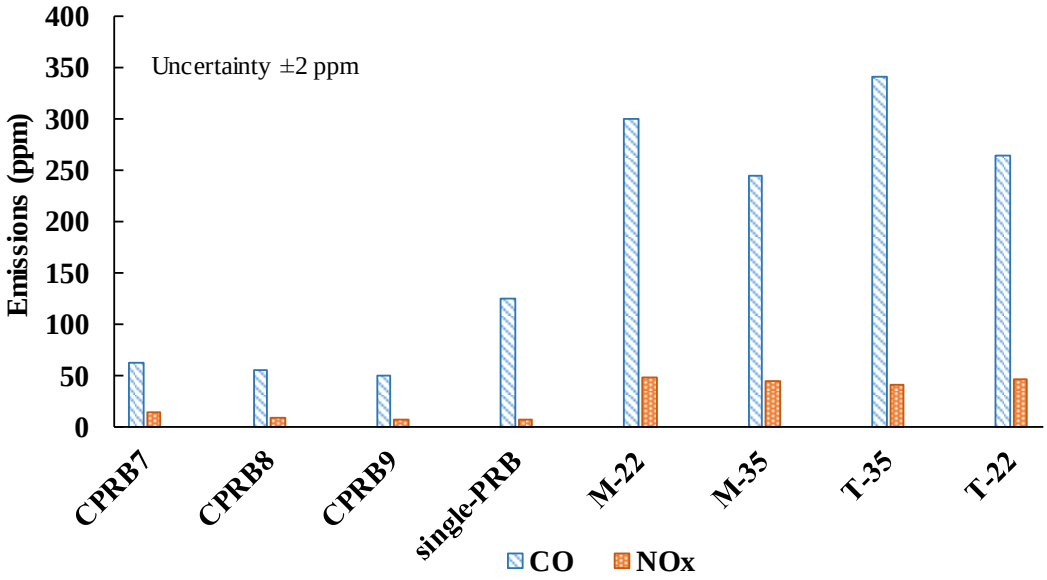

Fig. 3.35: Comparison of CO and NO_x emissions from CPRBs, PRBs and CBs

The emissions from various CBs and their comparison with CPRBs at power input of 12.5 kW are shown in Fig. 3.35. The maximum emissions of CO and NO_x from the CBs were measured to be 341 ppm and 48 ppm, respectively. In the case of the CBs, the CO/CO_2 ratio was found to be 0.00273, 0.00375, 0.00377 and 0.00682 for M-22, M-35, T-22 and T-35 burner, respectively. For the lowest Φ of 0.7, the CO/CO_2 ratio of CPRB was found to be lower than the CBs. CPRB9 yielded a maximum reduction of 60% and 85.3% in CO emissions when compared to single-PRB and CB, respectively. The NO_x emissions of CPRB9 was found to be comparable with that of a single-PRB. When compared to CBs, a maximum NO_x reduction of 83.3% could be obtained with CPRB9.

3.7 Summary

A Cluster Porous Radiant Burner (CPRB) consisting of 3 individual burners was developed and tested for its performance improvement over a single Porous Radiant Burner (PRB). Initially, experiments were conducted for a power input of 12.5 kW following the guidelines given in BIS 14612:1999. The system used air at 1.5 bar as oxidizer and LPG as fuel. Experimental results suggest that the performances of a PRB can be improved when smaller diameter PRBs, with equivalent top surface area as that of a single-PRB, were clustered. Maximum thermal efficiency (η_t) and lowest CO and NO_x emissions were obtained at an equivalence ratio of 0.7. Performance tests revealed that the CPRB7 yielded a maximum of 7% improvement in η_t and 50% reductions in CO emissions over a single-PRB.

Further, a detailed study on whether the CPRB is capable of delivering the improved performance at different power inputs so as to be suitable for cooking systems in small and medium scale applications. At an equivalence ratio of 0.7, the maximum reported thermal efficiencies for power inputs of 8, 11, and 14 kW were 59.7%, 57.3%, and 52.9%, respectively. The emissions of CO, NO_x and C_xH_y were found limited to 137, 21.5 and 318 ppm for the entire operational range.

Later, the performance of the CPRB was further improved by increasing its diameter. Amongst the CPRBs, CPRB8 produced the highest η_t, while CPRB9 yielded the lowest emissions. When compared to the CBs, a maximum η_t improvement of 27% was obtained with CPRB8, while a maximum reduction of 85.3% CO and 83.3%

NO_x emissions were obtained with CPRB9. CPRB was found to be more thermally efficient and cleaner than both the single-PRB and CBs. Therefore, it is concluded that clustering of smaller size individual burners is more efficient than a single-PRB. Also, all the CPRBs were found to operate well below the prescribed norms of emissions set by the BIS. Hence, the developed CPRB8 provides a substantial ground for the developments of alternative PRB based LPG cookstoves.

Chapter 4

Second Phase Investigations – Development of a self-aspirated Clustered Porous Radiant Burner

Preface

The previous chapter revealed insightful findings on the functioning of a Clustered Porous Radiant Burner (CPRB) as an effective tool to deliver the heat of combustion to the load while emitting less harmful pollutants. The operation of the CPRB was on forced draft mode requiring the supply and distribution of the combustion air equally amongst the individual burners of the CPRB. The use of pressurized air for combustion demanded an air compressor that not only required electrical power input but also increased the number of components required for air supply to the burner. If the proposed CPRB replaces the conventional medium-scale cookstoves in the market, the prime focus should be discarding the compressor and reducing the number of components required for hassle free and stable operation. Therefore, in order to offer an advantageous technology which can be ultimately used by the beneficiaries, a self-aspirated CPRB was developed and was tested for its thermal stability and performance. The developed self-aspirated CPRB was then assessed for its eco-friendliness against a conventional burner by conducting Life-Cycle Assessments.

4.1 Conversion of the CPRB from Forced Draft to Self-aspirated Mode

From the results of investigations on the performance improvement of the forced draft CPRB, individual burner diameter 80 mm was found to yield optimized thermal performance. Therefore, for the construction of a self-aspirated CPRB, the initial individual burner dimensions considered were diameter 80 mm, Combustion Zone (CZ) thickness 20 mm, Preheating Zone (PZ) thickness 10 mm and Mixing Chamber (MC) thickness of 20 mm. As described previously, the entrainment of air through natural draft in a cookstove is

accomplished through the phenomenon of Venturi effect in a Mixing Tube (MT) that acts as an eductor. The MTs of the forced draft CPRB were majorly used to provide an inlet for the incoming fuel and air streams and transport the air-fuel mixture to the individual burners. However, in self-aspirated burners, the MT performs the function of entraining surrounding air and serves as an eductor when coupled with jetpins. Therefore, the MTs of the forced draft CPRB were replaced by MTs wherein, jetpins mounted on nozzle valves (Fig. 4.1), were inserted for executing the process of natural air entrainment through Venturi action. Fig. 4.2 shows a typical MT employed in self-aspirated PRB cookstoves developed in IIT Guwahati.

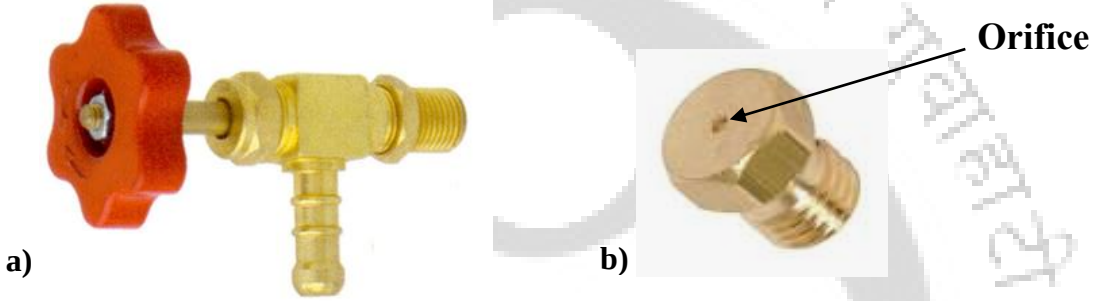

Fig. 4.1: Photographic views of a) nozzle valve and b) gas Jetpin

Fig. 4.2: Typical mixing tube used in self-aspirated PRB cookstoves

A typical MT used in the self-aspirated cookstove consists of a seamless mild steel tube containing two equidistant elliptical slots cut out on the periphery. The seamless tubes are welded to threaded pipes that are fitted inside a galvanized iron socket placed inside the casting to maintain the alignment of the MT and the burner.

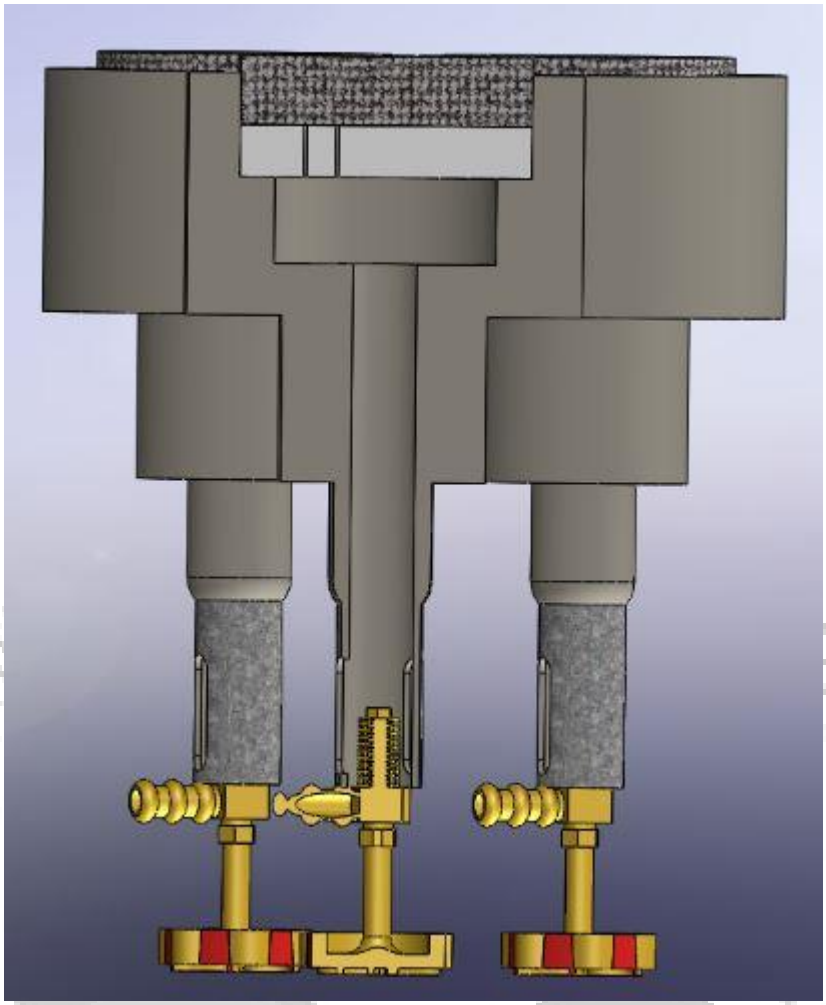

Fig. 4.3: Assembly of jet pin nozzle and mixing tube

Fig. 4.3 shows the assembly of the jet-pin inside the mixing tube. Initially, the jet-pins mounted on the nozzles were placed freely inside the MT at a certain offset from the bottom of the MT. After a few runs of experimentation, the CPRB started to behave unstably with one individual burner operating stably while the others exhibiting flame-quenching at one side of the sides. This was a result of an inappropriate and unequal supply of air-fuel mixture into the individual burners. Careful examination of the piping connections of the CPRB set-up led to the revelation that the nozzles carrying the jet pins were misaligned with the MT and were not positioned axially, leading to uneven air entrainment. Therefore, in order to establish a stable alignment of the nozzle and the MT and also to have a provision for easy dismantling of the assembly, a non-permanent fixture of the nozzle and the MT was opted.

A hexagonal nut was placed inside the MT at the bottom (Fig. 4.4) that provided a threaded joint between the nut and the nozzle to maintain proper alignment of the MT and nozzle

and maintain the burner symmetry. Such an assembly also supported the easy movement of the nozzle inside the MT for different offset positions of the jet-pins for further investigations.

Fig. 4.4: Hexagonal nut welded at the bottom of the mixing tube

Further to the advancement of a CPRB from operating in a forced draft mode to self-aspirated mode, the fuel headers were replaced with a four-way as shown in Fig. 4.5. Hose pipe connecting the cylinder to the four-way supplied fuel and the fuel was distributed to each individual burner by hose pipes connecting the other three outlets of the four-way.

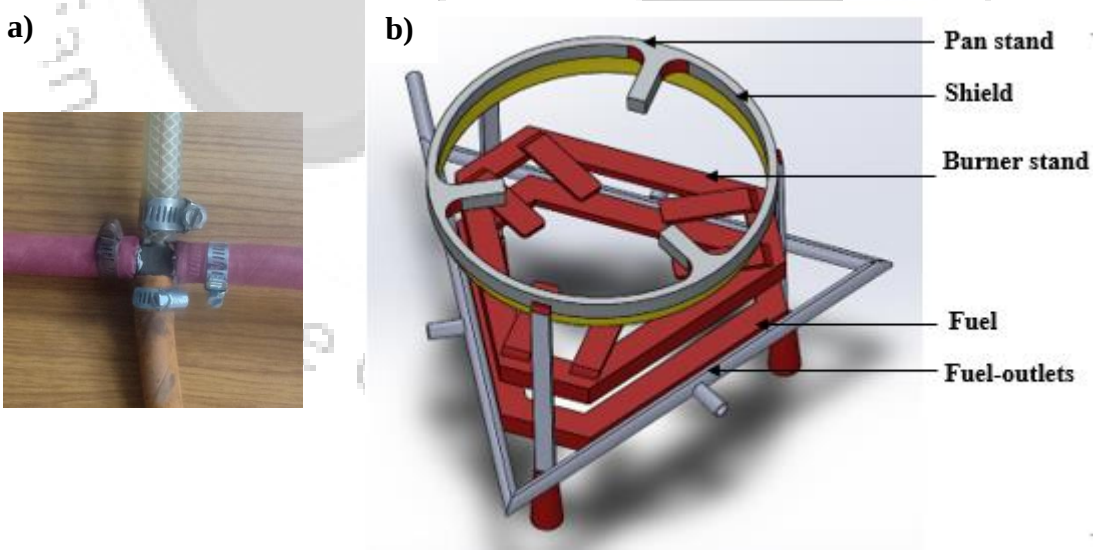

Fig. 4.5: Fuel distribution system a) Four way hose pipe connections, and b) Fuel header made of seamless steel tube

However, the four-way hose pipe connections when used for a long time resulted in leaks and therefore, a fuel header made of seamless steel tubes was fabricated and fixed with the

frame of the stove as shown in Fig. 4.5 (b). Starting with the introduction of a modified mixing tube for air entrainment, various design improvements of the CPRB were conducted to arrive at the final optimized design for best thermal performance. Initially all the experiments for the design optimization of self-aspirated CPRB were carried out for a fixed power input of 12.5 kW.

4.2 Stages of Design Optimization for the Self-aspirated CPRB

The schematic of the one of the individual burners of the self-aspirated CPRB showing the nomenclature of the geometrical parameters that varied for parametric study are displayed in Fig. 4.6. For the first experimental run of a self-aspirated CPRB set-up, the specifications of the CPRB are listed in Table 4.1.

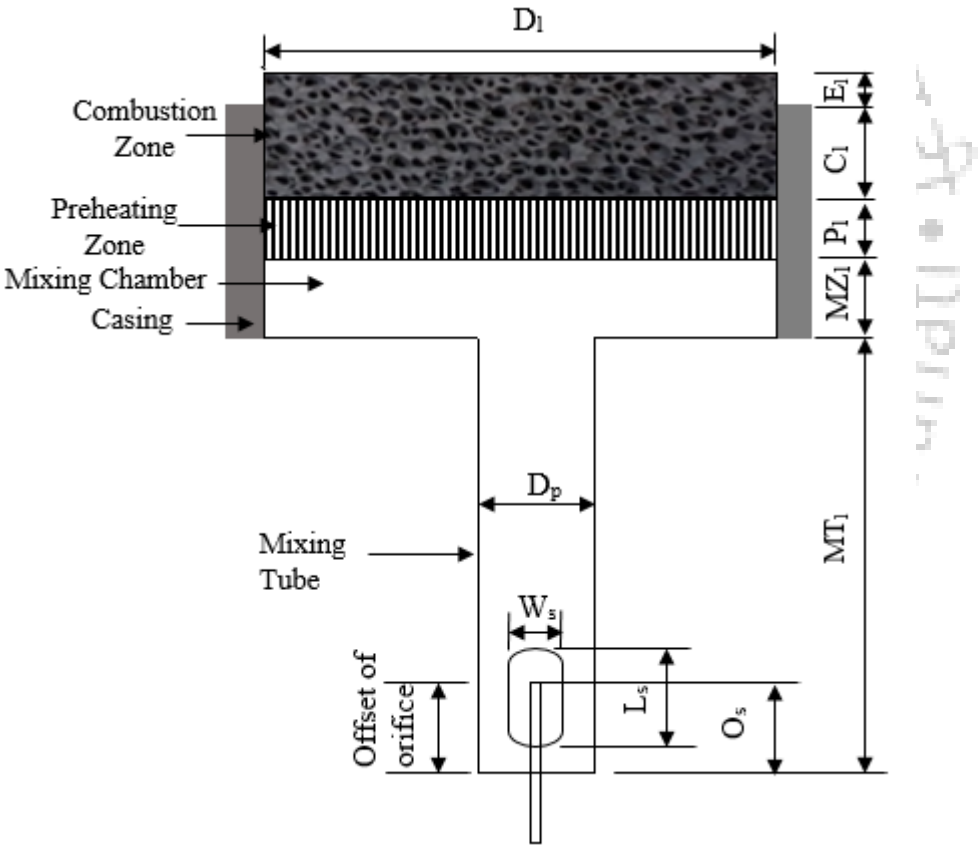

Fig. 4.6: Schematic of individual burner of CPRB depicting component nomenclature

Table 4.1: Specifications of the self-aspirated CPRB

Parameter		Measure (mm)	Parameter		Measure (mm)
Orifice	Offset from MT bottom (O_s)	5	Slot	Width (W_s)	10
	Diameter (O_d)	0.35		Length (L_s)	20
Mixing tube	Length (MT_l)	150	Combustion Zone	Diameter (D_l)	80
	Diameter (D_p)	19		Length (C_l)	20
Mixing Chamber	Length (MZ_l)	20	Preheating Zone	Diameter (D_l)	80
	Diameter (D_l)	75		Length (P_l)	10

The dimensions of these parameters were then changed up until a stable, least polluting and most energy-efficient burner configuration was obtained.

4.2.1 Burner modifications with variation in orifice diameter and position

As listed in Table 4.1, the initial diameter of the MT was 19 mm and the height was 150 mm. With the same configuration, unstable combustion with flashback was obtained. Therefore, the initial investigations on the development of the self-aspirated CPRB was carried out by changing the orifice diameter and orifice positions. The results of the stability assessment of the various combinations of orifice diameters and orifice positions are presented in Table 4.2.

Table 4.2: Stability assessment with various combinations of orifice diameters and positions

Orifice Diameter (O_d) (mm)	Orifice Position (O_s) (mm)	Stability
0.35 (30 lh)	5	• Lean combustion with surface flame
	10	• Submerged combustion • Flashback after ~10 min
	20	• Submerged combustion • Flashback after ~15 min
	30	• Partially submerged combustion • Extended flame ~ 300 mm (blowoff)
0.49 (45 lh)	5	• Submerged combustion • Flashback at the time of fuel shutoff

	10	• Flashback after submerged combustion for ~ 45 min to 1 h.
	20	• Partially submerged combustion with an extended flame • Flashback reported after ~ 45 min to 1 h
	30	• Partially submerged combustion with a swamping flame outside the combustion zone
0.59 (58 lh)	5	• Partially submerged combustion with an extended flame • Flashback reported after ~ 45 min to 1 h
	10	• Partially submerged flame with an extended flame • Flashback reported after ~ 30 to 45 min
	20	• Flashback reported after the 5 min of attaining partially submerged combustion

The results of stability assessment of various combinations of orifice diameter and positions reveal that both submerged and partially submerged combustion resulted in flashback. For the next set of investigations only those combinations of orifice diameters and positions were chosen that resulted in flashbacks after a longer period of time.

4.2.2 With variation in mixing tube diameter

Case 1: For mixing tube diameter 29 mm

Table 4.3: Results of stability analysis with various combinations of orifice diameters and positions for mixing tube diameter 29 mm

Orifice Diameter (O_d) (mm)	**Orifice Position (O_s) (mm)**	**Stability**
0.35	5	• Lean combustion (surface flame) • Flame quenching after ignition
	10	• Submerged combustion • Flashback after ~10 min
	20	• Partially submerged combustion • Flashback at the time of fuel shutoff
	30	• Partially submerged combustion with a longer extended flame • Cracks on the burner casing after 4 trial runs
0.49	5	• Submerged combustion

		• Flashback after 4 – 4.5 h of operation
	10	• Partially submerged combustion • Flashback after 4 – 4.5 h of operation
	20	• Partially submerged combustion with a swamping extended flame • Cracks on the burner casing after 3 trial runs
0.59	5	• Partially submerged combustion • Flashback after 2 h of operation
	10	• Partially submerged combustion with swamping flame • Flashback after 2 – 3 h of operation
	20	• Partially submerged combustion with swamping flame • Flashback after 2 – 3 h of operation • Cracks on the burner casing after 2 trial runs

Case 2: For mixing tube diameter 36 mm

Table 4.4: Results of stability assessment with various combinations of orifice diameters and positions for mixing tube diameter 36 mm

Orifice Diameter (O_d) (mm)	**Orifice Position (O_s) (mm)**	**Stability**
0.35	5	• Extremely lean combustion • Flame quenching within 1 min of ignition
	10	• Lean combustion • Surface flame
	20	• Submerged combustion • Low illumination of the porous matrix
	30	• Submerged combustion • Flashback after fuel shut off
0.49	5	• Submerged combustion • Flame quenching after a few minutes
	10	• Submerged combustion • Flashback after fuel shut off
	20	• Submerged combustion • Flashback after fuel shutoff
	30	• Submerged combustion • Flashback after 2.5 h of operation
0.59	5	• Submerged combustion • Flashback after 4 h of operation

10	• Partially submerged combustion • Flashback after fuel shut off
20	• Partially submerged combustion • Flashback after 2 – 3 h of operation

The observations of the stability conditions for the various combinations of MT and orifice diameters and orifice positions reveal that the increase in MT diameter was found to increase the possibilities of submerged combustion. Upon decreasing the MT diameter, the primary air entrainment decreases due to which there are increased possibilities of the excess fuel getting combusted outside the CZ, creating a partially submerged flame. The stability analyses also imply that the operation of the self-aspirated CPRB under submerged flame condition resulted in flashback due to excessive heat re-circulation towards upstream. Additionally, in some cases of operation on partially submerged mode, the occurrences of cracks in the burner casing implied that the heat of combustion was inadequately transferred to the load and was more than the tolerance of the burner casing. Therefore, in order to reduce the upstream heat recirculation and direct the heat more towards the load, a part of the CZ from the top was exposed to the surroundings. The height of the exposed part of the CZ was termed as 'E_l', as shown in Fig. 4.6.

4.2.3 Effect of exposing top part of the combustion zone

In the case of investigating the effects of exposing the top part of the CZ on burner stability, a few of the selected cases were considered for investigations. Only those combinations that resulted in flashback after more than 4 hours of operation and led to cracks in casing were chosen for further improvements. The results of stability conditions of the selected combinations are listed in Table 4.5.

Table 4.5: Results of stability analysis for selected combinations of orifice diameter, position and mixing tube diameter

Orifice Diameter (mm)	**Orifice Position (mm)**	**Mixing tube Diameter (D_p) (mm)**	**Extension Height (E_l) (mm)**	**Stability**
0.49	5	19	5	• Low illumination of porous matrix • Flame quenching
0.35	20	29	5	• Stable partially submerged combustion

0.49	30	29	10	• Stable partially submerged combustion
			5	• Stable partially submerged combustion
			10	• Partially submerged combustion • Swamping flame
	5	29	5	• Stable submerged combustion • Low illumination of matrix
			10	• Flame quenching
	10	29	5	• Stable partially submerged combustion

With an increase in the exposed portion of the CZ, the heat recirculation upstream of the CPRB was reduced, lowering the chances of flashback, thus enhancing burner stability.

4.3 Thermal Performance Investigation

4.3.1 Performance investigation at a fixed power input of 12.5 kW

Up till now, the stability assessments were carried out at a fixed power input of 12.5 kW. Upon finding geometrical configurations supporting the stable combustion, performance investigation of the CPRB was carried out and the scope for improving the thermal efficiency (η_t) was explored. The η_t and emissions of CO and NO_x were evaluated as per the procedures described in section 3.1.2 of Chapter 3. From the results of performance investigation of the forced draft CPRB and their comparison with Conventional Burner (CB), the CO/CO_2 ratio was found to be below the BIS limit of 0.02 for all the burners in consideration. Therefore, determination of the best performing configuration of the self-aspirated CPRB was based on the increase in η_t. From the literature, the η_t was found to vary with variation in loading height (LH). The loading height is the distance of the pan from the top surface of the burner. Therefore, the η_t of the burners were tested for different loading heights.

i) Evaluation of thermal efficiency at different loading heights

The η_t of the CPRB for the stable operating conditions obtained from Table 4.5 is listed in Fig. 4.7.

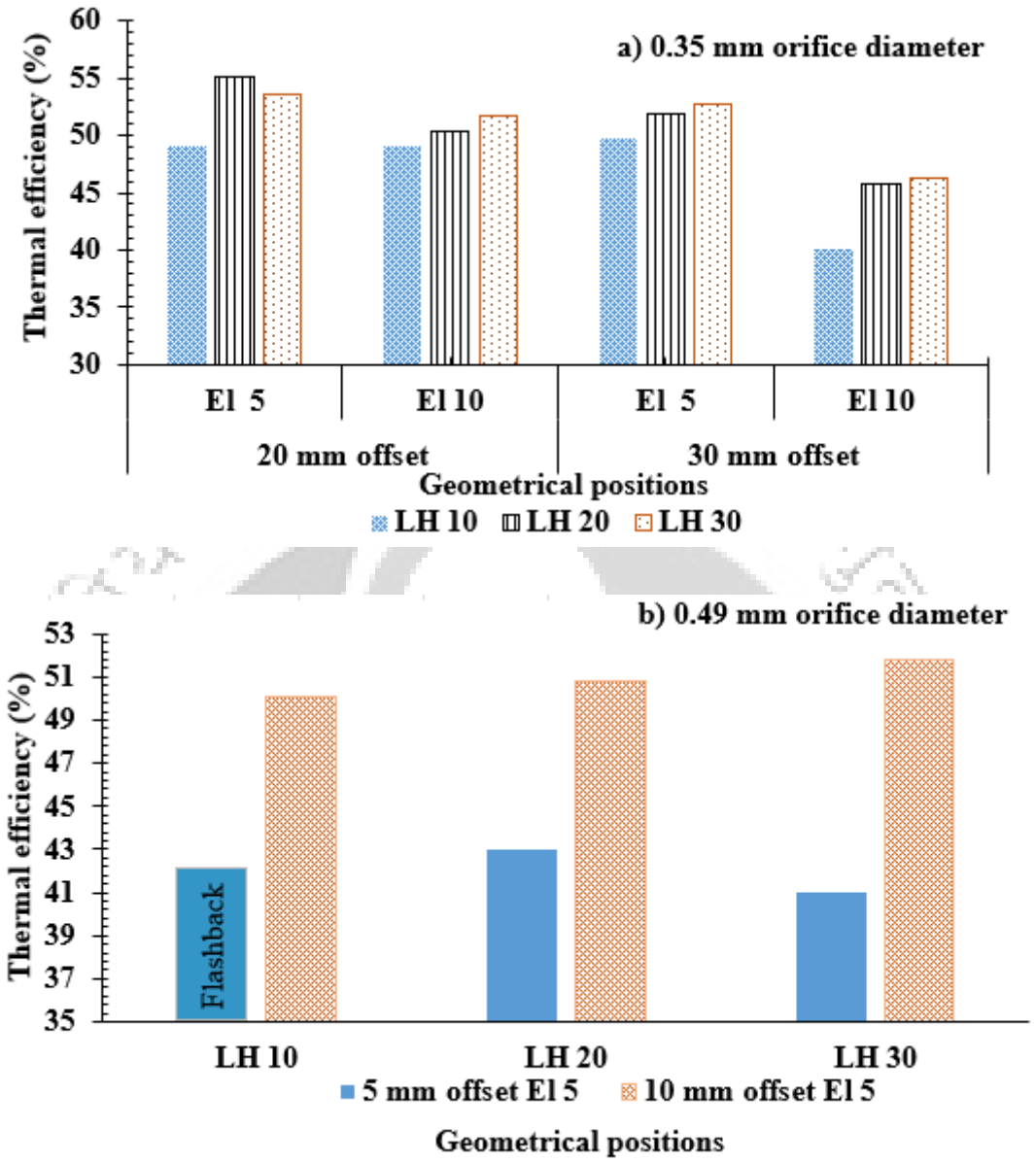

Fig. 4.7: Thermal efficiency at the stable operating conditions of the self-aspirated CPRB at orifice diameters a) 0.35 mm and b) 0.49 mm

In the case of orifice diameter 0.35 mm with orifice at 20 mm offset position, and extension height of 5 mm as shown in Fig. 4.7 a), with the increase in the LH, the η_t was observed to first increase and then decrease. At a given power input, as the LH increases from 10 mm to 20 mm, the spreading of the extended flame is reduced, which results in more concentrated heat at the bottom of the burner. However, upon a further increase in the LH, the heat losses increase and the η_t decreases. However, in case of the other geometrical positions with orifice diameter 0.35 mm, the η_t was noticed to marginally increase by a maximum value of 1% when the LH was increased from 20 to 30 mm, which lied within

the limits of uncertainty. In case of the CPRB with orifice diameter 0.49 at 5 mm offset and loading height of 10 mm (Fig. 4.7 b), flashback was observed. Due to the placement of the load nearer to the burner, the flame was pushed towards the upstream that resulted in flashback.

As inferred from Fig. 4.7, highest η_t of 55.1% was obtained when the CPRB operated for orifice diameter 0.35 mm, positioned at 20 mm offset, with E_l 5 mm and LH 20 mm. Therefore, above configuration was considered to be the optimized geometrical position. This geometrical configuration was taken up for further investigations.

ii) With variation of proximity (centre to centre distance) of the individual burners of the CPRB

The centre to centre distance or the proximity (C_s) of the individual burners of the CPRB, as shown in Fig. 4.7 (a), determines the proximity of the individual burners to each other. In case of the burner operation under partially submerged combustion mode, the extended flame impinges on the bottom surface of the load (pan) and spreads out towards the periphery. The increase in separation of the individual burners leads to the increased spreading of the flame beyond the diameter of the bottom surface of the pan as illustrated in Fig. 4.8 (b). This condition can lead to excessive heat loss from the extended flame and lead to decrease in efficiency.

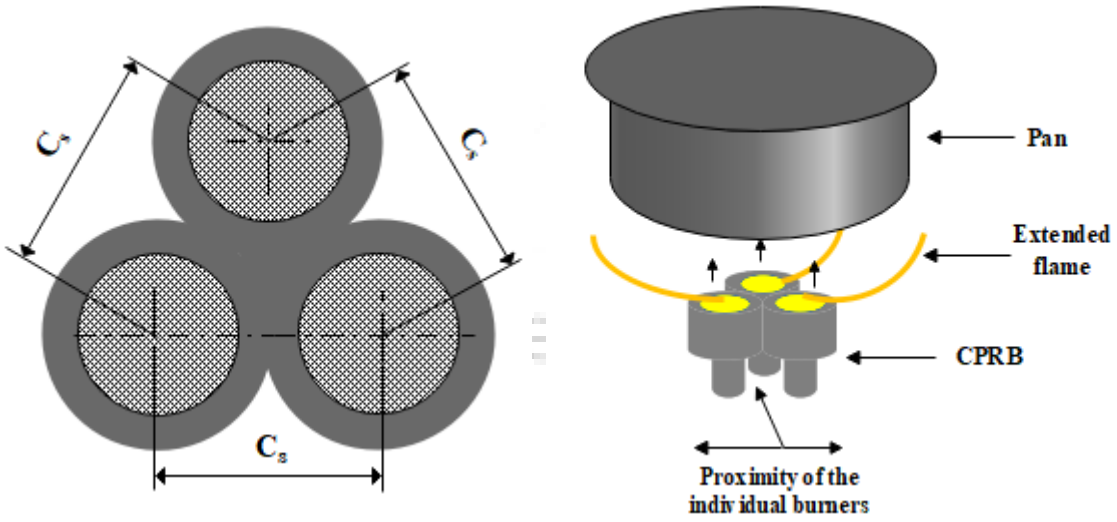

Fig. 4.8: Schematic of CPRB depicting a) centre to centre distance of each burner and b) spreading of extended flame over vessel bottom

On the other hand, when the individual burners are placed too close to each other, there is increased heat transfer among the individual burners leading to combustion instabilities and cracks in the burner casing. The η_t obtained with the change in proximity of the individual burners are listed in Table 4.6.

Table 4.6: Variation of thermal efficiency with proximity of individual burners

Proximity (cm)	Thermal efficiency (%)
15	48
13	55.1
11	Cracking of casing

4.3.2 Determination of turn-down ratio and performance of the CPRB

The self-aspirated CPRB developed was tested for its turn-down ratio and its performance for the stable range of power inputs. The performance parameters determined were stability, η_t and emissions of CO and NO_x. As mentioned previously, the stability was determined with the help of visual inspection of the burner for incidences of flashback, blow off or flame quenching and the rigidity of the burner components.

i) Determination of burner stability

As explained in Chapter 3, the stability of the CPRB was established when each individual burner operated stably and generated similar heat output. Similar to the stability conditions for forced draft operation, the stability was ascertained with the help of visual inspection for blow-off and flashback. Contrary to the forced draft CPRB, the self-aspirated CPRB was stabilized when operated on partially submerged combustion mode as observed from the results of geometrical optimization described in section 4.2. While determining the stable power input limits, the occurrence of an extended flame was not considered as a criterion of blow-off unless a swamping flame was observed. However, in addition to the above, the CPRB was checked for any damage to the burner components like the SiC foam, Alumina filter and the burner casing. The stability of the burner was ascertained when the burner components were damage free after repeated use. It is to be noted that for each power input, the CPRB was operated for a minimum of 4 h unless any visible instabilities was observed. Transient temperature mapping of the top surface of the CPRB was carried out in order to establish the similarity of the individual burners, obtain the time required to stabilize after ignition and cooling after fuel shut off.

The CPRB when operated within the power input range 8 to 14 kW, conformed to the above mentioned standards for stability. Below 8 kW, flame quenching was observed. When the CPRB was operated for power inputs above 14 kW up to 17 kW, cracks in the burner casing were observed after 2 trial runs along with swamping flame longer than 275 mm. For power inputs above 17 kW, melting of the SiC foam was observed after the first trial run. However, for all the studied range of power inputs flashback was not reported. The individual burners of the CPRB performed similarly as observed from the plots of the radial temperature variation with power input is shown in Fig. 4.9.

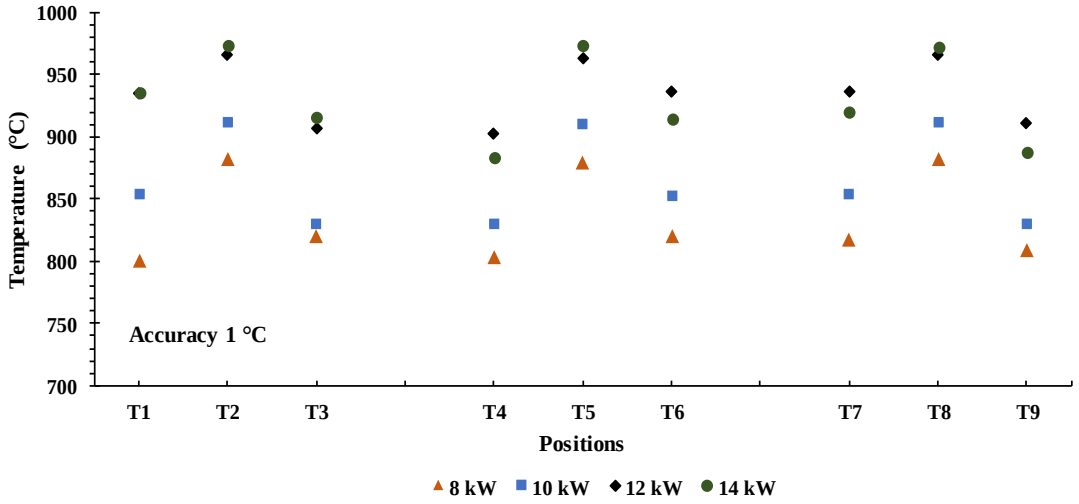

Fig. 4.9: Variation of top surface temperature of self-aspirated CPRB with power input

The maximum surface temperature was observed at the centre of each individual burner, the highest being 973 °C at a power input of 14 kW. In case of the self-aspirated CPRB, higher temperature difference (~ 90 °C) between the centre and the burner periphery was reported compared to the forced draft CPRB. The self-aspirated CPRB operated on partially submerged combustion mode because of which the excess fuel has burnt outside the CZ instead of being fully combusted inside the CZ as in submerged combustion mode. Therefore, the temperature distribution in a CPRB operating on partially submerged combustion mode is less uniform than when the CPRB is operated on submerged combustion. Nevertheless, the surface temperature distribution was considered to be uniform (Gao et al., 2011).

As mentioned previously, the CPRB for the power input range was already stable for more than 4 h. Hence, in order to determine the time required for stabilization and cooling after fuel shut off, the CPRB was operated for 2.5 h.

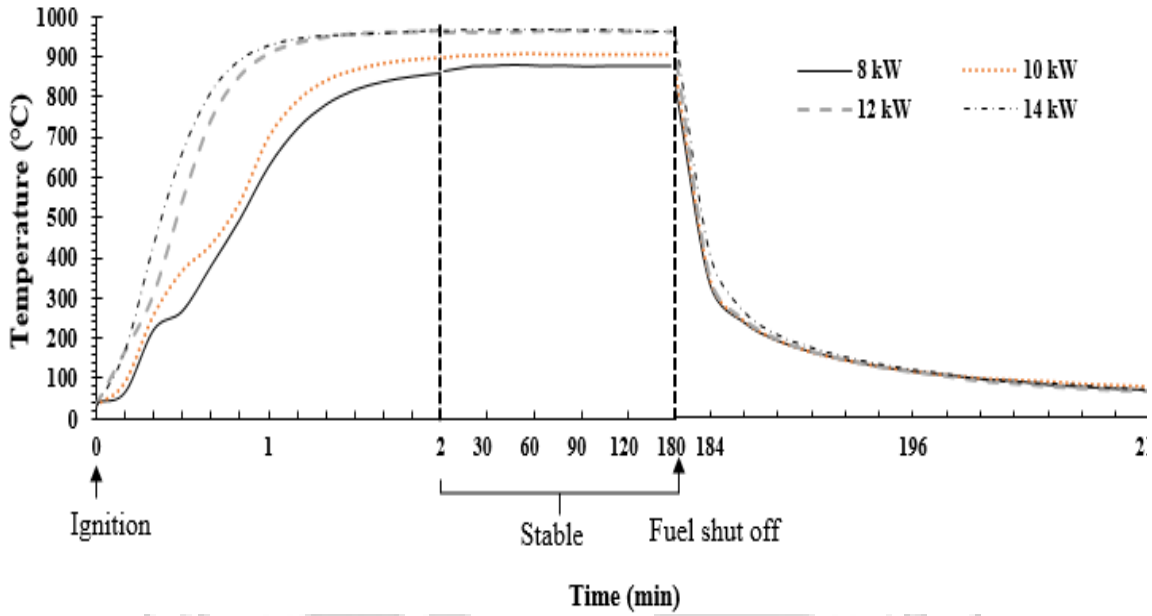

Fig. 4.10: Transient variation of top surface temperature at the centre with power input

The results of transient temperature mapping at the top surface of the CPRB for the stable range of power inputs 8 to 14 kW are illustrated in Fig. 4.9. For lower power inputs 8 and 10 kW, the CPRB stabilizes within less than 2 min. When operated at power inputs 12 and 14 kW, the CPRB takes shorter duration (~1 min) to attain invariant temperature after ignition. When the fuel was shut off, the top surface of the burner cooled rapidly from the maximum temperature to ~315 °C within 4 min. Thereafter, the CPRB cooled down to temperatures below 70 °C in 30 min. Evidently, the CPRB cooled down faster when operated at low power input, though the differences in cooling time were minuscule.

ii) Determination of thermal efficiency and emissions and comparison with Conventional Burner

The thermal efficiency and emissions of CO and NO_x of the self-aspirated CPRB and a comparison with a Conventional Burner (CB) for the stable range of power inputs are presented in Table 4.7. The results of the performance tests in terms of η_t and emissions as listed in Table 4.7 reveal that the self-aspirated CPRB performed similar to the forced draft CPRB. The highest η_t obtained was 58.8% at 8 kW and at the highest power input of 14 kW, the η_t obtained was 51.1%. The high η_t of the CPRB compared to the CB could be translated into fuel savings. Against 1 kg of fuel consumed by the CB, maximum savings of 422 g could be attained by the CPRB when operated at 14 kW. The self-aspirated CPRB performed successfully in reducing the CO and NO_x emissions. The highest CO and NO_x emissions were obtained at 14 kW and were limited to 122 ppm and 15.2 ppm, respectively.

The maximum improvements over a CB in terms of η_t and emissions were 42% and 97%, respectively.

Table 4.7: Thermal performance of self-aspirated CPRB at stable power inputs

Power input (kW)	**Thermal efficiency (%)**		**Emissions**					
			CO (ppm)		**NO_x (ppm)**		**CO/CO_2**	
	CPRB	**CB**	**CPRB**	**CB**	**CPRB**	**CB**	**CPRB**	**CB**
8	58.8	36.2	5	190	Untraceable	31	0.00007	0.0027
10	57.7	34.3	22	220	2	38	0.0003	0.003
12	55.1	32	67	341	6.2	42	0.0016	0.008
14	51.1	29.5	122	451	15.2	54	0.003	0.011

The performance of the cookstoves in terms of η_t and emissions are not sufficient to estimate the fuel and cost savings and the implications on health. In order to obtain a deeper insight to the environment friendliness availed when the CPRB is preferred over a CB, detailed Life Cycle Analyses were carried out as discussed in the following sections.

4.4 Assessment of the CPRB for its Environment Friendliness

Life Cycle Assessment (LCA) is an important evaluation method that determines the environmental and health charges incurred during the execution of a process or development, use or end-use of a product. An LCA helps to exhibit the actual environment friendliness of an item or a process, by closely evaluating associated individual. The impact characterization for the present study was carried out by midpoint and endpoint approaches. The midpoint approach exhibits indicators of the primary changes in the ecosystem like change in infrared radiation etc., and these usually occur early in the cause and effect chain. With the help of mid-point indicators, early changes occurring in the cause and effect chain can be detected without the complex modeling required in case of end-point method (Menoufi, 2011). Additionally, unwarranted conclusions on damage assessment can be avoided (Bare et al., 2000). The seven midpoint categories that represent different negative impacts on the environment include global warming measured in kg CO_2-equivalents (eq), human toxicity (kg 1,4-DB eq), terrestrial, freshwater and marine ecotoxicity (kg 1,4-DB), photochemical oxidant formation in kg NO_x-eq, and fossil fuel depletion in kg oil eq. Some of these parameters jointly or individually contribute to the damage in terms of health, resources and ecosystem. The characterization of the consequential damages to human

health, environment and resources resulting from the change in the midpoint indicators are obtained from the endpoint approach.

As described in the previous section, the CPRB was assessed for its capability to replace the conventional cookstove available in the market. These tests portrayed an overview of the benefits offered by the use of the CPRB in terms of fuel savings that can eventually lead to economic gains to the enterprises using medium scale cookstove. The results of the emission tests provided an inceptive depiction of the reduction in harmful emissions by the CPRB. These emissions released by the cookstoves are a result of combustion of LPG and are directly released to the surroundings. The results of emission were obtained for a short duration of time when the values were stable and hence the actual impact of the emissions on human lives and the environment cannot be ascertained. Apart from the emissions released from the burners, there are several other emissions released from the production of LPG, fabrication of the stoves, procurement of materials and their transport. With growing demands for sustainable products, the assessment of the cookstoves for their environment friendliness therefore becomes imperative. In order to fully comprehend the environmental implications of the newly developed CPRB and its following superiority over the CB, LCA becomes necessary.

4.4.1 Methodology for LCA study

To estimate the environmental and human health impacts of the self-aspirated CPRB in comparison to a CB, the principles for the LCA method set by ISO 14040:2006 have been adopted. The quantification of the resources consumption, environmental and health impacts throughout the entire life of the cookstoves, from their production to transport till the end of their use, can be obtained. SimaPro v.8.5.2.0 software with Ecoinvent database v3 has been used for the assessment. The ReCiPe method with the Hierarchist perspective was selected to characterize the emissions and resources used within the system boundaries.

4.4.2 Goal and scope of Life Cycle Assessment

In accordance with the studies to measure the thermal and emission performance of the CPRB, the goal of the present LCA is to compare and assess the environmental impacts of the newly developed self-aspirated CPRB and a CB. The study aims to provide a comparison of the environmental impacts of the use of medium scale cookstoves in a commercial enterprise. In this study the scope is from cradle-to-grave, in which the basic parameters like materials, transport, production, use and end-of-life (recycling) have been

considered. The domain of the study Subansiri (girls) hostel mess of Indian Institute of Technology Guwahati (IITG), where meals are prepared for 350 subscribers including hostel residents and day scholars. However, the analysis is conducted for a reference case of a single conventional burner when operated at power inputs of 8, 10, 12 and 14 kW and for a CPRB when operated at each of the corresponding power inputs. The functional unit for the CB amounts to 3109.8 kg (yearly consumption of LPG by a single CB) for a span of 1 year. The system boundary for the analysis is presented in Fig. 4.11.

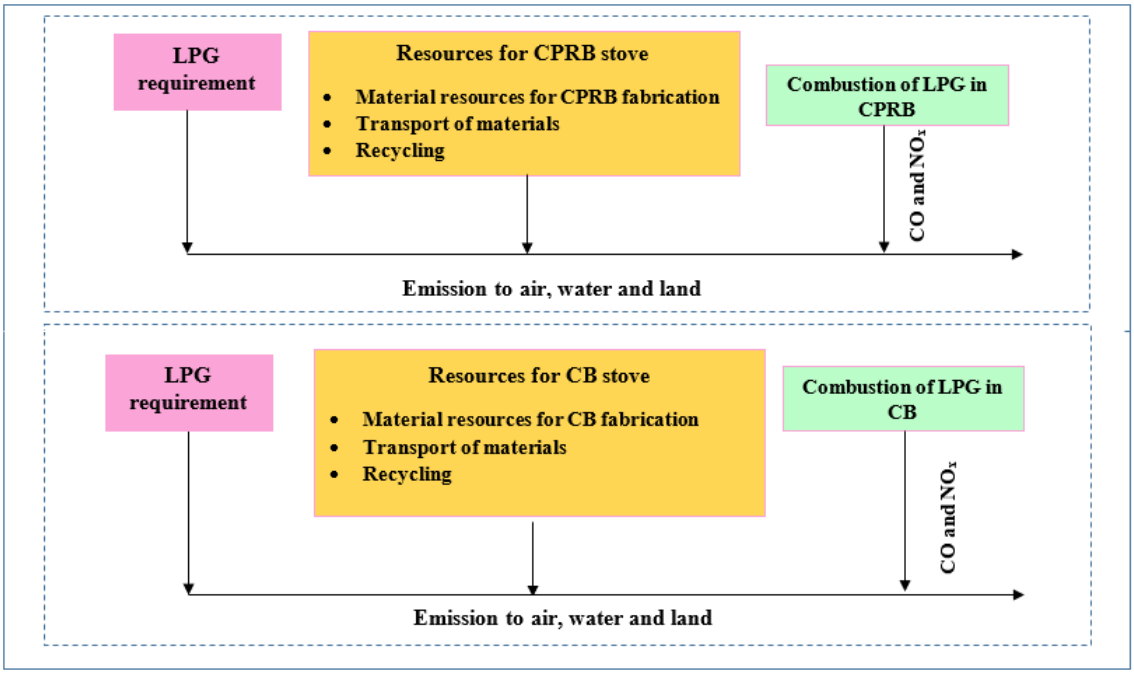

Fig. 4.11: System boundary for the Life-Cycle Assessment

The amount of LPG required by a CPRB against the functional unit (yearly fuel consumption by a CB) was calculated at each power input. The fuel consumption was calculated based on the results of η_t from the WBT conducted at each power input. The results of WBT and emission tests implied that the CPRB requires less resources and creates less damage to the environment. However, these results require to be quantified and the actual implications need to be presented. Apart from the fuel usage and the emissions, the stove consisting of the frame and burner components also impact the environment significantly. Thus the impact of the stove materials was also included in the analysis. The materials used for the CB and CPRB are listed in Table 4.8.

Table 4.8: Materials required for the stoves of CB and CPRB

CB		**CPRB**	
Material	**Weight (kg)**	**Material**	**Weight (kg)**
Brass eductor	0.096	Brass valve	0.135
Brass valve	0.085	Brass nozzle	0.076
Brass Burner head	0.303	GI socket	0.327
Copper Tube	0.061	SiC Reticulated foam	0.131
GI pipe (mixing tube)	0.071	Alumina	0.238
Mild Steel frame	9.117	Mild steel (mixing tube)	0352
		Mild Steel frame	10.142
		Refractory cement	2.5
		LPG hose pipe	0.573

4.4.3 Results of comparative LCA of CPRB and CB

The outcomes of the impact assessment through the midpoint approach are presented in Table 4.9. The results reveal that the use of CPRB for combustion can generate a minimum of 75% reduction in the climate change, fossil fuel depletion, human and ecological toxicity. The maximum reductions have been obtained at power input of 8 kW. Maximum reduction of 94% was obtained for the category marine ecotoxicity at 8 kW. Similar reduction (~92%) was obtained in the climate change category.

Table 4.9: Results of impact assessment through mid-point method

	14 kW		12 kW		10 kW		8 kW	
Impact category	CPRB	CB	CPRB	CB	CPRB	CB	CPRB	CB
Climate change (kg CO_2 eq)	11365	60964	7018	47139	3497	34649	2204	29777
Human toxicity (kg 1,4-DB eq)	6631	33488	4190	25984	2217	19047	1503	16466
Photochemical oxidant	41	198	27	155	15.4	114.4	11.4	99.55

formation (kg NMVOC)								
Terrestrial ecotoxicity (kg 1,4-DB eq)	0.61	3	0.41	2.55	0.26	1.97	0.2	1.7
Freshwater ecotoxicity (kg 1,4-DB eq)	182.12	1010	110	779	52	572	30	490
Marine ecotoxicity (kg 1,4-DB eq)	171.15	945	104	729	49	536	29.5	495
Fossil depletion (kg oil eq)	8240	33675	5713	26643	3692	19673	3026	17444

The end-point characterization indicators provide a quantified insight to the final damage caused to the environment, human health and resources. The results of the damage assessment obtained by the end-point method are listed in Table 4.10.

Table 4.10: Results of the damage assessment by the end-point method

Damage Category	**8 kW**		**10 kW**		**12 kW**		**14 kW**	
	CB	**CPRB**	**CB**	**CPRB**	**CB**	**CPRB**	**CB**	**CPRB**
Human health (DALY)	0.0838	0.00727	0.0971	0.0109	0.1327	0.0211	0.1713	0.0336
Ecosystem (species.yr)	3.2e-4	4.2e-5	3.7e-4	5.4e-5	5e-4	9.1e-5	6.3e-4	1.3e-4
Resources ($)	2985	505.7	3370	620	4566	966	5778	1400

The overall damages to the human health (DALY), ecosystems (species.yr) and resources ($) were ascertained at each power input and a comparison of the CPRB with the CB reveals that the damage reduction in each category reduced with power input. Maximum reductions

of 91%, 86.9% and 83% were obtained in damage categories of human health, ecosystems and resources.

4.5 Summary

A detailed account on the development and performance investigation of a self-aspirated Clustered Porous Radiant Burner (CPRB) has been presented. With the help of geometrical optimization, the final dimensions of the CPRB components, that supported burner stability and improved the thermal efficiency, were arrived at. Experimental investigations were carried out to find the stability, thermal efficiency and emissions. The self-aspirated CPRB was found to be stable for the power range 8 to 14 kW. The minimum time taken for achieving consistent surface temperature is less than 1 min. The highest thermal efficiency obtained was 58.8% at 8 kW. The emissions of CO and NO_x were remarkably low for the entire stable power range. Contrasting a Conventional Burner, the self-aspirated CPRB offers reduced fuel consumption and healthier environment. The Life-Cycle Analysis (LCA) conducted corroborated the findings that the use of a CPRB can bring about immense reduction in damage to human health, resources and ecosystem.

Chapter 5

Studies on Air Entrainment and Flame Stability of a Self-Aspirated Porous Radiant Burner

Preface

Design improvements of cookstove burners require detailed studies on the burner stability and combustion behavior. The use of Computational Fluid Dynamics (CFD) tool is useful in simulating burner operation and predicting parameters like temperature, pressure, velocity etc., that are useful in estimating the flow and heat transfer patterns for designing burners.

The present study exhibits the phenomenon of air entrainment and combustion of Liquefied Petroleum Gas (LPG) in a double layered Porous Radiant Burner (PRB) with the help of numerical simulations. The effects of the position and diameter of the orifice and the mixing tube diameter on the combustion parameters like flame length, uniformity in surface temperature and flashback are studied.

In the previous chapter, the development of a self-aspirated Clustered Porous Radiant Burner (CPRB) was demonstrated. As the research work on numerical simulation of air entrainment and flame stability in a double-layered PRB was not conducted, an attempt has been made to study the air entrainment and its impact on the combustion behaviour of a self-aspirated double-layered PRB. The burner used for accomplishing the objective is a self-aspirated double-layered PRB developed by Muthukumar et al. (2020). The description of the system and the results are presented in the following sections.

5.1 System Description

The present study is based on a medium-scale (5 – 7 kW) self-aspirated PRB cook-stove (Muthukumar et al., 2020). The photographic view of the set-up is shown in Fig. 5.1.

Fig. 5.1: Self-aspirated PRB (5 – 7 kW) developed by Muthukumar et al. (2020)

Table 5.1: Specifications of the self-aspirated PRB developed by Muthukumar et al. (2020)

Dimensions	Measure
Burner diameter (mm)	120
Thickness of Combustion Zone (CZ) (mm)	20
Porosity of CZ (%)	90
Thickness of Preheating Zone (PZ) (mm)	15
Porosity of PZ (%)	7
Thickness of Mixing Chamber (mm)	25
Casing wall thickness (mm)	15

The air entrainment, fuel supply and fluid flow in the PRB is the same as described in Chapter 4. The computational domain considered in this study, as shown in Fig. 2, is a simplified variant which represents the fluid flow and heat transfer in the zones. The flame propagation across the burner and beyond the top of the burner surface was captured by adding an Extended Flame Zone (EZ) (Fig. 5.2), which is a non-porous fluid zone downstream of the CZ. The locations of the radial temperature measurement and the air entrainment are shown in Fig. 5.2.

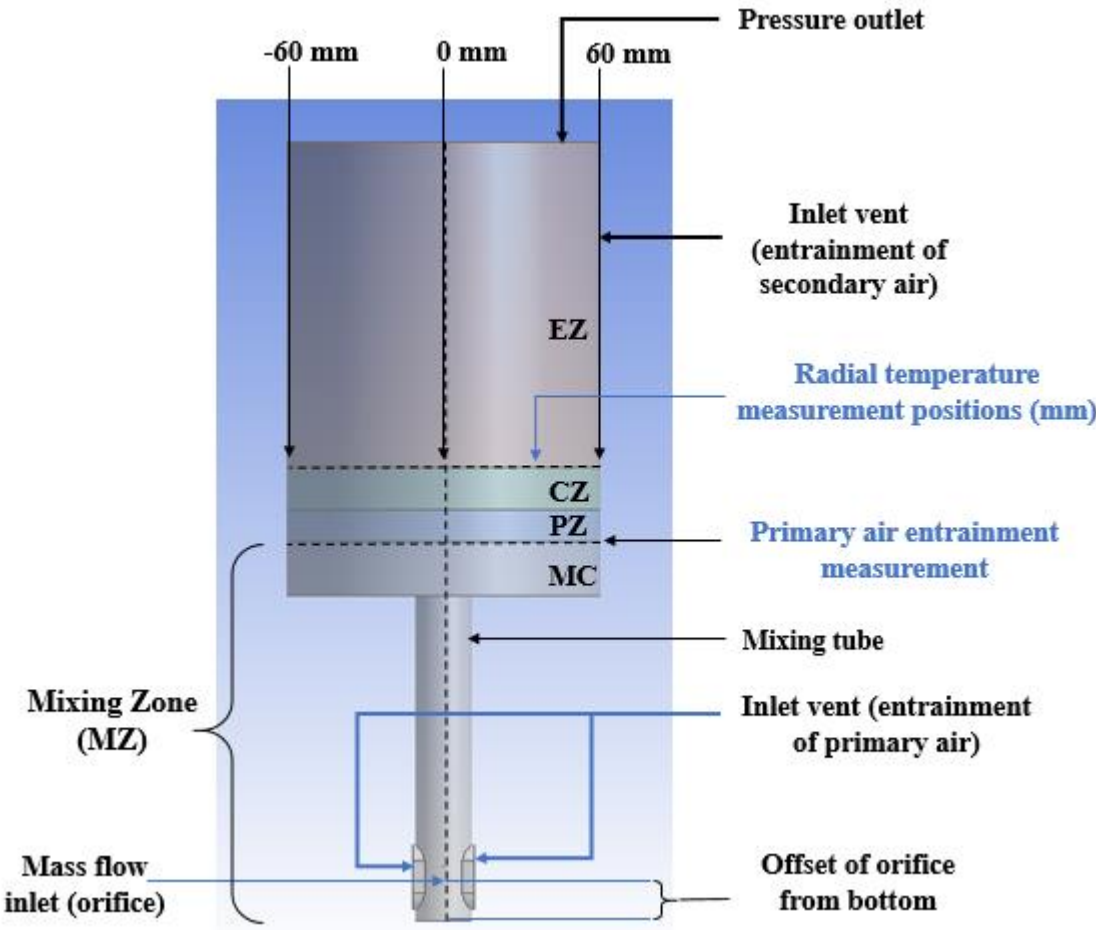

Fig. 5.2: Domain of simulation for PRB with extended flame

5.2 Numerical Methods

5.2.1 Governing equations and solution procedure

The simulations are carried out using the commercial code Ansys Fluent 20. The PMs are modelled by defining the zones as porous zones. The governing equations are based on the conservation equations of mass, momentum, energy and species (Eqs. (5.1) – (5.4b)). In the porous domains, a sink term 'S_i' in Eq. (2a) is added to the right hand side of the momentum equation (Eq. (2)) in order to account for the momentum dissipation. Along with the momentum equation, the conservation equations for the turbulent kinetic energy and its dissipation rate are also solved using the RNG k-ε model. From the results of investigation on the numerical investigations presented in Chapter 3, the Local Thermal Non-Equillibrium (LTNE) model was found to be appropriate. Therefore, LTNE model that accounts for separate energy conservation equations for the solid and the gaseous phases in the PMs, is adopted to express the energy conservation. The energy conservation

equation is solved separately for the gas and the solid phases. Eqs. (5.4a) and (5.4b) represent the energy conservation equations for the gas and the solid phases of the PMs, respectively. Eq. (5.3) represents the species conservation equation.

$$\nabla.\left(\rho_g \vec{u}\phi\right) = 0 \tag{5.1}$$

$$\nabla.\left(\phi\rho_g \vec{u}\vec{u}\right) = -\phi\nabla P + \nabla.\left(\phi\mu\nabla\vec{u}\right) \tag{5.2}$$

$$S_i = -\left(\frac{\mu}{K_1}\vec{u} + C_2\frac{1}{2}\rho_g|\vec{u}|\vec{u}\right) \tag{5.2a}$$

$$\nabla.\left(\rho_g \vec{u} Y_i\right) = -\nabla.\left(\rho_g D_m\right)\nabla Y_i + \dot{w}_i W_i \tag{5.3}$$

$$\phi\nabla\left(c_g\rho_g T_g\vec{u}\right) = \phi\nabla\left(k_g + c_g\rho_g D_t\right)\nabla T_g - \phi\sum_i \dot{w}_i h_i W_i - h_v\left(T_g - T_s\right) \tag{5.4a}$$

$$\nabla\left(k_s + \frac{16\sigma T_s^3}{3\alpha}\right)\nabla T_s - h_v\left(T_s - T_g\right) = 0 \tag{5.4b}$$

Initially, a grid independence test is carried out and the results from the optimized mesh are compared with the experimental results for the validation of the numerical model followed by subsequent simulations for PRB optimization. The model is simplified by assuming a steady flow and the gases are considered to be incompressible and having fixed thermo-physical properties. The properties of the materials constituting the PMs are listed in Table 3.2 in Chapter 3. The wall thickness was neglected, and the solid phases are assumed to be grey, diffuse and optically thick. Rosseland radiation model is used to model the radiative heat transfer in the solid phases while gas radiation has been neglected. A user defined function is employed to incorporate the radiation modelling. Mass flow inlet boundary condition is applied at the fuel inlet, whereas the air entrainment is represented by applying inlet vent condition at the primary and the secondary air inlets. Adiabatic heat transfer was applied to the walls; however, the heat transfer from the exposed zone of the CZ was realized by applying mixed heat transfer boundary condition. Finally, pressure outlet boundary condition was applied at the top of the extended flame zone.

The present case investigates the air entrainment and flame stability for different burner configurations for a power input of 5 kW. The chemical reactions were reduced to four step reactions (Eqs. (5.5a) – (5.5d)) and the reaction rate was determined using the eddy dissipation model.

$$C_3H_8 + 3.5O_2 \rightarrow 3\,CO + 4\,H_2O \tag{5.5a}$$

$$C_4H_{10} + 4.5O_2 \rightarrow 4\,CO + 5\,H_2O \quad (5.5b)$$

$$CO + 0.5\,O_2 \rightarrow CO \quad (5.5c)$$

$$N_2 + O_2 \rightarrow 2NO \quad (5.5d)$$

The convergence was considered to be obtained when the residuals of the energy equation was 10^{-6} and all other equations were 10^{-4}, respectively.

5.2.2 Determination of flame stability and Primary Aeration

The flame stability is a primary part of burner development and is a prerequisite for the performance measurement like thermal efficiency and emissions. The flame movement is obtained as a consequence of the combustion and the heat transfer processes in the PRB, which are in turn influenced by the air available for combustion, air-fuel mixture velocity and the geometrical parameters.

The flame movement, predicted from the shift in the maximum temperature locations, is deterministic of the stability of a burner and is useful in predicting the operational safety. Apart from the flame propagation, the amount of heat generated and its distribution across the burner also affects the stability. The flame movement was determined with the help of the axial temperature distribution, whereas the uniformity in the heat distribution was ascertained by the radial temperature distribution.

As the flame stability and amount of heat generated depend on the air-fuel mixture velocity and the amount of combustion air available, the study of the air entrainment is an essential requirement. The primary air entrainment or the percentage of Primary Aeration (PA) is determined as a fraction of the Stoichiometric Air Requirement (SAR) and is expressed as a percentage (Eq. 5.6f).

$$C_xH_y + \left(x + \frac{y}{4}\right) \times (O_2 + 3.76N_2) \rightarrow xCO_2 + \left(\frac{y}{2}\right) H_2O + 3.76\left(x + \frac{y}{4}\right) N_2 \quad (5.6a)$$

$$SAR = \left(x + \frac{y}{4}\right) \times 4.76 \quad (5.6b)$$

The reaction of LPG (40% C_3H_8 + 60% C_4H_{10}) with air can be expressed as

$$0.4\,C_3H_8 + 0.6C_4H_{10} + V_a\,(O_2 + 3.76\,N_2) \rightarrow \text{Products} \quad (5.6c)$$

$$V_a = \frac{\text{mol. fraction of Oxygen}}{1 - 4.76 \times (\text{mol. fraction of Oxygen})} \quad (5.6d)$$

$$PA = \frac{4.76 \times V_a}{SAR} \tag{5.6e}$$

$$\% PA = 0.17 \times V_a \times 100 \tag{5.6f}$$

The numerical model was validated by performing a grid independence test and corroborating the results with the experimental data. The experimental value of the PA was obtained by determining the oxygen concentration (by volume) in the mixing chamber by a flue gas analyser (TESTO 350) as shown in Fig. 5.3.

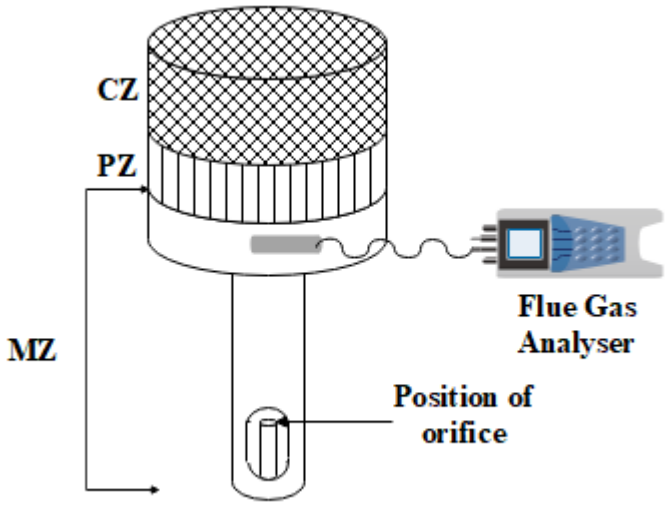

Fig. 5.3: Measurement of Primary Aeration

For the present investigation, the variation of PA and its influence on the air fuel mixture velocity, temperature and flame stability were studied for different combinations of orifice diameter, orifice position and MT diameter.

5.3 Results and Discussions

5.3.1 Validation of the numerical model

Grid independence test

A grid independence test was conducted for the first simulation whose geometrical dimensions are listed in Table 5.2 and the results are presented in Fig. 5.4. For the initial case, the diameter of the orifice was considered to be 0.5 mm positioned at an offset of 20

mm from the bottom of the MT for CZ, PZ and MC diameter of 120 mm. It is to be noted that the reference for all the axial positions is the bottom of the MT.

Table 5.2: Geometrical dimensions for grid independence test

	Diameter (mm)	Height (mm)	Porosity (%)
EZ	60	100	-
CZ	60	20	90
PZ	60	15	7
Mixing Chamber	60	25	-
Mixing Tube	29	150	-
Orifice diameter	0.5	+ 20 mm offset from bottom	

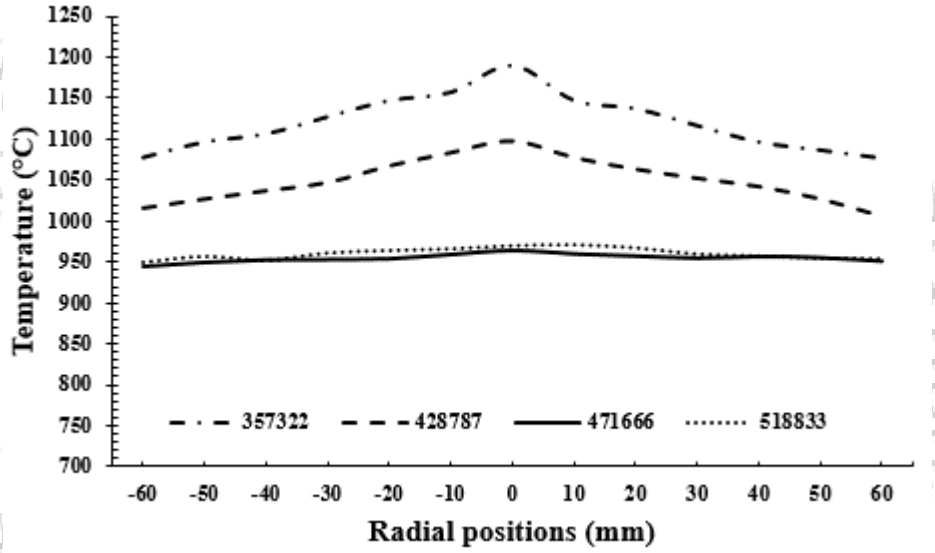

Fig. 5.4: Results of grid independence tests

Validation with experiments

For the same configuration as listed in Table 5.2, the results of experimental values of PA and radial temperature were compared with that of the numerical simulation and are presented in Table 5.3. In case of the results obtained for PA, the percentage error varied in the range of 26 – 31% while for the radial temperature, the maximum error was limited to 9.9%. The high percentage error in case of the numerical results of PA were mainly because of two reasons. The first reason is the consideration of 21% oxygen and 79% nitrogen in the derivation of the formula for percentage PA. In the experimental conditions, the percentage of oxygen varies in the range of 20.6 – 20.8% which affects the calculation

of percentage PA. The second reason is due to the accuracy of the instrument and placement of the probe at the specified positions.

Table 5.3: Comparison between results of numerical model and experiments

	Primary Aeration (%)			**Radial temperature (°C)**		
	Radial Positions in the mixing chamber			Radial Positions at the top surface of combustion zone		
	-60 mm	**0 mm**	**60 mm**	**-60 mm**	**0 mm**	**60 mm**
Experimental	40.4	41.2	40.8	1022.03	1060	1035.26
Numerical	52.3	52	53.7	944.6	963.0	950.6
Error	11.9	10.8	12.9	77.4	97	84.6

The errors in the numerical results of the radial temperature were due to the various assumptions considered for simplifying the numerical model. Nevertheless, the numerical results can be considered to be accurate as the temperature difference was within 100 °C (Dai et al., 2015).

5.3.2 Flame stability and Primary Aeration

The influence of the variation of orifice diameter, orifice position and mixing tube diameter on the flame stability and air entrainment are presented in the following as cases –

Case 1: - Variation of orifice diameter keeping the other geometrical parameters fixed

The impact of the change in orifice diameter on the temperature and primary air entrainment of the burner was numerically studied for an orifice position of 20 mm offset from the bottom of the mixing tube. The geometrical specifications of the computational domain are listed in Table 5.4.

Table 5.4: Dimensions of the computational domain for different orifice diameters

	Diameter (mm)	Length (mm)	Porosity (%)
EZ	60	150	-
CZ	60	20	90
PZ	60	15	7
Mixing Chamber	60	25	-
Mixing Tube	29	150	-
Orifice diameter	0.5, 0.25, 0.3,	+ 20 mm offset from bottom	

The operation of a PRB with an orifice diameter of 0.5 mm makes the fuel to enter the PRB with a velocity of 41 m/s as shown in Fig. 5.5. On flowing a little further (3 mm), this fuel stream gains velocity as it is joined by the air particles due to entrainment. The fluid stream consisting of air and fuel particles lose momentum as it flows through the length of the MT. As the fluid stream moves forward and enters the mixing chamber, the air-fuel mixture spreads across the MC while flowing towards the PZ.

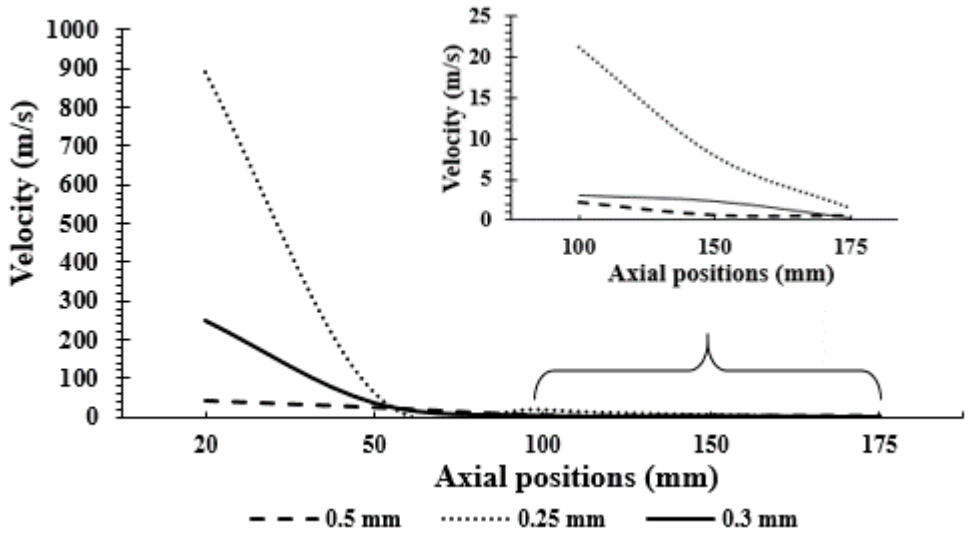

Fig. 5.5: Influence of orifice diameter on the air-fuel mixture velocity

This phenomenon favours further mixing of air and fuel and leads to a homogeneous mixture as can be seen from the plots of mole fraction of propane (Fig. 5.6) at a cross-section across the MC and the results can be further confirmed by the plots of the PA (Fig. 5.7) across the MC. As observed from Fig. 5.6, the mole fraction of propane is found to vary within range of 0.00455 to 0.00488 and thus can be regarded as uniform over the cross-sectional area of the MC. Similarly, as shown in Fig. 5.7, the percentage of PA is found to be ~53%.

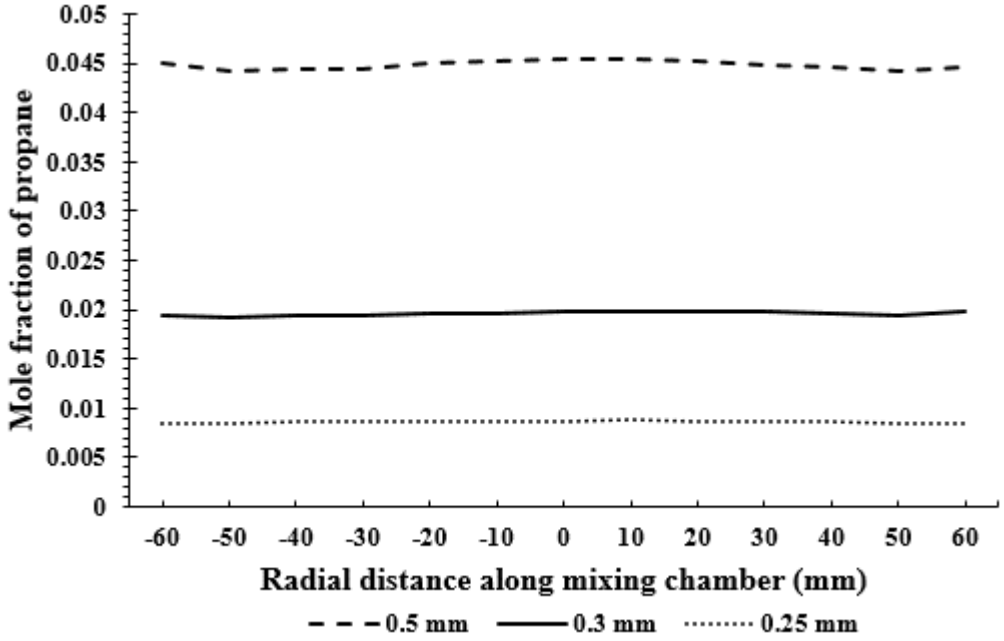

Fig. 5.6: Plots of distribution of propane across the Mixing Chamber

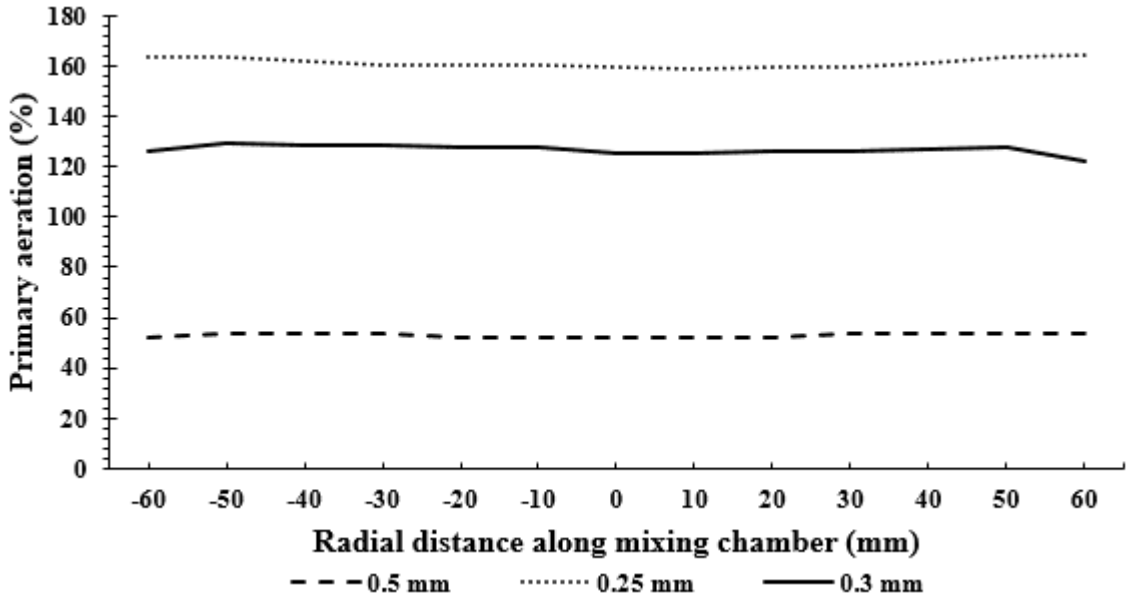

Fig. 5.7: Influence of orifice diameter on Primary Aeration

The top surface and the axial temperature distributions are plotted as shown in Fig. 5.8 and Fig. 5.9, respectively. In case of PRB of orifice diameter 0.5 mm, highest top surface temperature of 963 °C is obtained at the center and is found to vary within ±15°C with that at the peripheral positions (Fig. 5.8). The highest temperature is obtained above the top surface of the CZ for orifice diameter 0.5 mm as observed from the variation of axial temperature with orifice diameter shown in Fig. 5.9. The attainment of the highest temperature downstream of the CZ reflects the incomplete combustion in the PM due to

lack of sufficient air. Countering this shortcoming, the diameter of the orifice is decreased from 0.5 to 0.25 mm, a lower surface temperature of 693°C is obtained. This is due to increased air entrainment up to ~160% (Fig. 5.7) resulting from a high fuel jet velocity of 709 m/s (Fig. 5.5). The flame is observed to stabilize at the middle of the CZ for orifice diameter 0.25 mm.

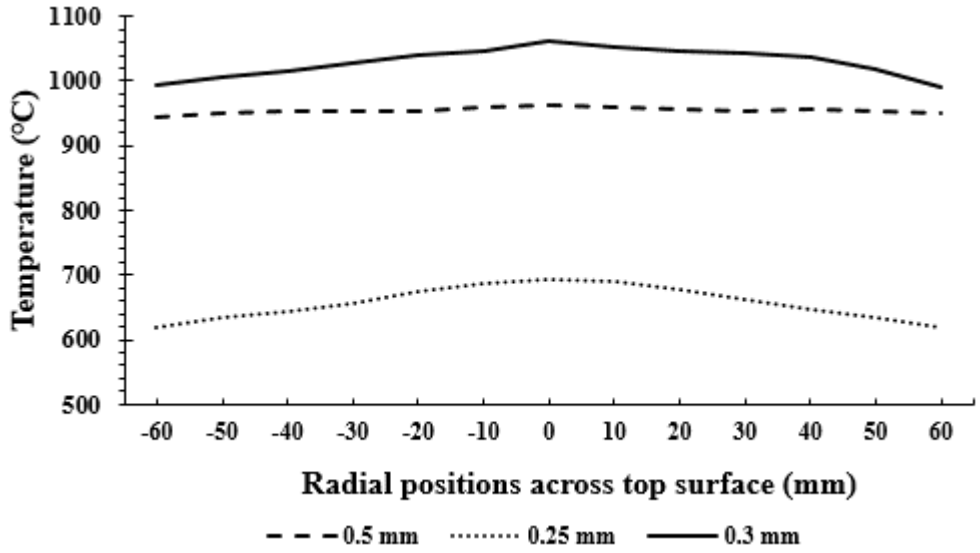

Fig. 5.8: Influence of orifice diameter on the radial temperature

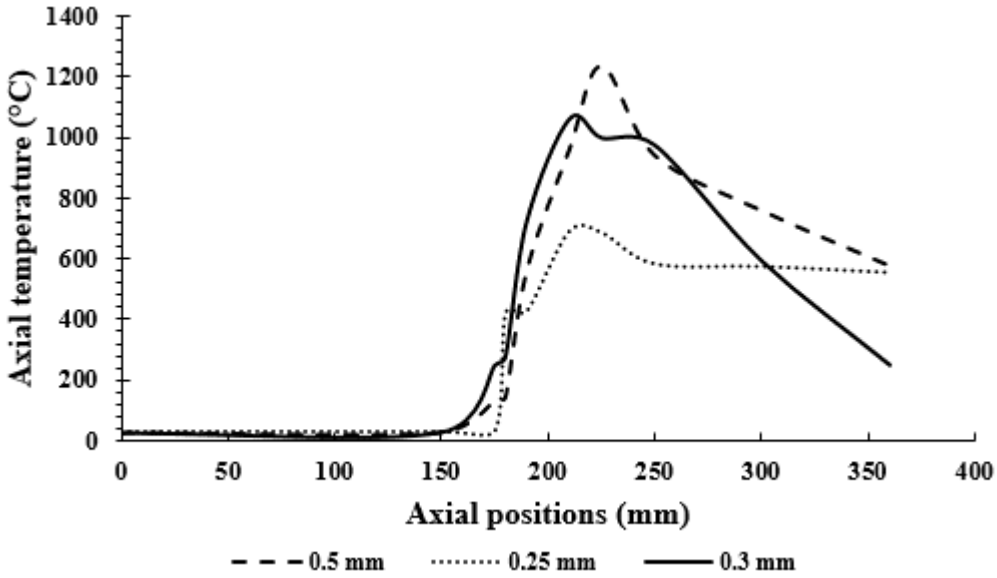

Fig. 5.9: Variation of axial temperature with change in orifice diameter

As decreasing the diameter of the orifice to 0.25 mm lead to excessive lowering of the top surface temperature, the orifice diameter is increased from 0.25 mm to 0.3 mm. Increasing the orifice diameter from 0.25 to 0.3 mm results in a reduction in the excess primary air

entrainment from 161% to 128%, leading to the increase in the top surface temperature from ~693 °C to ~1062 °C. A reduction in the fuel jet velocity in the MT makes the flame shift upstream and increases the temperature in the MC. However, a shorter exposed flame length of 110 mm compared to that obtained for orifice diameter 0.5 mm is observed (Fig. 5.9), which can be considered as a desirable feature for operational safety and reduction in heat losses to the surroundings.

The orifice diameter of 0.3 mm is therefore chosen as the optimum parameter for the subsequent simulations for geometrical optimization and performance assessment.

Case 2: - Variation of orifice position for orifice diameter 0.3 mm keeping the other geometrical parameters fixed

The results of simulation of the PRB configuration in case 1 reveal that application of orifice diameter of 0.3 mm results in the attainment of an optimum top surface temperature and flame length. However, the temperature of the mixing chamber is increased which can increase the possibilities of flashback. Further steps of optimization are carried out by changing the orifice position, keeping a fixed orifice diameter of 0.3 mm. The geometrical parameters for the numerical simulations are listed in Table 5.5.

Table 5.5: Dimensions of the computational domain for different orifice positions

	Diameter (mm)	Length (mm)	Porosity (%)
EZ	60	150	-
CZ	60	20	90
PZ	60	15	7
Mixing Chamber	60	25	-
Mixing Tube	29	150	-
Orifice diameter	0.3	+ 20, + 10, +30 offset	

The orifice positions are changed in steps of 10 mm. A change in orifice position from 20 mm offset to 10 mm offset from the bottom of the mixing tube results in a decrease in the primary aeration from 125% to 69% (Fig. 5.10). This is due to the reduced velocity of the fuel jet as it has to traverse a longer distance, thus reducing the air entrainment. As shown in Fig. 5.11, the velocity of the fuel jet is 251 m/s at the orifice for both the offset positions. However, in case of the offset position 10 mm, the mixture velocity reduces as the air-fuel mixture flows downstream beyond 13 mm.

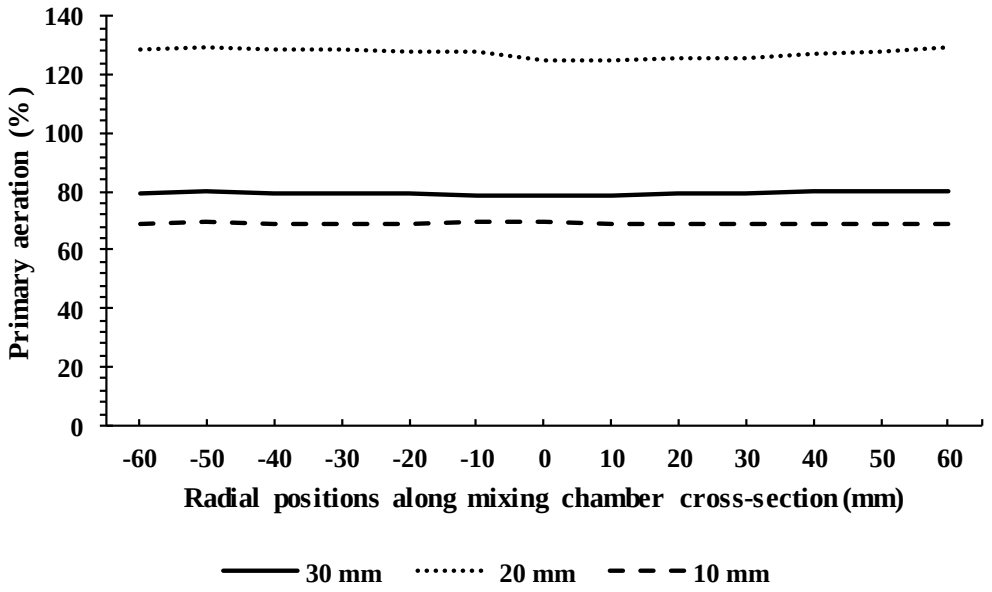

Fig. 5.10: Variation of primary air entrainment with change in orifice position

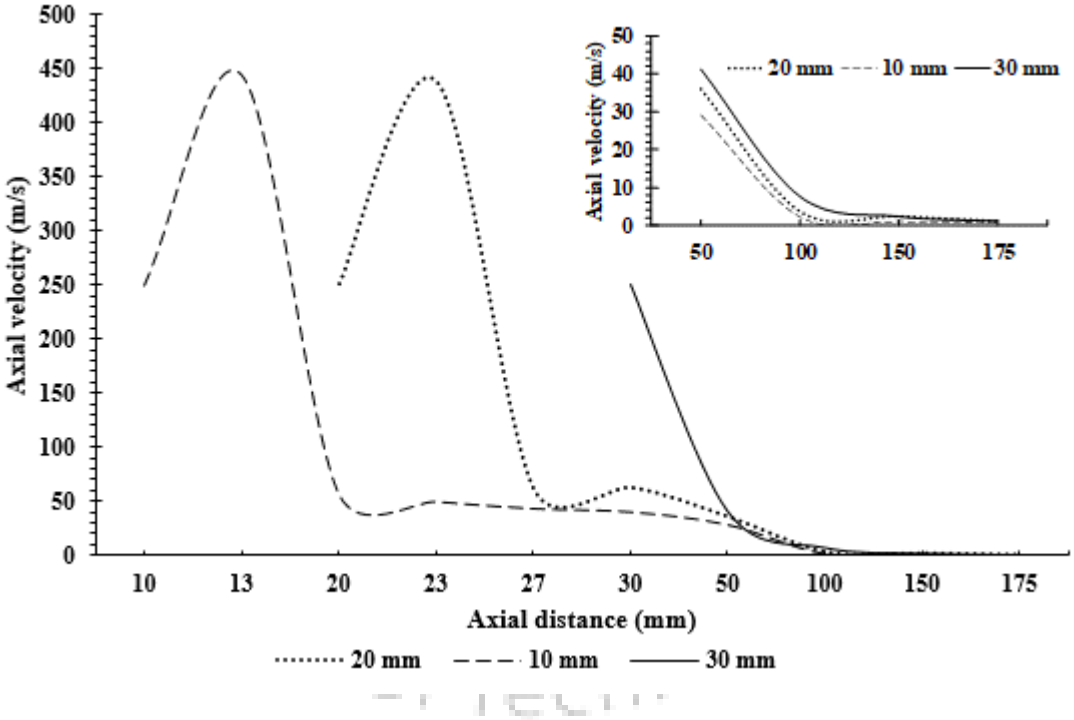

Fig. 5.11: Variation of axial velocity with change in orifice position

Despite the homogeneity in the air-fuel mixture as indicated from the plot of PA shown in Fig. 5.10, there is inhomogeneity in the top surface temperature in the case of orifice position 10 mm offset (Fig. 5.12). The highest surface temperature is obtained at 752°C, at the centre, while that at the peripheral positions is ~380°C. This non-uniformity in temperature can be attributed to the heat lost from the burner periphery and the occurrence

of combustion outside the burner as observed from the plots of the axial temperature distribution shown in Fig. 5.13.

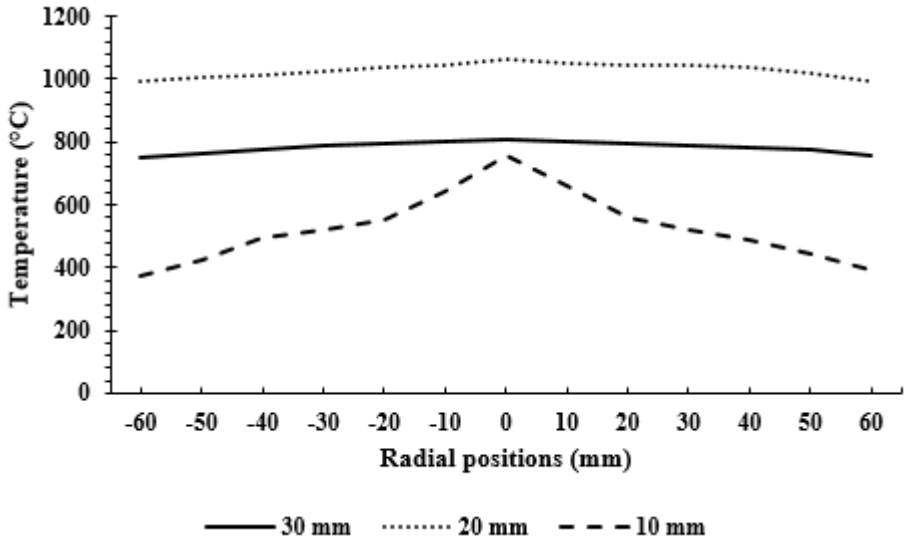

Fig. 5.12: Variation of radial temperature with change in orifice position

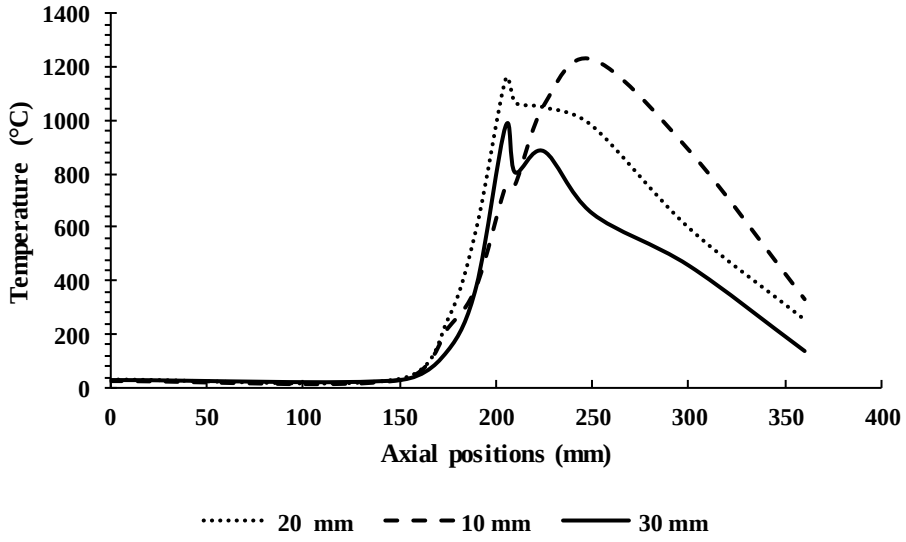

Fig. 5.13: Variation of axial temperature with change in orifice position

The unavailability of excess air for combustion due to the low PA lead to the excess fuel being burnt diffusively outside the PM and lead to the attainment of higher temperature downstream of the CZ. The maximum flame temperature attained is 1225°C, attained at a distance of 40 mm above the top surface of the burner (Fig. 5.13). However, the length of the exposed flame can be obtained as 140 mm which can be considered as a condition of blow-off, an undesirable characteristic of a PRB.

The positioning of the orifice to 30 mm, still yields reduced PA of 79%, compared to the position 20 mm, however, an increase is obtained as compared to the position 10 mm. The increase in the PA as compared to the position 20 mm favours some of the combustion to take place inside the PM and thus results in the attainment of two highest temperature points; one inside the CZ and the other outside the CZ as observed from the axial temperature plots shown in Fig. 5.13. Highest temperature of 979°C is obtained inside the CZ resulted from the combustion of fuel with the primary air entrained. The temperature decreases further downstream and increases to 886°C at a height of 15 mm above the CZ implying the occurrence of partially submerged combustion. Additionally, with the placement of the orifice at 30 mm offset lead to the reduction in the MC temperature to below 137°C, which is less than the MC temperature for the positions 20 mm and 10 mm. As the temperature at the bottom of the PZ is much below the ignition temperature of LPG (480 – 510°C), the incidences of flashback can be ruled out. The flame height is extended up to a little more than 40 mm, thus ensuring operational safety and minimum heat loss to the environment from the exposed flame.

Apart from the orifice diameter and orifice position, the air ingress into the MT is significantly influenced by the mixing tube diameter (Mishra et al., 2014; Singh et al., 2003). Towards obtaining an improved burner design, the influence of the mixing tube diameter on the air entrainment and its consequent effects on the temperature is to be determined.

Case 3: - Variation of mixing tube diameter for orifice diameter 0.3 mm at orifice offset of 30 mm

The dimensions of the various components of the PRB considered for numerical simulation for variation in mixing tube diameters are listed in Table 5.6.

Table 5.6: Dimensions of the computational domain for different Mixing Tube diameters

	Diameter (mm)	Length (mm)	Porosity (%)
EZ	60	150	-
CZ	60	20	90
PZ	60	15	7
Mixing Chamber	60	25	-
Mixing Tube	29, 36, 19	150	-

Orifice diameter	0.3	+ 30 offset from bottom

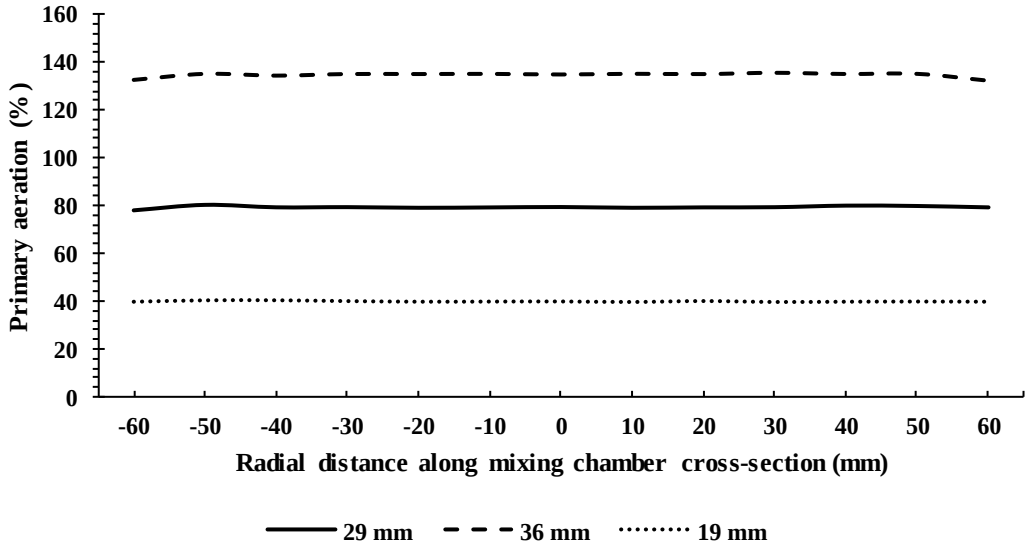

Fig. 5.14: Variation of Primary Aeration with Mixing Tube diameter

Initially, the diameter of the MT is increased from 29 to 36 mm. As perceived from Fig. 5.14, the PA is observed to increase from 79% to 135%, implying excess air in the premixed air-fuel mixture. Increasing the MT diameter decreases the static pressure inside the MT, which leads to an increase in the pressure difference between the surroundings and MT. Similar results are obtained by Mishra et al. (2014). Subsequently, increase in the PA leads to higher air-fuel mixture velocity of 1.01 m/s at the MC (Fig. 5.15) compared to 0.32 m/s in case of MT diameter 29 mm.

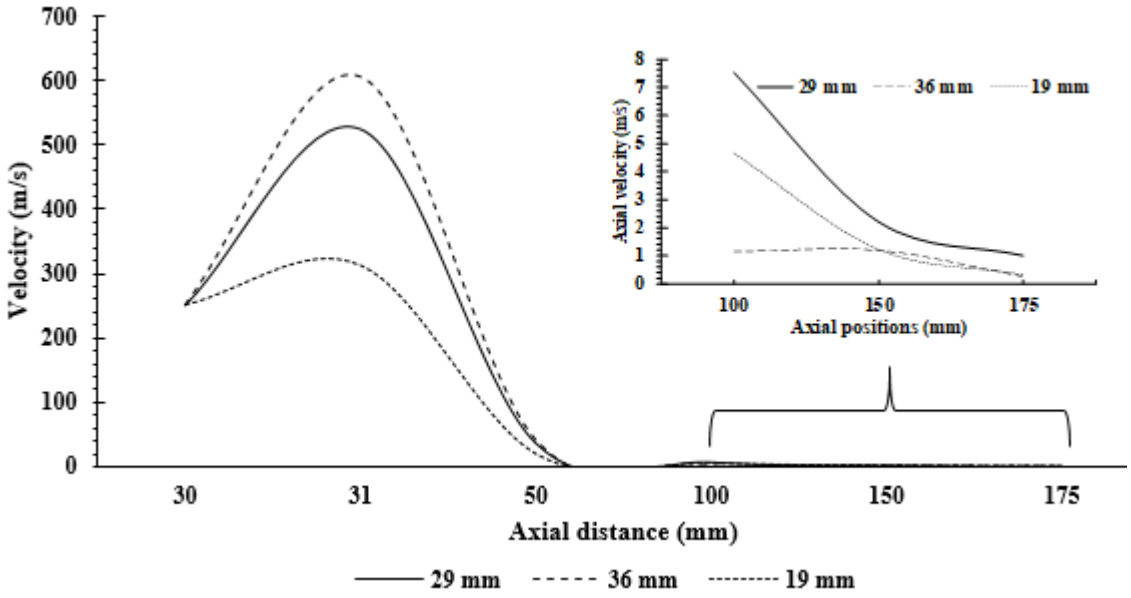

Fig. 5.15: Influence of Mixing Tube diameter on axial velocity

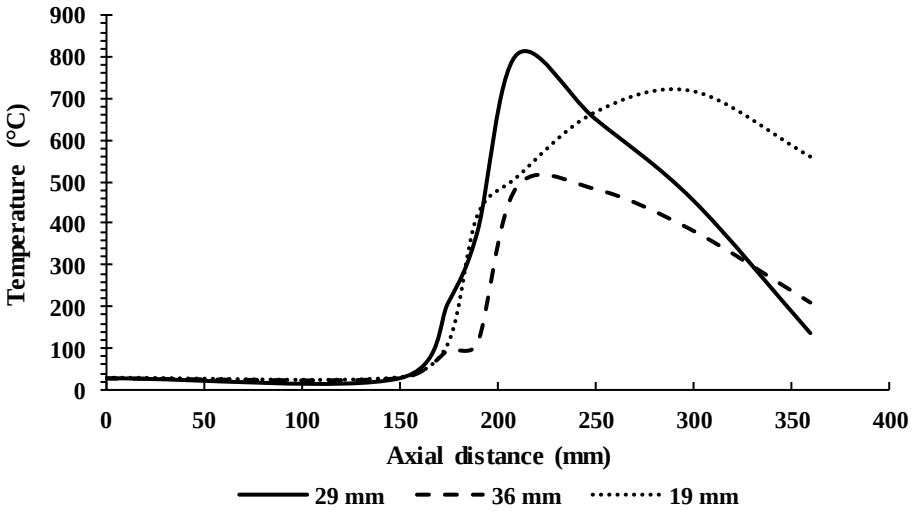

Fig. 5.16: Influence of Mixing Tube diameter on axial temperature

Consequently, after ignition at the top surface, the flame is restricted from travelling upstream (Turns, 2000) and stabilizing inside the PM, which is evident from the plots of variation axial temperature with MT diameter illustrated in Fig. 5.16. Maximum temperature of 487°C is obtained at the top surface of the CZ and the combustion is not sustained beyond 40 mm top of the CZ (Fig. 5.16). This condition can be considered as a lean blow-off as the highest temperature is not obtained more than the ignition temperature of 480°C.

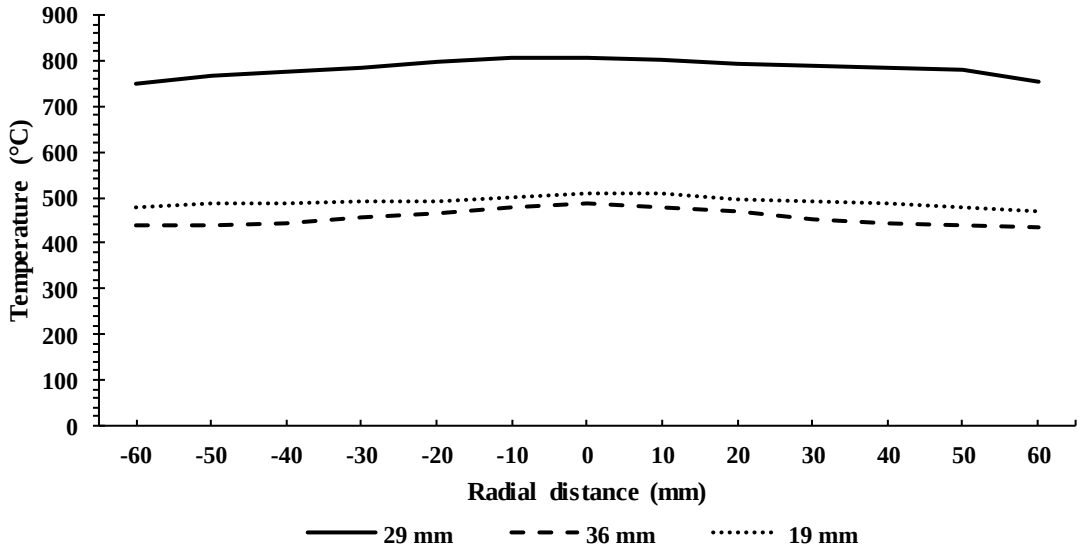

Fig. 5.17: Variation of top surface temperature with Mixing Tube diameter

As observed from Fig. 5.17, apparently the temperature distribution across the top surface of the burner was more uniform than that obtained in PRB with MT diameter 29 mm,

however, the temperature at the peripheral locations were less than the ignition temperature depicting no flame in the CZ near the walls.

Upon decreasing the diameter of the mixing tube from 29 mm to 19 mm, the PA is observed to reduce from 79% to 40.1% (Fig. 5.14), owing to the increase in the static pressure inside the MT. Due to the reduction in the air ingression, the air-fuel mixture velocity is also observed to be reduced to 0.25 m/s as compared to 0.3289 m/s for MT diameter of 29 mm at the entry of the PZ (Fig. 5.15). An advantage of such reduction in the air fuel mixture velocity is the attainment of a more uniform distribution of air fuel mixture across the MC, as the mixture does not flow quickly towards the PZ.

As observed from Fig. 5.16, in the present case of MT diameter 19 mm too, ignition is observed to occur at the top of the CZ similar to the case of MT diameter 36 mm. However, unlike the case of MT diameter 36 mm, the maximum temperature of 718°C is attained at a distance of 9 cm above the burner top surface indicating surface combustion. This is attributed to the unavailability of sufficient primary air due to decrease in the PA. As soon as excess air is made available for sustained combustion through secondary air entrainment, increase in the temperature rise can be attained outside the CZ.

Despite the advantage of the velocity reduction obtained by using MT diameter 21 mm, the variation of PA from the centre of the mixing chamber towards the periphery is within 0.05%, in the PRB with 29 mm mixing tube diameter. This can be considered as acceptable and thus the mixture can be represented as homogeneous. The homogeneity in the air fuel mixture also leads to the uniformity in the top surface temperature as observed from Fig. 5.17. Therefore, MT diameter 29 mm is considered to be the optimum diameter for PRB operation.

5.4 Summary

The present chapter explored the effect of the geometrical dimensions of the orifice, mixing tube and the orifice position on the Primary Aeration (PA) and consequently, the stability of a self-aspirated double layered Porous Radiant Burner (PRB) through numerical simulations. The results of simulation are validated with experimental results. The flame movement is traced with the help of axial temperature mapping, while the radial temperature plots shows the uniformity in heat distribution. Results shows that with

increase in the orifice diameter, the primary air entrainment decreases. Conversely, an increase in the mixing tube diameter increases the primary air entrainment. With increase in the orifice offset from the bottom of the mixing tube, the jet velocity is the same at the orifice outlet. However, the air-fuel mixture velocity is found to increase and then decrease as the mixture streamed through the mixing tube. Hence, the lowest air fuel mixture velocity of 0.69 m/s is obtained for orifice offset 10 mm. Flame instabilities like flashback and surface combustion with blow-off were reported from the orifice offsets 10 mm and 20 mm while offset of 30 mm with orifice diameter of 0.3 mm results in stable partially submerged flame. Percentage of PA and maximum temperature obtained with the stable partially submerged flame configuration are 79% and 979°C, respectively. The mixing tube diameters 19 mm and 36 mm create unstable surface flames and therefore mixing tube diameter of 29 mm is considered to be the optimized diameter.

The insights from the numerical investigation of primary air entrainment and flame stabilities in a self-aspirated PRB can be applied to study the behavior and subsequently conduct geometrical optimization of a Clustered Porous Radiant Burner (CPRB) for different operating conditions and material properties.

Chapter 6

Conclusions and Future Scope

Preface

The present chapter on the conclusion and future scope compiles the important findings of the work presented in this thesis. The exemplified investigations add another dimension to the ongoing research work in the domain of development of fuel saving and clean burners and particularly to the wing of Porous Radiant Burners (PRBs). This thesis work was focused on the development of energy-efficient and environment friendly PRB applicable for medium scale (5 – 15 kW) uses such as cooking and industrial applications.

The developments were presented in a phased manner depicting the extension and progress of the research work. Initially, by carrying out the investigations on forced draft mode of operations, the superiority of the Clustered Porous Radiant Burner (CPRB) over a single PRB was demonstrated for a fixed power input. Further investigations were conducted to study the power modulation, stability and performance characteristics and later design optimizations to obtain an optimized CPRB geometry for best performance.

Thereafter the research work was extended to develop a self-aspirated CPRB and studies on the thermal behavior and the performance were carried out. Life-Cycle Assessments were carried out to estimate the damage potential in terms of human health, resources and eco-system.

Through numerical simulations the flame stability and primary air entrainment was investigated for a self-aspirated PRB operating on partially submerged combustion mode. The optimized dimensions of the orifice diameter, position and mixing tube diameter which supported a stable flame were obtained.

6.1 Conclusions on the First Phase Developments on Forced Draft Clustered Porous Radiant Burner

- *Development of a novel burner to improve the performance of a single-PRB for commercial applications*

Towards improving the energy efficiency and reducing the emissions of Porous Radiant Burners (PRBs), a simple and innovative option of using three small sized burners in place of a single and large size PRB was presented. The reference PRB was of diameter 120 mm and the competing Clustered Porous Radiant Burner (CPRB) had individual diameter of 70 mm. By the virtue of increasing the peripheral surface area of the PRB for the same cross-sectional area, the heat distribution in the PRB was enhanced and resulted in reduced surface temperature. Initially, the investigations were conducted for a fixed power input of 12.5 kW. With respect to a single PRB, considerable improvement of thermal efficiency of 7% was obtained and massive reductions of CO emissions up to 50% was obtained.

- *Determination of suitability of the novel burner for different power requirements*

To test the CPRB for its compatibility for different applications requiring varied power inputs, the stability and performance assessments were studied at different power inputs. The stable power inputs were found to be 8 to 20 kW. Thermal efficiency in the stable band of power inputs (8 to 14 kW) ranged between 59.7% - 52.9% at equivalence ratio of 0.7. The minimum emissions were obtained at power input of 8 kW and equivalence ratio 0.7. The values of CO and NO_x at this condition were 42 and 8 ppm, respectively. Temperature and emissions were found to increase with equivalence ratio while thermal efficiency showed a negative trend.

- *Design optimization of forced draft CPRB*

Further to the developments, the prospects of improving the thermal efficiency and reducing the emissions of the CPRB were explored. With stepwise increase in the individual burner diameter, the geometry of the CPRB was optimized. CPRB with individual burner diameter of 80 mm was reported to yield the maximum thermal efficiency (59.2%), while the CPRB of diameter 90 mm yielded the lowest emissions of CO and NO_x.

6.2 Conclusions on the Second Phase Developments on Self-aspirated Clustered Porous Radiant Burner

For the CPRB to be applicable for cookstove applications, the mode of operation of the CPRB was converted from forced draft mode to self-aspirated mode. The conversion to self-aspirated mode required several modifications. The burner dimensions (diameter of preheating zone and the combustion zone) were derived from the results of optimization of the forced draft CPRB. The ensemble of components that supported the fuel and air distribution were replaced by only a single fuel header supplying equal quantities of fuel to each burner. The most significant modification was in the mixing tube that facilitated the natural air entrainment when coupled with an orifice. Thereafter, the optimized burner geometries for stable operation were determined for a fixed power input of 12.5 kW. The stability was assessed for different combinations of position and diameter of the orifice and the diameter of the mixing tube.

Various combinations of orifice diameters ad orifice positions resulted in submerged and partially submerged combustions. The duration of stability varied for each case, and that depended on the amount of heat generated, heat recirculated, and heat loss to the surroundings. Finally, stable combustion was obtained when the height of the exposed length of the combustion zone was 5 mm, for a few combinations of orifice diameter, position, and mixing tube diameter. Stable combustion was obtained when the CPRB was operated in partially submerged combustion mode. The thermal efficiency was then tested, and a maximum of 55.1% was obtained at 12.5 kW for a loading height of 20 mm. The influence of the centre to centre distance of the individual burners on the CPRB operation was also checked. Subsequently, the stability at different power inputs was determined. The CPRB was found to be stable for the power input range 8 to 14 kW. For this stable input range, the minimum time for stabilization was reported to be 1 min, while the maximum thermal efficiency obtained was 58.8%. The maximum emissions of CO and NO_x were limited to 152 and 15 ppm, respectively. Results of Life Cycle Analyses showed that the CPRB could immensely reduce damages to the environment, human health, and resources compared to a conventional burner. Maximum fuel saving of 422 g per 1 kg of LPG was obtained at a power input of 14 kW. Therefore, the CPRB was recognized as a better alternative than a conventional burner. However, the CPRB requires to be tested by

performing CCT and KPT so that the performance in actual kitchens can be tested, which is left as a future scope of the research work.

6.3 Conclusions on studies on primary air entrainment and flame stability of a Porous Radiant Burner

The design of energy-efficient burners requires knowledge of the fluid flow and heat transfer phenomenon, which are instrumental in carrying out burner optimization. Some of the factors influencing burner operation are the operating parameters such as power input, fuel type, amount of combustion air, and the geometrical parameters like the burner dimensions and the specifications of the eductor. A numerical study was conducted to find the primary air entrainment and the flame stability in a double-layered PRB.

The numerical model was well-validated with experiments and thus can also be used to study the flame behavior of the CPRB. The results show that there exists an optimized orifice and mixing tube diameter and orifice offset from the bottom of the mixing tube for stable combustion in a PRB. With a decrease in orifice diameter, the velocity of the fuel jet was observed to increase, resulting in increased Primary Aeration (PA). PA significantly influences burner stability as the heat generated from combustion depends on the amount of primary air. Maximum PA obtained was 160% for a PRB of orifice diameter of 0.25 mm at 20 mm offset and mixing tube of diameter 29 mm. The PRB was found to operate stably under partially submerged mode of combustion with an orifice of diameter 0.3 mm placed at 30 mm offset from the bottom of the mixing tube of diameter 29 mm.

The valuable insights from the above study can be employed to perform geometrical optimization and studies on flame stability while designing and characterizing future PRBs, especially for designing CPRBs with multiple individual burners.

6.4 Future Scope

The major findings observed from the present thesis work contribute to the knowledge in the design of new burners and pave paths for further investigations in similar areas. The research work can be extended to the following –

i) The impact of clustering more than 3 PRBs on the thermal performance

ii) Studies on improving the eductor for CPRB for improvement in air entrainment and improving stability

iii) Influence of increasing the peripheral surface area through clustering on the chemical kinetics

iv) Numerical studies can be carried on time dependent model to obtain detailed knowledge on flame stability

References

Addamane, S.R., Hajilou, M., Belmont, E.L., 2016. Experimental and analytical study of a porous media reformer with passive air entrainment. Int. J. Hydrogen Energy 41, 12738–12746. https://doi.org/10.1016/j.ijhydene.2016.05.035

Al-attab, K.A., Ho, J.C., Zainal, Z.A., 2015. Experimental investigation of submerged flame in packed bed porous media burner fueled by low heating value producer gas. Exp. Therm. Fluid Sci. 62, 1–8. https://doi.org/10.1016/j.expthermflusci.2014.11.007

Aroonjarattham, P., 2016. The parametric studied of high pressure gas burner affect thermal efficiency. Eng. J. 20, 33–48. https://doi.org/10.4186/ej.2016.20.3.33

Avdic, F., Adzic, M., Durst, F., 2010. Small scale porous medium combustion system for heat production in households. Appl. Energy 87, 2148–2155. https://doi.org/10.1016/j.apenergy.2009.11.010

Babkin, V.S., Korzhavin, A.A., Bunev, V.. A., 1991. Propagation of Premixed Gaseous Explosion Flames in Porous Media. Combust. Flame 87, 182–190.

Baiquan, L., Huaming, D., Chaoqun, W., Qingzhao, L., Ke, W., Yuanzhen, Z., 2014. Combustion characteristics of low concentration coal mine methane in divergent porous media burner. Int. J. Min. Sci. Technol. 24, 671–676. https://doi.org/10.1016/j.ijmst.2014.03.027

Bakry, A., Al-Salaymeh, A., Al-Muhtaseb, A.H., Abu-Jrai, A., Trimis, D., 2011. Adiabatic premixed combustion in a gaseous fuel porous inert media under high pressure and temperature: Novel flame stabilization technique. Fuel 90, 647–658. https://doi.org/10.1016/j.fuel.2010.09.050

Bare, J.C., Hofstetter, P., Pennington, D.W., Udo De Haes, H.A., 2000. Life Cycle Impact Assessment Workshop Summary: LCIA Midpoints versus Endpoints: The Sacrifices and Benefits. Int. J. Life Cycle Assess. 5, 319–326.

Bouma, P.H., Eggels, G.M., Goey, L.P.H., Nieuwenhuizen, J.K., Drift, A. Van Der, 1995. A Numerical and Experimental Study of the No-Emission of Ceramic Foam Surface

Burners. Combust. Sci. Technol. 108, 193–203. https://doi.org/10.1080/00102209508960398

Bubnovich, V., Toledo, M., Henríquez, L., Rosas, C., Romero, J., 2010. Flame stabilization between two beds of alumina balls in a porous burner. Appl. Therm. Eng. 30, 92–95. https://doi.org/10.1016/j.applthermaleng.2009.04.001

Bureau of Indian Standards, 1999. Indian Standard Commercial Burners using LPG at inlet pressure up to 147.1 k-N/m2 (1500 gf/cm2) - Specification.

Chaelek, A., Grare, U.M., Jugjai, S., 2019. Self-aspirating/air-preheating porous medium gas burner. Appl. Therm. Eng. 153, 181–189. https://doi.org/10.1016/j.applthermaleng.2019.02.109

Chen, C.-H., Gowdagiri, S., Kumar, S., Ronney, P.D., 2009. Numerical and Experimental Study in Swiss Roll Heat-Recirculating Burner. PowerMEMS 2009 Work. 605–608.

Dai, H., Lin, B., Zhai, C., Hong, Y., Li, Q., 2015. Subadiabatic combustion of premixed gas in ceramic foam burner. Int. J. Heat Mass Transf. 91, 318–329. https://doi.org/10.1016/j.ijheatmasstransfer.2015.07.122

Data, O.W. in, 2021. low-carbon-energy-vs-global [WWW Document]. URL https://ourworldindata.org/grapher/low-carbon-energy-vs-global

Donoso-García, P., Henríquez-Vargas, L., 2015. Numerical study of turbulent porous media combustion coupled with thermoelectric generation in a recuperative reactor. Energy 93, 1189–1198. https://doi.org/10.1016/j.energy.2015.09.123

Du, Z., Sarofim, A.F., Longwell, J.P., Tognotti, L., 1991. The CO/CO2 Ratio in the Products of the Carbon-Oxygen Reaction, in: Lahaye, J., Ehrburger, P. (Eds.), Fundamental Issues in Control of Carbon Gasification Reactivity. Springer Netherlands, Dordrecht, pp. 91–106. https://doi.org/10.1007/978-94-011-3310-4_5

Durst, F., Trimis, D., Dimaczek, G., 1996. Burners having porous material of varying porosity. 5522723.

Facts on Cooking Energy - energypedia [WWW Document], n.d. URL https://energypedia.info/wiki/Facts_on_Cooking_Energy (accessed 9.23.21).

Gal, P., Jecha, D., Jícha, J., Stehlík, P., 2017. Selective non-catalytic reduction (SNCR) and its efficiency with respect to various combustion parameters. Chem. Eng. Trans. 56, 1915–1920. https://doi.org/10.3303/CET1756320

Gao, H., Qu, Z., Tao, W., He, Y., Zhou, J., 2011. Experimental study of biogas combustion in a two-layer packed bed burner. Energy and Fuels 25, 2887–2895. https://doi.org/10.1021/ef200500j

Global Energy Review 2021, 2021.

H.R.N. Jones, 2005. THE APPLICATION OF COMBUSTION PRINCIPLES TO DOMESTIC GAS BURNER DESIGN. Taylor & Francis e-Library, London.

Hanamura, K., Echigo, R., Zhdanok, A., 1993. Superadiabatic combustion in a porous medium. Int. J. Heat Mass Transf. 36, 3201–3209.

Hardesty, D.R., Weinberg, F.J., 1973. Burners Producing Large Excess Enthalpies. Combust. Sci. Technol. 8, 201–214. https://doi.org/10.1080/00102207308946644

Hashemi, S.M., Hashemi, S.A., 2017. Flame stability analysis of the premixed methane-air combustion in a two-layer porous media burner by numerical simulation. Fuel 202, 56–65. https://doi.org/10.1016/j.fuel.2017.04.008

Herrera, B., Cacua, K., Olmos-Villalba, L., 2015. Combustion stability and thermal efficiency in a porous media burner for LPG cooking in the food industry using Al2O3 particles coming from grinding wastes. Appl. Therm. Eng. 91, 1127–1133. https://doi.org/10.1016/j.applthermaleng.2015.08.079

Hoda, S.N., Nassab, S.A.G., Ebrahim, J.J., 2019. Three dimensional numerical simulation of combustion and heat transfer in porous radiant burners. Int. J. Therm. Sci. 145, 106024. https://doi.org/10.1016/j.ijthermalsci.2019.106024

Holman, J.P., 2012. Experimental Methods for Engineers, 8th ed. McGraw-Hill, New York.

Hsu, P.F., Evans, W.D., Howell, J.R., 1993. Experimental and Numerical Study of Premixed Combustion Within Nonhomogeneous Porous Ceramics. Combust. Sci. Technol. 90, 149–172. https://doi.org/10.1080/00102209308907608

Indian Food Services Industry - Market Analysis - StockTalk [WWW Document], n.d. URL https://www.stocktalk.in/indian-food-services-industry-market-analysis/ (accessed 9.23.21).

Janvekar, A.A., Miskam, M.A., Abas, A., Ahmad, Z.A., Juntakan, T., Abdullah, M.Z., 2017. Effects of the preheat layer thickness on surface/submerged flame during porous media combustion of micro burner. Energy 122, 103–110. https://doi.org/10.1016/j.energy.2017.01.056

Jugjai, S., Rungsimuntuchart, N., 2002. High efficiency heat-recirculating domestic gas burners. Exp. Therm. Fluid Sci. 26, 581–592. https://doi.org/10.1016/S0894-1777(02)00164-4

Jugjai, S., Sanitjai, S., 1996. Parametric studies of thermal efficiency in a proposed porous radiant recirculated burner (PRRB): A design concept for the future burner. RERIC Int. Energy J. 18.

Kapsalyamova, Z., Mishra, R., Kerimray, A., Karymshakov, K., Azhgaliyeva, D., 2021. Why energy access is not enough for choosing clean cooking fuels? Evidence from the multinomial logit model. J. Environ. Manage. 290, 112539. https://doi.org/10.1016/j.jenvman.2021.112539

Kolluri, P., Kamal, A., Gollahalli, S.R., 1996. Application of Noncircular Primary-Air Inlet Geometries in the Inshot Burners of Residential Gas Furnaces. Trans. ASME 118, 58–64.

Kotani, Y., Takeno, T., 1982. An experimental study on stability and combustion characteristics of an excess enthalpy flame, in: Nineteenth Symposium (International) on Combustio. pp. 1503–1509. https://doi.org/10.1016/S0082-0784(82)80327-5

Kulkarni, M.R., Peck, R.E., 1996. Analysis of a bilayered porous radiant burner. Numer. Heat Transf. Part A Appl. 30, 219–232. https://doi.org/10.1080/10407789608913837

Laphirattanakul, P., Laphirattanakul, A., Charoensuk, J., 2016. Effect of self-entrainment and porous geometry on stability of premixed LPG porous burner. Appl. Therm. Eng. 103, 583–591. https://doi.org/10.1016/j.applthermaleng.2016.03.079

Leonardi, S.A., Viskanta, R., Gore, J.P., 2003. Analytical and experimental study of combustion and heat transfer in submerged flame metal fiber burners/heaters. J. Heat Transfer 125, 118–125. https://doi.org/10.1115/1.1527910

Liquified Petroleum Gas Burners and Equipment, 2009.

Liu, H., Wu, D., Xie, M., Liu, H., Xu, Z., 2019. Experimental and numerical study on the lean premixed filtration combustion of propane/air in porous medium. Appl. Therm. Eng. 150, 445–455. https://doi.org/10.1016/j.applthermaleng.2018.12.155

Menoufi, K.A.I., 2011. Life Cycle Analysis and Life Cycle Impact Assessment methodologies: A state of the art. Disertation.

Min, D.K., Shin, H.D., 1991. Laminar premixed flame stabilized inside a honeycomb ceramic. Int. J. Heat Mass Transf. 34, 341–356.

Mishra, D.P., Paramanik, S.C., 2019. Computation of air entrainment into a mixing pipe: An experimental and numerical analysis. J. Mech. Eng. 16, 11–28.

Mishra, D.P., Samantaray, M.K., Dash, S.K., 2014. Maximum air entrainment into a mixing pipe through optimum design. Ships Offshore Struct. 9, 605–618. https://doi.org/10.1080/17445302.2014.881246

Mishra, N.K., 2015. Development of Self-Aspirated Two-Layer Porous Radiant Burners for LPG Cooking Applications. Indian Institute of Technology Guwahati.

Mishra, N.K., Mishra, S.C., Muthukumar, P., 2015. Performance characterization of a medium-scale liquefied petroleum gas cooking stove with a two-layer porous radiant burner. Appl. Therm. Eng. 89, 44–50. https://doi.org/10.1016/j.applthermaleng.2015.05.077

Mishra, N.K., Muthukumar, P., 2018. Development and testing of energy efficient and environment friendly porous radiant burner operating on liquefied petroleum gas. Appl. Therm. Eng. 129, 482–489. https://doi.org/10.1016/j.applthermaleng.2017.10.068

Mujeebu, M.A., Abdullah, M.Z., A. Bakar, M.Z., Mohamad, A.A., 2011a. A mesoscale premixed LPG burner with surface combustion in porous ceramic foam. Energy

Sources, Part A Recover. Util. Environ. Eff. 34, 9–18. https://doi.org/10.1080/15567030903515062

Mujeebu, M.A., Abdullah, M.Z., Mohamad, A.A., 2011b. Development of energy efficient porous medium burners on surface and submerged combustion modes. Energy 36, 5132–5139. https://doi.org/10.1016/j.energy.2011.06.014

Muthukumar, P., Kaushik., L.K., Arun Kumar, M., 2020. Eco-Frindly and Energy-Efficient LPG Cooking Stove with Naturally-Aspirated Porous Radiant Burner for Ccommercial Kitchens. 202031009304.

Muthukumar, P., Kaushik, L.K., 2020. Energy Efficient and Eco-Friendly LPG Domestic Cooking Stove With A Two-Layer Porous Radiant Burner. 202031009356.

Muthukumar, P., Shyamkumar, P.I., 2013. Development of novel porous radiant burners for LPG cooking applications. Fuel 112, 562–566. https://doi.org/10.1016/j.fuel.2011.09.006

Nakayama, A., Kuwahara, F., 1999. A macroscopic turbulence model for flow in a porous medium. J. Fluids Eng. Trans. ASME 121, 427–433. https://doi.org/10.1115/1.2822227

Namkhat, A., Jugjai, S., 2010. Primary air entrainment characteristics for a self-aspirating burner: Model and experiments. Energy 35, 1701–1708. https://doi.org/10.1016/J.ENERGY.2009.12.020

Nimvari, M.E., Maerefat, M., Jouybari, N.F., El-hossaini, M.K., 2013. Numerical simulation of turbulent reacting flow in porous media using two macroscopic turbulence models. Comput. Fluids 88, 232–240. https://doi.org/10.1016/j.compfluid.2013.09.012

NIST Property Data Summary - NIST Ceramics Data Portal [WWW Document], n.d. URL https://srdata.nist.gov/CeramicDataPortal/Pds/Scdscs (accessed 11.18.20).

Panigrahy, S., Mishra, N.K., Mishra, S.C., Muthukumar, P., 2016. Numerical and experimental analyses of LPG (liquefied petroleum gas) combustion in a domestic cooking stove with a porous radiant burner. Energy 95, 404–414.

https://doi.org/10.1016/j.energy.2015.12.015

Panigrahy, S., Mishra, S.C., 2016. Analysis of combustion of liquefied petroleum gas in a porous radiant burner. Int. J. Heat Mass Transf. 95, 488–498. https://doi.org/10.1016/j.ijheatmasstransfer.2015.12.017

Pantangi, V.K., Karuna Kumar, A.S.S.R., Mishra, S.C., Sahoo, N., 2007. Performance Analysis of Domestic LPG Cooking Stoves with Porous Media. Int. Energy J. 8, 139–144.

Pantangi, V.K., Mishra, S.C., Muthukumar, P., Reddy, R., 2011. Studies on porous radiant burners for LPG (liquefied petroleum gas) cooking applications. Energy 36, 6074–6080. https://doi.org/10.1016/j.energy.2011.08.008

Pedras, M.H.J., de Lemos, M.J.S., 2001. Macroscopic turbulence modeling for incompressible flow through undefromable porous media. Int. J. Heat Mass Transf. 44, 1081–1093. https://doi.org/10.1016/S0017-9310(00)00202-7

Petroleum Planning & Analysis Cell, 2021. Lpg profile (Data on LPG Marketing).

Primary energy consumption by source, 2020 [WWW Document], n.d. URL https://ourworldindata.org/grapher/primary-energy-source-bar?country=USA~CHN~CAN~IND~BRA~ZAF~GBR~FRA~SWE (accessed 3.12.22).

Pritchard, R., Guy, J. J., and Connor, N. E., 1977. Handbook of industrial gas utilization: engineering principles and practice. United States: N. p., Web.

Reis, L.C.B.S., Carvalho, J.A., Nascimento, M.A.R., Rodrigues, L.O., Dias, F.L.G., Sobrinho, P.M., 2014. Numerical modeling of flow through an industrial burner orifice. Appl. Therm. Eng. 67, 201–213. https://doi.org/10.1016/j.applthermaleng.2014.02.036

Shi, J.-R., Xie, M.-Z., Liu, H., Liu, H.-S., Zhang, X.-S., Xu, Y.-N., 2011. Two-dimensional numerical study of combustion and heat transfer in porous media combustor-heater. Proc. Combust. Inst. 33, 3309–3316. https://doi.org/10.1016/j.proci.2010.07.026

Singh, G., Sundararajan, T., Bhaskaran, K.A., 2003. Mixing and Entrainment

Characteristics of Circular and Noncircular Confined Jets. J. Fluids Eng. 125, 835–842. https://doi.org/10.1115/1.1595676

Singh, G., Sundararajan, T., Shet, U.S.P., 1999. Entrainment and mixing studies for a variable density confined jet. Numer. Heat Transf. Part A Appl. 35, 205–224. https://doi.org/10.1080/104077899275335

Singh, N., Chhabra, S., Sehgal, S.S., Singh, I., 2017. Performance analysis of porous radiant burners for cooking applications. Int. J. Eng. Technol. 6, 65. https://doi.org/10.14419/ijet.v6i3.7868

Takeno, T., Sato, K., 1979. An Excess Enthalpy Flame Theory. Combust. Sci. Technol. 20, 73–84. https://doi.org/10.1080/00102207908946898

Trimis, D., Wawrzinek, K., 2004. FLAME STABILIZATION OF HIGHLY DIFFUSIVE GAS MIXTURES IN POROUS INERT MEDIA, Journal of Computational and Applied Mechanics.

Turns, S.R., 2000. An Introduction to Combustion Concepts and Applications, 2nd ed. The McGraw-Hill Co, Singapore.

Veríssimo, A.S., Rocha, A.M.A., Costa, M., 2013. Importance of the inlet air velocity on the establishment of flameless combustion in a laboratory combustor. Exp. Therm. Fluid Sci. 44, 75–81. https://doi.org/10.1016/j.expthermflusci.2012.05.015

Wasinarom, K., Charoensuk, J., Lilavivat, V., 2019. Non-equilibrium numerical modeling for combustion of LPG within porous media. Int. J. Heat Mass Transf. 143, 118551. https://doi.org/10.1016/j.ijheatmasstransfer.2019.118551

Weinberg, F.J., 1971. Combustion temperatures: The future? Nature 233, 239–241. https://doi.org/10.1038/233239a0

Wood, S., Harris, A.T., 2008. Porous burners for lean-burn applications. Prog. Energy Combust. Sci. 34, 667–684. https://doi.org/10.1016/j.pecs.2008.04.003

Wu, C.Y., Chen, K.H., Yang, S.Y., 2014. Experimental study of porous metal burners for domestic stove applications. Energy Convers. Manag. 77, 380–388. https://doi.org/10.1016/j.enconman.2013.10.002

Yoksenakul, W., Jugjai, S., 2011. Design and development of a SPMB (self-aspirating, porous medium burner) with a submerged flame. Energy 36, 3092–3100. https://doi.org/10.1016/j.energy.2011.02.054

Zhang, G., Cai, X., Liu, M., Lin, B., Chen, Y., Wang, L., 2006. Characteristic analysis of low-velocity gas filtration combustion in an inert packed bed. Combust. Theory Model. 10, 683–700. https://doi.org/10.1080/13647830600647426

Zhao, P., Chen, Y., Liu, M., Ding, M., Zhang, G., 2007. Numerical simulation of laminar premixed combustion in a porous burner. Front. Energy Power Eng. China 1, 233–238. https://doi.org/10.1007/s11708-007-0032-8

Zhou, X.Y., Pereira, J.C.F., 1998. Comparison of Four Combustion Models for Simulating the Premixed Combustion in Inert Porous Media. Fire Mater. 22, 187–197. https://doi.org/10.1002/(SICI)1099-1018(199809/10)22:5<187::AID-FAM652>3.0.CO;2-T

Zhou, X.Y., Pereira, J.C.F., 1997. Numerical study of combustion and pollutants formation in inert nonhomogeneous porous media. Combust. Sci. Technol. 130, 335–364. https://doi.org/10.1080/00102209708935748

APPENDIX – I

Properties of Fuels

1. LPG (http://www.gasindia.in)

Particulars	Value
Chemical Formula	Propane (C_3H_8) - 40% and Butane (C_4H_{10}) - 60%
Ignition temperature (°C)	488-502
Max. flame temperature (°C)	1985
Higher calorific value (kJ/kg)	49540
Lower calorific value (kJ/kg)	45605.6
Density (kg/m^3)	1.9

APPENDIX – II

Technical Specifications of the Instruments Used in the Experiments

1. Compressor

Make	Ingersoll Rand
Type	Reciprocating
Maximum Pressure	12 kg/cm2
Free air delivery	400-450 lpm
Type	2 stage
Tank capacity	250 liters
Accessories	Precise Pressure regulator, air filter

2. Weighing balance

Make	SARTORIUS COMBICS LITE
Model	CLWP1 – 30ED-I
Capacity	30kg
Platform size	400X300mm
Readability	1g
Power Supply	90 to 260V AC & DC
Indicator	18mm LCD 7 segment backlit

3. Thermocouples

Make	Industrial Heators
Type:	metal sheathed K-type
Junction	Grounded
Range	20 ºC to 1400 ºC

4. Mass flow meter for fuel

Type	Coriolis mass flow meter
Make	Emerson Process Management Pvt. Ltd.

Model	CMF010P323NQB2E222
Flow range	0 to 50 g/min
Flow accuracy	± 0.35% of full scale
Sensitivity	0.001g
Temperature range	-10 to 100 °C
Operating pressure range	0 to 150 bar

5. Mass flow meter for air

Type	Thermal mass flow meter
Make	Mass Stream
Model	D-6370-HGD-CC-AV-99-D-S-DR
Flow range	0.2 to 20 g/s
Flow accuracy	± 0.5% of full scale
Sensitivity	0.001g
Temperature range	20 to 35 °C
Operating pressure range	0 to 2 bar

6. Portable gas analyzer

Make	Testo
Model	340
O_2	0-25 Vol%
Resolution	0.01 Vol%
Accuracy	±0.2Vol.%
CO	0-10000ppm
Accuracy	±10ppm (0-200 ppm)
Resolution	1 ppm
NO	0-3000 ppm
Accuracy	±5ppm (0-99 ppm)
Resolution	1 ppm
NO_2	0-500ppm
Accuracy	± 10ppm (0-199)
Resolution	0.1 ppm

7. Data Acquisition Unit (DAQ)

Make	Agilent technologies
Model	34970A
Scan rate	60 to 250 channels/second
Scan intervals	0 to 99 hours; 1 ms time step
Accuracy	6 digits of resolution with 0.004%

APPENDIX – III

Uncertainty Analysis

Estimation of uncertainty in the estimated quantities radiation efficiency (η_r), thermal efficiency (η_t), Equivalence Ratio (Φ), and CO/CO_2 ratio have performed according to the sequential perturbation technique (Holman, 2012). A sample calculation for the uncertainty in η_t is shown below. The expression for error ($\delta(\eta_t)$) associated with the calculation of η_t (1) is found from the following:

$$\eta_t(\%) = \frac{(m_w c_w + m_p c_p) \times \Delta T}{m_f \times LCV} \times 100 \quad (1)$$

$$\delta(\eta_t) = \left(+ \left(\frac{\partial \eta_t}{\partial m_p}\right)^2 \times (\delta m_p)^2 + \left(\frac{\partial \eta_t}{\partial m_w}\right)^2 \times (\delta m_w)^2 + \left(\frac{\partial \eta_t}{\partial m_f}\right)^2 \times (\delta m_f)^2 + \left(\frac{\partial \eta_t}{\partial \Delta T}\right)^2 \times (\delta \Delta T)^2 \right)^{\frac{1}{2}} \quad (2)$$

$$\delta(\eta_t) = \sqrt{(E_1 + E_2 + E_3 + E_4} \quad (3)$$

Maximum relative uncertainty of thermal efficiency ($\frac{\delta(\eta_t)}{\eta_t} \times 100$) is 0.98% for m_p = 2.99 kg, m_w= 16.5 kg, ΔT = 62°C, and m_f = 175.51 g. Details of the uncertainties are given in the Table below

Pan mass (E_1)	Water mass (E_2)	Fuel weight (E_3)	Water temp. (E_4)	$\delta\eta_t$	$\frac{\delta(\eta_t)}{\eta_t}\times 100$
4.52×10^{-13}	1.048×10^{-9}	1.005×10^{-5}	2.005×10^{-5}	± 0.00541	± 0.98%

Similarly, the maximum uncertainties in the measurement of η_r, Φ and CO/CO_2 ratio are 0.6%, 0.03 and 0.00022, respectively.

APPENDIX – IV

User Defined Function for Radiation model

1. User defined function for incorporating Rosseland radiation model in the Combustion Zone (SiC)

```
#include "udf.h"
 DEFINE_PROPERTY(krad,c,t)
 {
 real a; // extinction co-efficient value.
 real sig;          //boltzman's constant
 real T = C_T(c,t); //storing cell temperature
 sig = 5.67*pow(10,-8);
 a = 270;
 return 120 + 16*sig*pow(T,3)/(3*a);

 }
```

2. User defined function for incorporating Rosseland radiation model in the Preheating Zone (Al_2O_3)

```
#include "udf.h"
 DEFINE_PROPERTY(krad,c,t)
 {
 real a; // extinction co-efficient value.
 real sig;          //boltzman's constant
 real T = C_T(c,t); //storing cell temperature
 sig = 5.67*pow(10,-8);
 a = 270;
 return 35 + 16*sig*pow(T,3)/(3*a);

 }
```

List of Publications

Patent

P. Muthukumar, **Deb S.**, Self-Aspirated Clustered Porous Radiant Burner Stove for Clean and Efficient Largescale Commercial Cooking Applications. Indian Patent, Application no. Patent application No. 202131040236 published on 12-11-2021.

Journal Papers

[1] **S. Deb**, P. Muthukumar, Development and performance assessment of LPG operated cluster Porous Radiant Burner for commercial cooking and industrial applications, Energy. 219 (2021) 119581. https://doi.org/10.1016/j.energy.2020.119581.

[2] **S. Deb**, L.K. Kaushik, M.A. Kumar, S.H. V. Satish, P. Muthukumar, Clustered Porous Radiant Burner: A cleaner alternative for cooking systems in small and medium scale applications, J. Clean. Prod. 308 (2021) 127276. https://doi.org/10.1016/j.jclepro.2021.127276.

[3] **S. Deb**, L.K. Kaushik, M.A. Kumar, P. Muthukumar, Performance characterization of a cluster porous radiant burner for clean and efficient LPG combustion, Chem. Eng. Trans. 81 (2020) 361–366. https://doi.org/10.3303/CET2081061.

Conferences

[1] **S. Deb**, S. H. V. Satish, P. Muthukumar, Numerical Study of Combustion Modes in a Clustered Porous Radiant Burner, International Conference on Applied Energy 2021, Nov. 29 - Dec. 2, 2021, Bangkok (Virtual), Thailand